NONLINEAR PROPERTIES OF DENSE COHERENT MEDIA

A Dissertation

by

EUGENIY EUGENIEVICH MIKHAILOV

Submitted to the Office of Graduate Studies of
Texas A&M University
in partial fulfillment of the requirements for the degree of

DOCTOR OF PHILOSOPHY

August 2003

Major Subject: Physics

NONLINEAR PROPERTIES OF DENSE COHERENT MEDIA

A Dissertation

by

EUGENIY EUGENIEVICH MIKHAILOV

Submitted to Texas A&M University
in partial fulfillment of the requirements
for the degree of

DOCTOR OF PHILOSOPHY

Approved as to style and content by:

George R. Welch (Chair of Committee)	
Edward S. Fry (Member)	M. Suhail Zubairy (Member)
Paul S. Cremer (Member)	Edward S. Fry (Head of Department)

August 2003

Major Subject: Physics

ABSTRACT

Nonlinear Properties of Dense Coherent Media. (August 2003)
Eugeniy Eugenievich Mikhailov, B.S., Moscow State Engineering Physics Institute
Chair of Advisory Committee: Dr. George R. Welch

Properties of coherent media in the regime of electromagnetically induced transparency (EIT) are studied. A study of the shape and width of the EIT resonance is presented for coherent media with buffer gas. Observation of an absorption-like resonance for large one-photon detunings in a medium with buffer gas and its properties are shown. The regime of "slow" and "fast" group velocities are studied. Observation of narrow resonances with a phase broadened probe field is presented, and possible application of this regime are outlined.

To my lovely wife Irina.

ACKNOWLEDGMENTS

There are many people who influenced, guided, taught, and helped me. I am thankful to every one of them.

First of all, I would like to thank my advisor, Prof. George R. Welch for his support, advice, and especially for being the perfect role model of a successful physicist and a devoted father. I also want to thank Dr. Vladimir A. Sautenkov, Vladimir L. Velichansky, and Alexander S. Zibrov. Their help with the experiment and ideas for new ones cannot be overestimated. I am grateful to Dr. Yuri V. Rostovtsev who taught me a lot about theory and experiment connections. It was an honor to meet and have a discussion with such great scientists as Dr. Marlan O. Scully, Edward S. Fry, M. Suhail Zubairy, A. B. Matsko, Olga Kocharovskaya, A. Sokolov, I. Marienko, H. Lee, D. Budker, V. V. Yashchuk, V. I. Yudin, and A. V. Taichenachev. My special appreciation goes to the physics professor on the undergraduate admission committee, whose name I do not know, but whose advice turned me toward the physics.

I also want to acknowledge the support of the Office of Naval Research and the Welch Foundation.

Finally, I would like to thank all my friends and family, especially my beloved wife Irina Novikova for her patience, help and support.

TABLE OF CONTENTS

CHAPTER Page

CHAPTER Page

LIST OF FIGURES

FIGURE Page

FIGURE Page

FIGURE Page

FIGURE Page

FIGURE Page

FIGURE Page

FIGURE Page

CHAPTER I

INTRODUCTION

A. Review of the study of electromagnetically induced transparency

The importance of atomic coherence has been recognized in physics for quite a long period of time. This field started with the Hanle effect [1–3] and now encompasses a wide range of current experiments [4].

The phenomenon of coherent population trapping (CPT) was first observed experimentally by Adriano Gozzini and coworkers in 1976 [5]. They discovered that under the condition of matching the two-photon detuning of two laser fields to the atomic level splitting, the fluorescence in a medium is highly suppressed. This can be explained by considering a picture of "bright" and "dark" states, which are coherent superpositions of atomic levels. In the CPT process, atoms are repumped to the "dark" state which does not interact with light, and thus no fluorescence is observed [6–17].

The same mechanism leads to EIT of a weak probe field in the presence of a strong drive field in the medium where the two-photon resonance condition is satisfied [18–29]. Without a drive field, such media is opaque for probe field.

The EIT regime highly modifies properties of the media giving rise to many new phenomena. Hundreds of experimental and theoretical publications are devoted to the study EIT of the regime and to possible applications. Several configuration of atomic levels and laser fields are suggested and experimentally demonstrated for the EIT regime, such as a Λ scheme, where 2 ground levels are coupled by two fields with a single upper level [30–32], a V scheme, where one ground level is coupled with 2

This dissertation follows the style and fomat of Physical Review A.

higher levels [33–37], a cascade, where the upper level is coupled with the ground level through an intermediate one [38–43], and many others utilizing more than 2 fields coupling higher numbers of levels.

Cancelation of absorption in the EIT regime [3, 22, 23] makes possible the realization of amplification without inversion (AWI) [44–47], gain without inversion (GWI) [48–50] and lasing without inversion (LWI) [24, 27, 28, 34, 46, 51–58]. Two teams of Texas A&M University researches first conducted proof of principle experiments of LWI in 1995 [44, 59, 60]

The EIT regime shows resonance features with subnatural resonance width [61–68]. Resonance widths as narrow as several Hz have been observed in cells with buffer gas [61, 63, 69] and with antirelaxation coatings [70]. Such narrow resonances make possible state of the art sensitive magnetometry [29, 71–76] and precision spectroscopy [69], as well as frequency standards [77].

The narrow EIT resonance is accompanied by steep dispersion [3, 78–80] which makes possible observation of enhanced index of refraction [25, 81–87]. Furthermore, the steep dispersion enables the observation of low group velocity as low as several meters per second [78, 79, 88–91]. Future breakthroughs in quantum computing will require a new type of quantum memory. Slow and halted light pulses, or even light storage schemes for quantum computing memory utilizing EIT have been suggested [92–102]. An EIT medium with low group velocity makes possible forward Brillouin scattering [103, 104] which is usually forbidden in bulk media because of the phase matching condition.

Opposite to slow light, superluminal group velocity has been observed in the EIT regime with extra incoherent pumping [105]. In the case when the upper level degeneracy is smaller than the lower level degeneracy, the CPT process leads to observation of electromagnetically induced absorption (EIA) [66, 106–108]. Because the slope

of the dispersion curve is opposite to the one in the EIT case, superluminal group velocity is observed [106]. Large negative delay (-400μS) associated with superluminal group velocity is observed in lambda scheme with an additional microwave field [91].

Nonlinear properties of the media are greatly enhanced by the EIT regime in orders of magnitude [26, 109–111]. In the EIT regime, nonlinear processes at energy as low as a few photons per atomic cross section are allowed [18]. Scully suggested the new so-called "phaseonium" regime where high atomic density and a strong drive laser field prepares coherence in very optically dense media [112]. In this regime, phase dependent measurements are greatly enhanced. This property of EIT leads to sensitive magnetometry [71, 113, 114].

Another important application of nonlinear properties of EIT is enhanced four-wave mixing due to coherence constructed on coupled atomic sublevels [64, 115–121]. Such processes lead to the enhancement of generation of ultraviolet radiation in the mixing scheme where the probe field operates in two-photon resonance [122–124].

A scheme for generating ultra short light pulses was suggested by Harris *et al.* [125]. In this case, the coherence gives rise to an amplitude and phase modulated signal, and thereby allows compression by the group velocity dispersion of the medium.

Several papers show that quantum statistics of light are changed by propagating through a medium in the EIT regime. For example, the outgoing light can be in a "squeezed" state [70, 112, 126–130]. Light in such a state may be more favorable for ultra high precision experiments such as search for gravitational waves [131].

It is practically impossible to mention all of the hundreds of papers devoted to the study of CPT and EIT regimes as well as all possible applications based on them. Several useful reviews covering this area include [17, 22, 23] and references included therein.

B. Motivation

Because the EIT regime allows us to dramatically modify properties of the medium in a controllable fashion, numerous experimental and theoretical studies are devoted to the properties of EIT. However, there are several areas which still need to be explored.

For example, despite the use of buffer gas as tool to increase ground level coherence time [132, 133] and its common usage to achieve ultranarrow resonances [61, 63, 69] in the EIT regime, the influence of buffer gas on the shape of the EIT resonance with a change in one-photon drive detuning is not studied in the high drive power regime to the best of our knowledge. Below we will show that the high power EIT regime with large one-photon drive detuning is quite different from the low drive power regime already studied [134, 135]. We show that even a small amount of buffer gas changes the resonance shape significantly changes.

Since the low group velocity regime is important for quantum memory, we present a study of the low group velocity regime in EIT . We demonstrate several dependences on power of the drive field and show that the power of the probe field should be taken in account, since it has a significant effect on the speed (delay time) of light pulses propagation.

Also we study four-wave mixing in the EIT regime. We demonstrate that the width of the generated new field is comparable but larger than the width of the EIT resonance for the probe field. We show that the shape of the generated new (Stokes) field is dramatically altered by seeding at the entrance of the medium. We show that buffer gas addition to the medium modifies the shape of the far detuned Stokes field in the four-wave mixing regime as the drive field is detuned. We study a new regime of absorption-like resonances appearing as this detuning becomes large. This regime has unique properties, such as higher signal to noise ratio and narrower width than

the traditional EIT regime.

Theoretical study shows that phase noise on the drive or probe field should broaden the EIT resonance, yet we show a way to observe a narrow EIT resonance with a width equal to the case with no phase noise.

CHAPTER II

THEORY

A. General equations of light interacting with media

1. Maxwell's equations

Maxwell's equations describe propagation of the electromagnetic field in a medium [136, 137]:

$$\vec{\nabla} \times \vec{E} = -\frac{1}{c}\frac{\partial \vec{B}}{\partial t}; \tag{2.1}$$

$$\vec{\nabla} \times \vec{H} = \frac{4\pi}{c}\vec{j} + \frac{1}{c}\frac{\partial \vec{D}}{\partial t}; \tag{2.2}$$

$$\vec{\nabla} \cdot \vec{D} = \rho \tag{2.3}$$

$$\vec{\nabla} \cdot \vec{B} = 0. \tag{2.4}$$

Here $\vec{E}$ is the electric field, and $\vec{H}$ is the magnetic field, $\vec{D}$ is the displacement, $\vec{D} = \vec{E} + 4\pi\vec{P}$, where $\vec{P}$ is the polarization of the medium, $\vec{B}$ is the magnetic induction, and $\vec{B} = \vec{H} + 4\pi\vec{M}$ where $\vec{M}$ is the magnetization of the medium, and ρ and $\vec{j}$ are the electric charge and current densities in the medium.

An atomic vapor is characterized by the absence of free charges $\rho = 0$ and lack of electric current $\vec{j} = 0$. In this case $\vec{B} \equiv \vec{H}$, and the equation for the electric component of the light field is:

$$-\nabla^2\vec{E} + \frac{1}{c^2}\frac{\partial^2\vec{E}}{\partial t^2} = -\frac{4\pi}{c^2}\frac{\partial^2\vec{P}}{\partial t^2} \tag{2.5}$$

where $\vec{P} = N\langle\vec{d}\rangle$ is the induced macroscopic polarization of the atomic vapor which is proportional to a number of interacting atoms N, and the individual dipole moment is averaged over an atomic ensemble $\langle\vec{d}\rangle = -e\langle\vec{r}\rangle$ where e is electron charge, $\vec{r}$ is the

radius vector of this electron.

Using the density operator of the atomic system the average dipole moment can be easily found by [3, 138]:

$$\hat{\rho} = |\psi\rangle\langle\psi| = \sum_{\{i\},\{j\}} \rho_{i,j}|i\rangle\langle j| \tag{2.6}$$

where $\{|i\rangle\}$ is a complete set of atomic states. The average dipole moment is expressed in terms of the dipole moments of the individual transitions and the density matrix elements of the atomic system as:

$$\langle\vec{d}\rangle = Tr(\vec{d}\hat{\rho}) = -\sum_{\{i\},\{j\}} e\langle j|\vec{r}|i\rangle\rho_{i,j} = \sum_{\{i\},\{j\}} d_{i,j}\rho_{i,j}. \tag{2.7}$$

In general case

$$|i\rangle = |nFm\rangle \tag{2.8}$$

where n is the principle quantum number, F total atomic angular momentum, m projection of F. Levels with similar quantum numbers n and F but different $m = \{-F \dots 0 \dots F\}$ are called Zeeman or magnetic sublevels.

In the following calculations we always consider a plane wave, circularly polarized in the $x-y$ plane propagating along the z direction. Then we can separate terms with left σ_- and right σ_+ circular polarization in Eq.(2.5) and rewrite it in scalar form, keeping in mind that $\vec{E}(\vec{r}) = E_{\sigma_+,\sigma_-}(z)(\vec{e_x} \pm i\vec{e_y})/\sqrt{2}$:

$$-\frac{\partial^2 E_{\sigma_+,\sigma_-}}{\partial z^2} + \frac{1}{c^2}\frac{\partial^2 E_{\sigma_+,\sigma_-}}{\partial t^2} = \frac{4\pi}{c^2} N \sum_{\{i,j\}} d_{i,j}^{(\sigma_+,\sigma_-)} \frac{\partial^2}{\partial t^2}\rho_{i,j}, \tag{2.9}$$

where $d_{i,j}^{(\sigma_+,\sigma_-)} = -e\langle j|\frac{1}{2}(x \pm iy)|i\rangle$ is the matrix element of the electric dipole moment of the transition, and σ_+ and σ_- polarization correspond to transition with $\Delta m = \pm 1$.

Let us now write the electromagnetic field in the following form:

$$E(z,t) = \mathcal{E}(z,t)e^{ikz - i\nu t} + \mathcal{E}^*(z,t)e^{-ikz + i\nu t} \tag{2.10}$$

where $k = 2\pi/\lambda$ is wave vector of the field with wavelength λ and v is its frequency of oscillations.

We assume that characteristic changes of the amplitude of the electromagnetic wave take place at the time scale much larger than one cycle of the oscillations and distances much longer then wavelength.

$$\frac{\partial \mathcal{E}}{\partial z} \ll k\mathcal{E}; \;\; \frac{\partial \mathcal{E}}{\partial t} \ll \omega\mathcal{E} \tag{2.11}$$

Then we can rewrite Eq.(2.9) for the amplitude $\mathcal{E}$, keeping only the first time and spatial derivatives of the slowly-varying amplitude:

$$\frac{\partial \mathcal{E}}{\partial z} + \frac{1}{c}\frac{\partial \mathcal{E}}{\partial t} = 2\pi i k N \sum_{\{i,j\}} d_{i,j}\tilde{\rho}_{i,j}, \tag{2.12}$$

where $\rho_{i,j} = \tilde{\rho}_{i,j}e^{ikz-i\nu t}$. This is called slowly varying amplitude approximation.

The polarization can be expressed through susceptibility (χ)

$$P = \varepsilon_0 \chi E \tag{2.13}$$

so

$$\chi = \frac{N}{\varepsilon_0 E}\sum_{\{i,j\}} d_{i,j}\rho_{i,j} \tag{2.14}$$

2. Interaction Hamiltonian

The time evolution of the density matrix is described by following equation [3]

$$\frac{d}{dt}\rho = -\frac{i}{\hbar}[H, \rho]. \tag{2.15}$$

We separate the Hamiltonian in two parts, H_0 which is the Hamiltonian in the absence of any external electro-magnetic field, and H_I which is the part responsible for the

interaction of the atom with the electro-magnetic field. Thus

$$H = H_0 + H_I \tag{2.16}$$

where $H_I = -e\vec{r} \cdot \vec{E}$. We can rewrite this equation in component form

$$H_{0ij} = \hbar\omega_i \delta_{ij} |i\rangle\langle j| \tag{2.17}$$

$$H_{Iij} = \sum_p d_{ij_p} E_{t_p}(t) |i\rangle\langle j| \tag{2.18}$$

where ω_i is energy of i-th level divided by $\hbar$, d_{ij_p} is dipole moment of transition $i \rightarrow j$ for polarization p and $E_{t_p}(t)$ is total electric field with polarization p, i and j are the full set of atomic levels.

We treat our system from the point of view of perturbation theory assuming that laser electro-magnetic field is much smaller then the interatomic electro-magnetic field, this condition holds for whole range of laser intensities used in our lab.

If we would like to include the decay of the atomic state in our system, we have to add the decay operator Γ to our Hamiltonian.

$$\frac{d}{dt}\rho = -\frac{i}{\hbar}[H, \rho] - \Gamma\rho. \tag{2.19}$$

where the matrix elements of Γ are

$$\Gamma_{ij} = \frac{1}{2}(\gamma_i + \gamma_j) + \gamma_{ij}. \tag{2.20}$$

Here γ_i and γ_j are the population decay rate of the states $|i\rangle$ and $\langle j|$. The pure dephasing rate γ_{ij} is due to the phase relaxation. Often γ_i and γ_{ij} are expressed through longitudinal (T_1) and transverse (T_2) relaxation time also called population and coherence decay time. The connection between them is $\gamma_i = 1/T_1$, $\gamma_{ij} = 1/T_2$, $\gamma_{ij} \neq 0$ only when $i \neq j$.

3. Liouville operator

Sometimes it is convenient to introduce a Liouville operator L in terms of which the evolution of the density matrix can be described through the action of the Liouville operator on the density matrix [138].

$$\frac{d\rho}{dt} = -\frac{i}{\hbar} L\rho \tag{2.21}$$

or in matrix form

$$\frac{d\rho_{jk}}{dt} = -\frac{i}{\hbar} \sum_{m,n} L_{jk,mn}\rho_{mn} \tag{2.22}$$

where

$$L_{jk,mn} = H_{jm}\delta_{kn} - H^*_{kn}\delta_{jm} + \frac{\hbar}{i}\left(\left(\frac{\Gamma_k}{2} + \frac{\Gamma_j}{2} + \widehat{\Gamma}_{jk}\right)\delta_{jm}\delta_{kn} - \delta_{mn}\delta_{jk}\gamma_{mj}\right) \tag{2.23}$$

or with $H^*_{kn} = H_{nk}$

$$L_{jk,mn} = H_{jm}\delta_{kn} - H_{nk}\delta_{jm} + \frac{\hbar}{i}\left(\left(\frac{\Gamma_k}{2} + \frac{\Gamma_j}{2} + \widehat{\Gamma}_{jk}\right)\delta_{jm}\delta_{kn} - \delta_{mn}\delta_{jk}\gamma_{mj}\right) \tag{2.24}$$

where $\widehat{\Gamma}_{jk}$ is decay rate of coherence ρ_{jk} associated with its dephasing,

$$\Gamma_k = \sum_m \gamma_{km} \tag{2.25}$$

and

$$\gamma_{km} = \gamma_{k\to m} \tag{2.26}$$

is the decay rate from the k-th state to the m-th.

Lets assume that

$$\rho_{jk}(t) = \sum_{\omega_\alpha} \rho_{jk_{\omega_\alpha}}(t) e^{i\omega_\alpha t} \tag{2.27}$$

similarly

$$L_{jk,mn}(t) = \sum_{\omega_\alpha} L_{jk,mn_{\omega_\alpha}}(t) e^{i\omega_\alpha t} \tag{2.28}$$

where $\rho_{jk_{\omega_\alpha}}(t)$ and $L_{jk,mn_{\omega_\alpha}}(t)$ are slowly varying amplitude of the Fourier components with frequency ω_α of ρ and L correspondingly.

This way Eq. 2.22 is transformed to

$$\begin{aligned}\sum_{\omega_\alpha}\frac{d\rho_{jk_{\omega_\alpha}}(t)e^{i\omega_\alpha t}}{dt} &= \sum_{\omega_\alpha}\left(i\omega_\alpha\rho_{jk_{\omega_\alpha}}(t)+\frac{d}{dt}\rho_{jk_{\omega_\alpha}}(t)\right)e^{i\omega_\alpha t}\\ &= -\frac{i}{\hbar}\sum_{m,n}\sum_{\omega_{\alpha'}}L_{jk,mn_{\omega_{\alpha'}}}(t)e^{i\omega_{\alpha'}t}\sum_{\omega_{\alpha''}}\rho_{mn_{\omega_{\alpha''}}}(t)e^{i\omega_{\alpha''}t}\end{aligned}\tag{2.29}$$

Collecting terms with $e^{i\omega_\alpha t}$ we obtain

$$\frac{d\rho_{jk_{\omega_\alpha}}(t)}{dt}=-i\omega_\alpha\rho_{jk_{\omega_\alpha}}(t)-\frac{i}{\hbar}\sum_{m,n}\sum_{\omega_{\alpha'}}\sum_{\omega_{\alpha''}}L_{jk,mn_{\omega_{\alpha'}}}(t)\rho_{mn_{\omega_{\alpha''}}}(t)\delta_{\omega_{\alpha''}\omega_\alpha-\omega\alpha'}\tag{2.30}$$

Lets express $E_{t_p}(t)$ through slowly varying Fourier components

$$E_{t_p}(t)=\int E_{p_{\omega_\alpha}}e^{i\omega_\alpha t}d\omega_\alpha=\sum_{\omega_\alpha}E_{p_{\omega_\alpha}}(t)e^{i\omega_\alpha t}\tag{2.31}$$

Thus

$$L_{jk,mn_0}=H_{0_{jm}}\delta_{kn}-H_{0_{nk}}\delta_{jm}+\frac{\hbar}{i}\left(\left(\frac{\Gamma_k}{2}+\frac{\Gamma_j}{2}+\widehat{\Gamma}_{jk}\right)\delta_{jm}\delta_{kn}-\delta_{mn}\delta_{jk}\gamma_{mj}\right)\tag{2.32}$$

$$L_{jk,mn_{\omega_\alpha}}(t)=H_{I_{jm_{\omega_\alpha}}}\delta_{kn}-H_{I_{nk_{\omega_\alpha}}}\delta_{jm}=\sum_p\left(d_{jm_p}\delta_{kn}-d_{nk_p}\delta_{jm}\right)E_{p_{\omega_\alpha}}(t)\tag{2.33}$$

These formulas are very useful when the electric field consists of just several monochromatic components. Then it is very easy to numerically solve Eq. 2.30.

B. Simple three level model of an atom interacting with bichromatic light

1. Three level Λ system in bichromatic electro-magnetic field

Let us consider the simple but realistic 3 level system interacting with a bichromatic electro-magnetic field as shown in Fig. 1. Such a system is often called Λ configuration because probe and drive fields (Ω_p, Ω_d) form Λ like configuration connecting two

ground levels ($|b\rangle, |c\rangle$) with upper level ($|a\rangle$).

In such a system the Hamiltonian has the following form [3]

$$H = \hbar\omega_a|a\rangle\langle a| + \hbar\omega_b|b\rangle\langle b| + \hbar\omega_c|c\rangle\langle c| - \hbar\left(\Omega_d e^{-i\omega_d t}|a\rangle\langle c| + \Omega_p e^{-i\omega_p t}|a\rangle\langle b|\right) + h.c. \quad (2.34)$$

where Ω_d and Ω_p are the Rabi frequency of a strong and weak fields respectively. The strong field is called the "drive" or coupling field, and the weak field is called the "probe" field. They are expressed through the drive electro-magnetic field amplitude ($\mathcal{E}_d$) and the probe field amplitude ($\mathcal{E}_p$) as

$$\Omega_d = \frac{d_{ac}\mathcal{E}_d}{\hbar}; \Omega_p = \frac{d_{ab}\mathcal{E}_p}{\hbar} \quad (2.35)$$

Lets define $\hat{\rho}(t)$ such that it satisfies Eq. 2.19 then let solve it by the method of slow varying amplitude. We define

$$\hat{\rho}_{aa}(t) = \rho_{aa} \quad (2.36)$$

$$\hat{\rho}_{bb}(t) = \rho_{bb} \quad (2.37)$$

$$\hat{\rho}_{cc}(t) = \rho_{bb} \quad (2.38)$$

$$\hat{\rho}_{ab}(t) = \rho_{ab}e^{-i\omega_p t} \quad (2.39)$$

$$\hat{\rho}_{ac}(t) = \rho_{ac}e^{-i\omega_d t} \quad (2.40)$$

$$\hat{\rho}_{bc}(t) = \rho_{bc}e^{-i(\omega_p-\omega_d)t} \quad (2.41)$$

where ω_d and ω_p frequency of drive and probe fields, then evolution of density matrix element is given in rotation wave approximation [139]

$$\dot{\rho}_{aa} = -i\Omega_p^*\rho_{ab} + i\Omega_p\rho_{ba} - i\Omega_d^*\rho_{ac} + i\Omega_d\rho_{ca} - 2\gamma\rho_{aa} \quad (2.42)$$

$$\dot{\rho}_{bb} = i\Omega_p^*\rho_{ab} - i\Omega_p\rho_{ba} + \gamma\rho_{aa} - \gamma_{bc}\rho_{bb} + \gamma_{bc}\rho_{cc} \quad (2.43)$$

$$\dot{\rho}_{cc} = i\Omega_d^*\rho_{ac} - i\Omega_d\rho_{ca} + \gamma\rho_{aa} - \gamma_{bc}\rho_{cc} + \gamma_{bc}\rho_{bb} \quad (2.44)$$

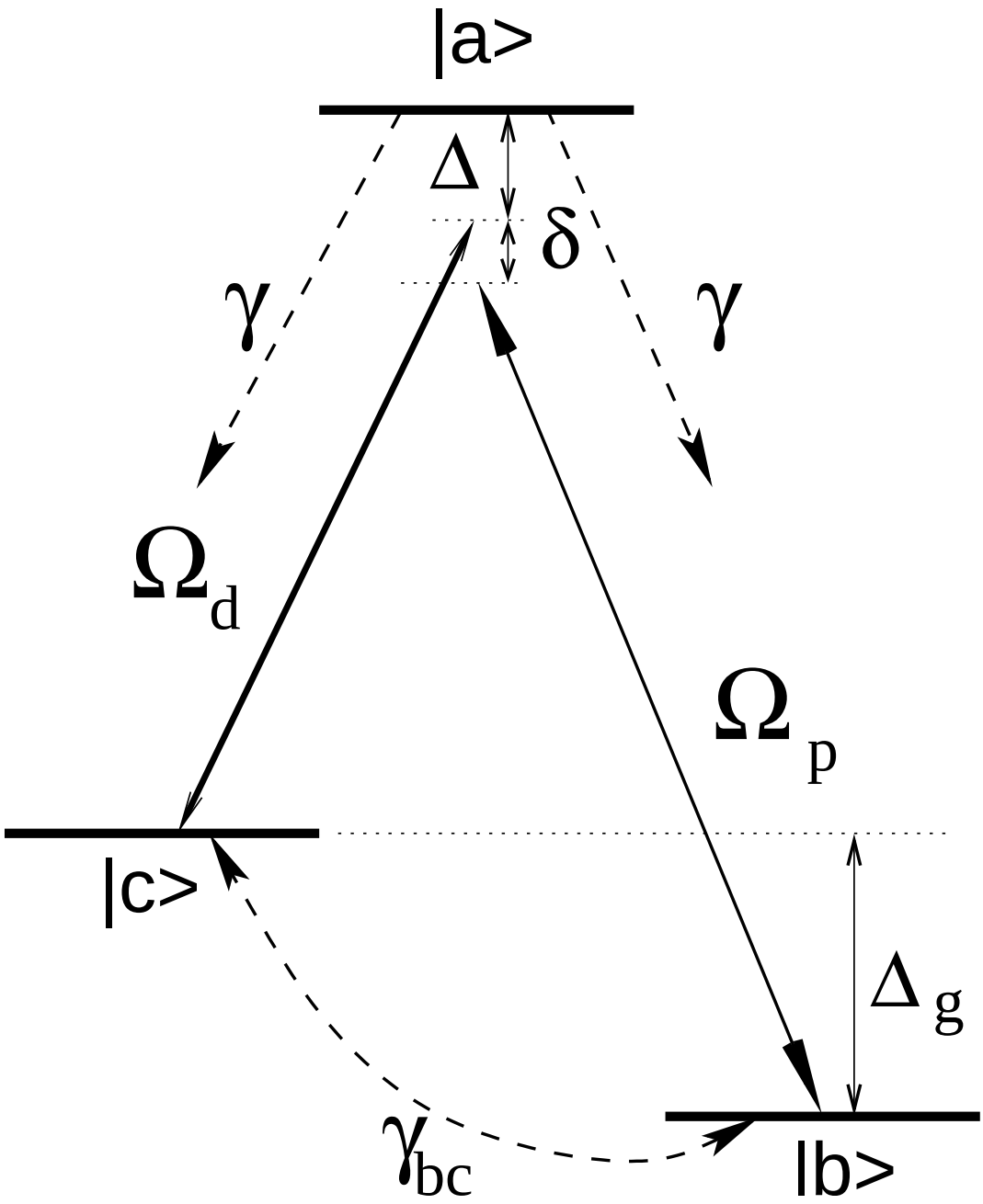

Fig. 1. Λ configuration.

$$\dot{\rho}_{ab} = -\Gamma_{ab}\rho_{ab} + i\Omega_p(\rho_{bb} - \rho_{aa}) + i\Omega_d\rho_{cb} \quad (2.45)$$

$$\dot{\rho}_{ca} = -\Gamma_{ca}\rho_{ca} + i\Omega_d^*(\rho_{aa} - \rho_{cc}) - i\Omega_p^*\rho_{cb} \quad (2.46)$$

$$\dot{\rho}_{cb} = -\Gamma_{cb}\rho_{cb} - i\Omega_p\rho_{ca} + i\Omega_d^*\rho_{ab} \quad (2.47)$$

with

$$\Gamma_{ab} = \gamma + i(\Delta + \delta) = \Gamma_{ba}^* \quad (2.48)$$

$$\Gamma_{ca} = \gamma - i\Delta = \Gamma_{ac}^* \quad (2.49)$$

$$\Gamma_{cb} = \gamma_{bc} + i\delta = \Gamma_{bc}^* \quad (2.50)$$

where we assume $\gamma_{bc} \ll \gamma$.

The solution of the above equations in the steady state regime ($\dot{\rho}_{ij} = 0$) is [139]

$$\rho_{ab} = i\Omega_p \frac{(\rho_{bb} - \rho_{aa})(\Gamma_{ac}^*\Gamma_{cb} + |\Omega_p|^2) + |\Omega_d|^2(\rho_{aa} - \rho_{cc})}{\Gamma_{ab}\Gamma_{ac}^*\Gamma_{cb} + \Gamma_{ac}^*|\Omega_d|^2 + \Gamma_{ab}|\Omega_p|^2} \quad (2.51)$$

$$\rho_{ca} = i\Omega_d^* \frac{(\rho_{aa} - \rho_{cc})(\Gamma_{ab}\Gamma_{cb} + |\Omega_d|^2) + |\Omega_p|^2(\rho_{bb} - \rho_{aa})}{\Gamma_{ab}\Gamma_{ac}^*\Gamma_{cb} + \Gamma_{ac}^*|\Omega_d|^2 + \Gamma_{ab}|\Omega_p|^2} \quad (2.52)$$

$$\rho_{cb} = i\Omega_p\Omega_d^* \frac{(\rho_{aa} - \rho_{cc})\Gamma_{ab} - (\rho_{bb} - \rho_{aa})\Gamma_{ac}^*}{\Gamma_{ab}\Gamma_{ac}^*\Gamma_{cb} + \Gamma_{ac}^*|\Omega_d|^2 + \Gamma_{ab}|\Omega_p|^2} \quad (2.53)$$

2. Four wave mixing in Λ system

In the previous consideration we neglected a term that drives our atomic system, namely probe field operating at $a \to c$ transition, and drive field operating at $a \to b$ transition. Let's now consider these off resonance fields (see Fig. 2) and also we add to consideration the additional electro-magnetic field Ω_s which is the Stokes component here with a frequency $\omega_s = \omega_d - \omega_g$, where ω_g is ground level frequency splitting.

The Hamiltonian of the system is

$$H = \hbar\omega_a|a\rangle\langle a| + \hbar\omega_b|b\rangle\langle b| + \hbar\omega_c|c\rangle\langle c| \quad (2.54)$$
$$+\hbar((\Omega_d e^{-i\omega_d t} + \Omega_s e^{-i\omega_s t})|a\rangle\langle c| + (\Omega_p e^{-i\omega_p t} + \Omega_d e^{-i\omega_d t})|a\rangle\langle b|) + h.c.$$

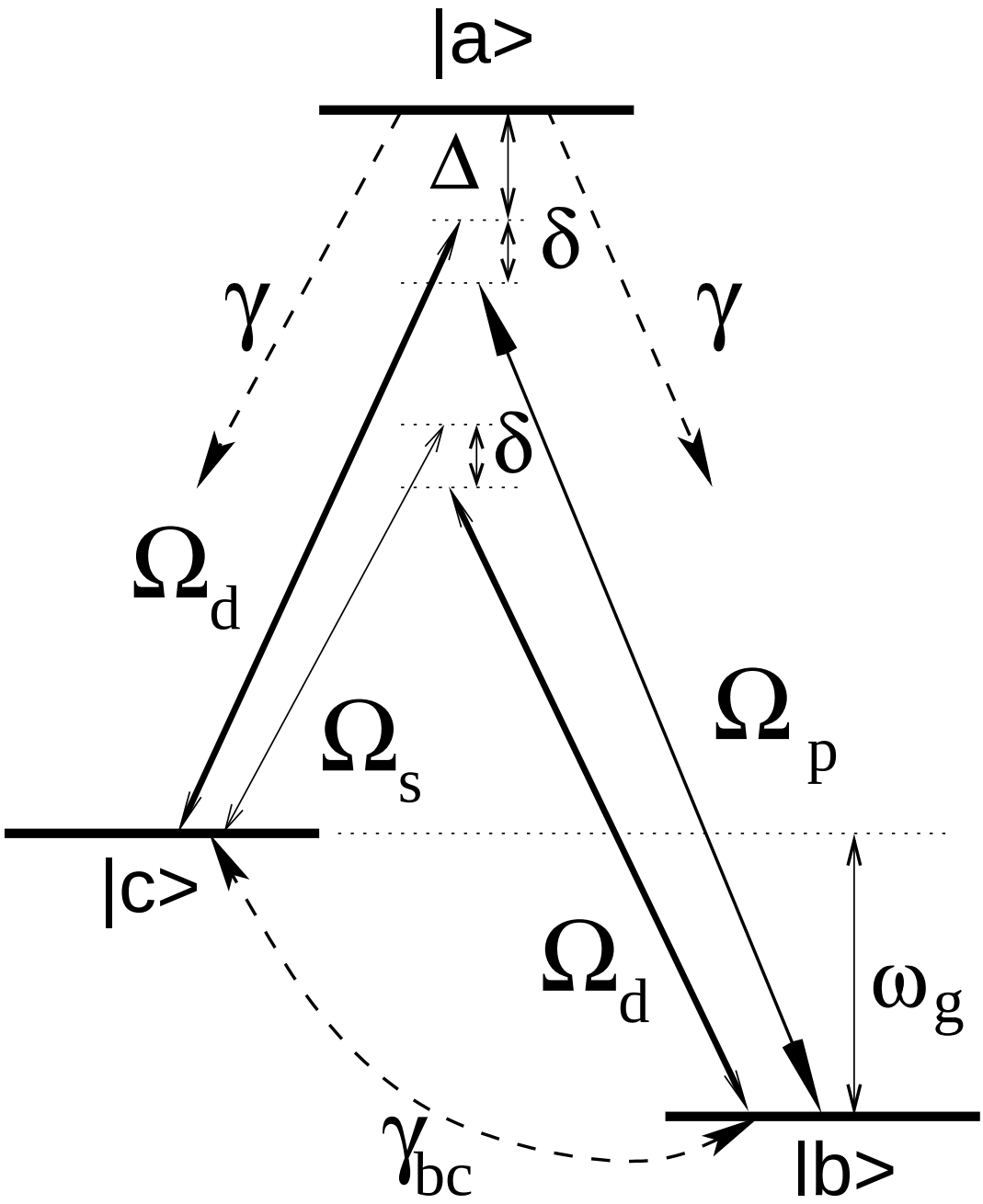

Fig. 2. Double Λ configuration formed by drive and probe, drive and Stokes fields.

Similarly to Eqs. (2.36 - 2.41) we introduce

$$\hat{\rho}_{aa}(t) = \rho_{aa} \tag{2.55}$$

$$\hat{\rho}_{bb}(t) = \rho_{bb} \tag{2.56}$$

$$\hat{\rho}_{cc}(t) = \rho_{cc} \tag{2.57}$$

$$\hat{\rho}_{ab}(t) = \rho_{ab}e^{-i\omega_p t} + \rho'_{ab}e^{-i\omega_d t} \tag{2.58}$$

$$\hat{\rho}_{ac}(t) = \rho_{ac}e^{-i\omega_d t} + \rho'_{ac}e^{-i\omega_s t} \tag{2.59}$$

$$\hat{\rho}_{bc}(t) = \rho_{bc}e^{-i(\omega_p-\omega_d)t} \tag{2.60}$$

The evolution of the Fourier components of the density matrix is described by

$$\begin{aligned}\dot{\rho}_{aa} &= -i\Omega_p^*\rho_{ab} + i\Omega_p\rho_{ba} - i\Omega_d^*\rho_{ac} + i\Omega_d\rho_{ca} - 2\gamma\rho_{aa} \\ &\quad -i\Omega_d^*\rho'_{ab} + i\Omega_d\rho'_{ba} - i\Omega_s^*\rho'_{ac} + i\Omega_s\rho'_{ca} \end{aligned}\tag{2.61}$$

$$\begin{aligned}\dot{\rho}_{bb} &= i\Omega_p^*\rho_{ab} - i\Omega_p\rho_{ba} + \gamma\rho_{aa} - \gamma_{bc}\rho_{bb} + \gamma_{bc}\rho_{cc} \\ &\quad +i\Omega_d^*\rho'_{ab} - i\Omega_d\rho'_{ba} \end{aligned}\tag{2.62}$$

$$\begin{aligned}\dot{\rho}_{cc} &= i\Omega_d^*\rho_{ac} - i\Omega_d\rho_{ca} + \gamma\rho_{aa} - \gamma_{bc}\rho_{cc} + \gamma_{bc}\rho_{bb} \\ &\quad +i\Omega_s^*\rho'_{ac} - i\Omega_s\rho'_{ca} \end{aligned}\tag{2.63}$$

$$\dot{\rho}_{ab} = -\Gamma_{ab}\rho_{ab} + i\Omega_p(\rho_{bb} - \rho_{aa}) + i\Omega_d\rho_{cb} \tag{2.64}$$

$$\dot{\rho}'_{ab} = -\Gamma'_{ab}\rho'_{ab} + i\Omega_d(\rho_{bb} - \rho_{aa}) + i\Omega_s\rho_{cb} \tag{2.65}$$

$$\dot{\rho}_{ca} = -\Gamma_{ca}\rho_{ca} + i\Omega_d^*(\rho_{aa} - \rho_{cc}) - i\Omega_p^*\rho_{cb} \tag{2.66}$$

$$\dot{\rho}'_{ca} = -\Gamma'_{ca}\rho'_{ca} + i\Omega_s^*(\rho_{aa} - \rho_{cc}) - i\Omega_d^*\rho_{cb} \tag{2.67}$$

$$\begin{aligned}\dot{\rho}_{cb} &= -\Gamma_{cb}\rho_{cb} - i\Omega_p\rho_{ca} + i\Omega_d^*\rho_{ab} \\ &\quad -i\Omega_d\rho'_{ca} + i\Omega_s^*\rho'_{ab} \end{aligned}\tag{2.68}$$

with

$$\Gamma_{ab} = \gamma + i(\Delta + \delta) = \Gamma^*_{ba} \tag{2.69}$$

$$\Gamma_{ca} = \gamma - i\Delta = \Gamma^*_{ac} \tag{2.70}$$

$$\Gamma_{cb} = \gamma_{bc} + i\delta = \Gamma^*_{bc} \tag{2.71}$$

$$\Gamma'_{ab} = \gamma + i(\omega_g + \Delta + \delta) = \Gamma'^*_{ba} \tag{2.72}$$

$$\Gamma'_{ca} = \gamma - i(\Delta + \omega_g) = \Gamma'^*_{ac} \tag{2.73}$$

where we assume $\gamma_{bc} \ll \gamma$.

It is important to notice that $\rho'_{ij} \ll \rho_{ij}$ since they correspond to off resonance term and $\omega_g \gg \Delta$. Under this condition we consider only near resonant terms as we did in the previous subsection.

Coupling between Ω_p and Ω_s occurs through the ground level coherence term ρ_{cb}. Since ρ_{cb} is quite high due to coherent preparation by the probe and drive fields we could expect ρ'_{ac} (the term responsible for propagation of the Stokes field Ω_s) to be bigger than in the case when there is no drive Ω_d and probe Ω_p (pure Raman scattering process). Thus due to high ground level coherence off resonant Stokes component highly interacts with the medium.

Notice that in the steady state regime from Eq. 2.67

$$\rho'_{ca} = \frac{i\Omega^*_s(\rho_{aa} - \rho_{cc}) - i\Omega^*_d\rho_{cb}}{\Gamma'_{ca}} \tag{2.74}$$

which looks similarly to

$$\rho_{ab} = \frac{i\Omega_p(\rho_{bb} - \rho_{aa}) - i\Omega_d\rho_{cb}}{\Gamma_{ab}} \tag{2.75}$$

thus in case when $\Omega_s, \Omega_p \ll \Omega_d$ and $\Delta, \delta \ll \gamma \ll \omega_g$

$$\rho'_{ca} = \frac{-i\Omega_d^* \rho_{cb}}{i\omega_g} \tag{2.76}$$

$$\rho_{ab} = \frac{-i\Omega_d \rho_{cb}}{\gamma} \tag{2.77}$$

we can see that

$$\rho'_{ca} = i\frac{\gamma}{\omega_g}\rho_{ab} \tag{2.78}$$

Recalling Eq. 2.14 we can see $\chi(\omega_p) \sim \rho_{ab}$ and $\chi(\omega_s) \sim \rho'_{ca} \sim i\rho_{ab}$ thus $\chi''(\omega_s)$ mimics $\chi'(\omega_p)$. In other words frequency dependence of the absorption of the Stokes field behaves similarly to the index of refraction of the probe field frequency dependence.

CHAPTER III

SETUP

In our experiments we mainly use two type of configurations. One consists of two laser and another consists of one laser and electro-optic modulator (EOM) . First has ability to change power of the probe and drive fields independently and in easy fashion, the second is more robust and easy to maintain. Both types of setup described below.

A. Two laser setup

A schematic of the experiment is shown in Fig. 3. Two external cavity diode lasers (ECDL) were used, one of them as a strong drive laser and the second as a relatively weak probe laser. The drive laser was tuned to the $5S_{1/2}(F = 2) \rightarrow 5P_{1/2}(F = 2)$ transition of the ^{87}Rb resonance line ($\lambda = 794.7$ nm), which is called D_1 line. The probe laser was phase-locked to the drive laser with a frequency offset approximately equal to the ground-state hyperfine splitting (6.835 GHz), so its frequency was close to the $5S_{1/2}(F = 1) \rightarrow 5P_{1/2}(F = 2)$ transition. This is shown in Fig. 4.

The laser frequency is controlled via observation of fluorescence in a reference cell containing a natural mix of ^{87}Rb and ^{85}Rb. This allows us easily choose the required transition for the laser field.

The co-propagating beams of both lasers were combined and passed through a polarization preserving single mode optical fiber in order to obtain good spatial overlap and spatial modes. The beam width was adjusted with a telescope and diaphragm and the light was circularly polarized with a quarter-wave plate just before it entered the ^{87}Rb cell.

During the experiments we use different cells containing a mix of isotopically

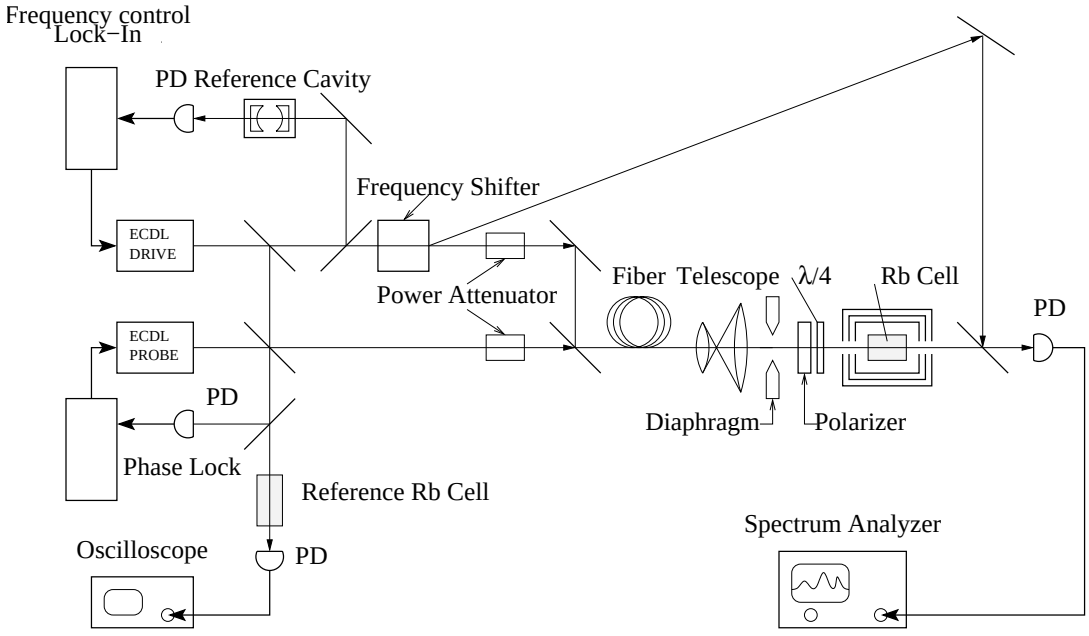

Fig. 3. Experimental setup.

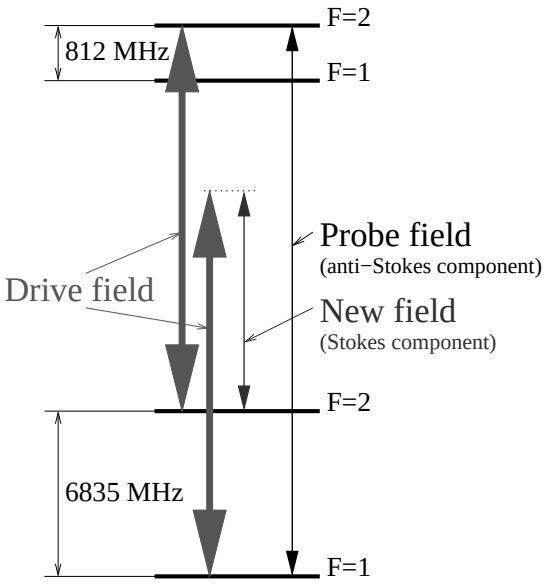

Fig. 4. Level scheme in ^{87}Rb

enhanced ^{87}Rb. The cells vary by length, diameter, kind and pressure of buffer gas. Typical range of length is 1–5 cm, and with typical buffer gas pressure laying in range .12–100 Torr. Several buffer gases are used such as Ne, Kr, N_2. Different concentrations of Rb vapor are achieved by adjusting the temperature of the cell. The cell was placed inside a three-layer magnetic shield to screen the earth's magnetic field.

The power of the drive and the probe fields can be adjusted separately by two set of crossed polarizers (depicted as power attenuators in Fig. 3). Also, probe power field can be smoothly electronically attenuated with an acousto-optic modulator (AOM) which deflects part of the beam. This allow us to control the temporal shape of the probe field for time delay measuring experiments.

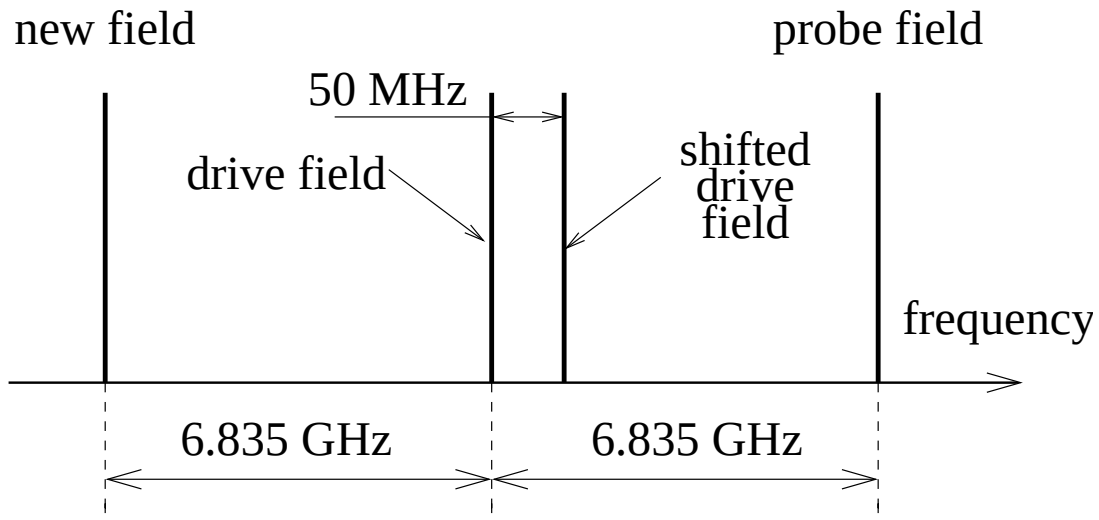

Fig. 5. Diagram showing relative frequency of the laser fields present in the experiment. The drive field is tuned to the $S_{1/2}(F = 2) \rightarrow P_{1/2}(F = 2)$ transition of the ^{87}Rb D_1 resonance line ($\lambda = 794.7$ nm). The probe laser is tuned near the the $S_{1/2}(F = 1) \rightarrow P_{1/2}(F = 2)$ transition.

B. Width measurement procedure

As described in the theory chapter, the "new" field (Stokes component) is generated by nonlinear four-wave mixing of the drive and probe fields. The difference between the probe (anti-Stokes) and drive field frequencies is equal to the difference between the drive and new field frequencies (see Figs. 4 and 5).

Rather than measure the DC component of the transmitted light, which contains drive, probe, and new fields, we detect the ac component near the beat frequency of the probe and drive lasers. This allows a clean measurement of both probe and generated (Stokes) field amplitudes. The amplitude of the beat signal at the frequency difference of the probe and drive fields (which is near the hyperfine frequency of 6.835 GHz) contains a contribution from the beat between the probe and drive fields,

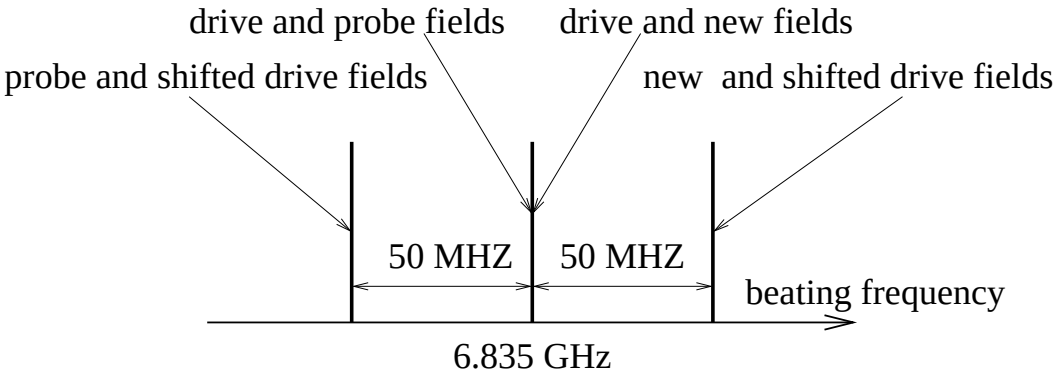

Fig. 6. Diagram showing the beat frequencies present in the experiment.

and a contribution from the beat between the drive and new fields (see Fig. 6.)

To separate the individual frequency components, another field is introduced on the detector which is derived from the drive field but shifted up slightly (50 MHz) in frequency by an AOM (See Fig. 3). This introduces side-bands in the beat spectrum. Because the shifted field does not pass through the cell these sidebands are just proportional to the transmitted field amplitude of the probe and new fields. The beat spectrum is shown in Fig. 6. Measurement of the transmitted probe field (anti-Stokes component) gives us information about the EIT resonance. Similarly, measurement of the transmitted new field (Stokes component) provides us with information about the resonance of the new field.

C. One laser and EOM setup

The two laser setup requires phase-locking the two lasers. Unfortunately, our electronic realization of it was not perfect. The beatnote of the probe and drive laser fields has a quite narrow spectrum with width less then 100 Hz (without phase lock

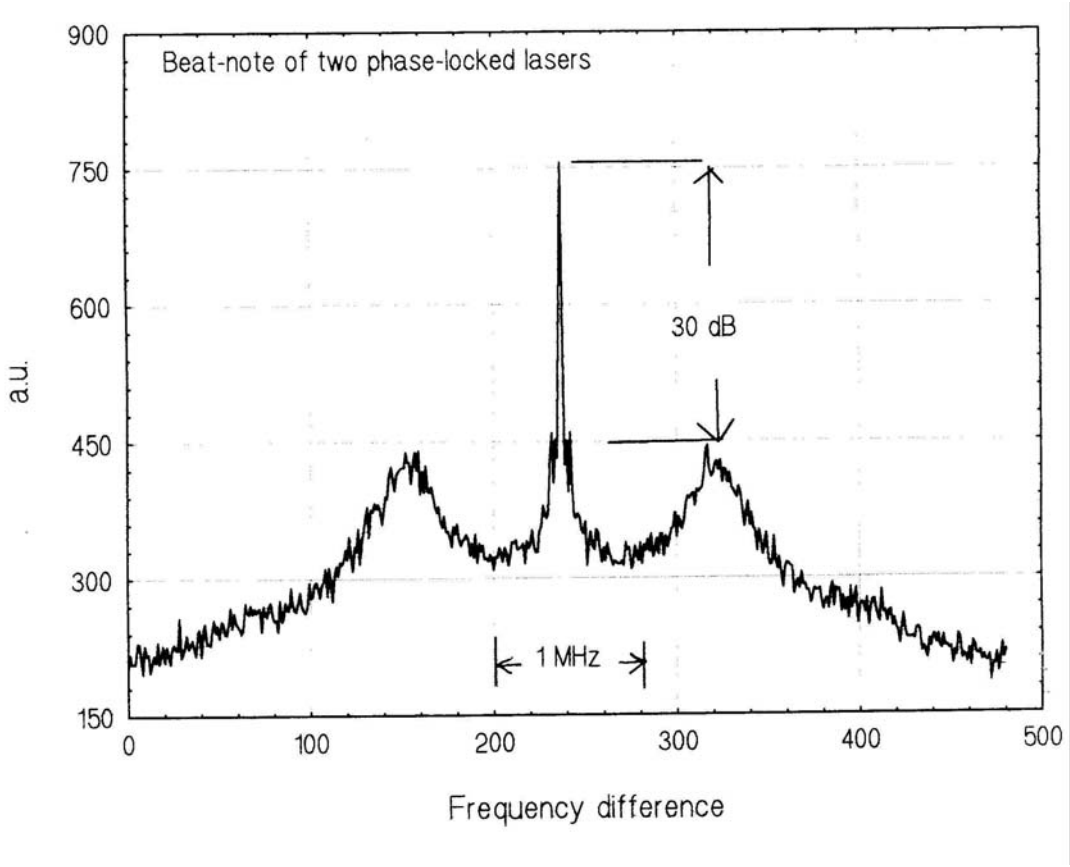

Fig. 7. Beatnote of two phase-locked lasers.

it is about 3 MHz) and a broad plato (3-4 Mhz) suppressed by 30 dB with respect to the central peak (see Fig. 7). But a crucial disadvantage is that our realization of the phase lock is not stable enough during long running times and unable to track a large drift of the probe laser. Thus every 10-15 minutes, the lasers must be readjusted, which is very inconvenient and slows down all data taking processes.

For these reasons we also use a setup using only one laser. The laser is tuned to the drive transition, and modulated by an EOM (see Fig. 8) which is driven at the frequency of the ground level splitting (6.835 GHz). This way we obtain two

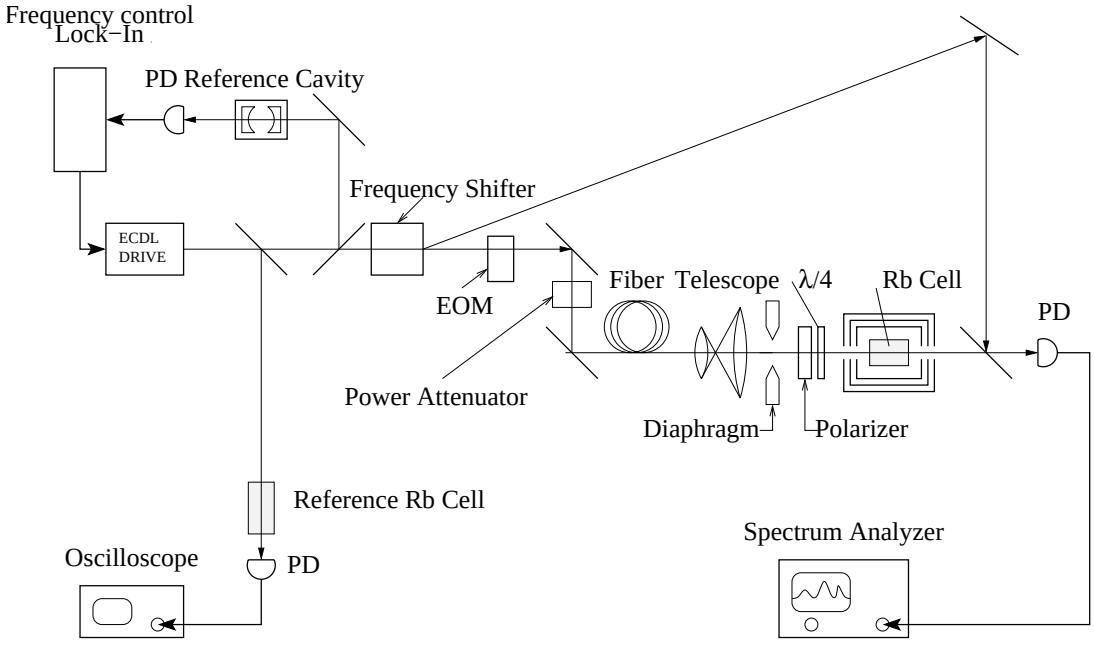

Fig. 8. Experimental setup with one laser and EOM .

sidebands, one with the frequency of the probe field (anti-Stokes component) and another with the frequency down shifted by 6.835 GHz with respect to the drive field (Stokes component). The power of the sidebands is varried by changing the EOM driving power, which is useful for time delay measurements.

A disadvantage of this setup that it is practically impossible to suppress the Stokes component of the field, as well as that it requires extra work to measure sideband power with respect to the drive field. However great stability and simplification of the setup is the main reason why we choose this scheme.

The main difference from two lasers setup is that 3 fields are entering into the ^{87}Rb cell instead of 2 as before. Other aspect of the setup are similar to the setup with two lasers.

D. Setup for phase noised probe field

For experiments which required broad ($\sim$ 1 MHz) probe field spectra we utilize the one-laser setup with EOM. But now we drive the EOM with a carrier frequency (about 6.835 MHz) and modulate its phase by "white" noise. Thus the sidebands of the Stokes and anti-Stokes component are now noise broadened with characteristic width 1 Mhz.

E. Experimental parameters estimation

Rabi frequency for ^{87}Rb can be estimated by the following formula [140]

$$\Omega = \gamma_r \sqrt{\frac{I \frac{\mathrm{cm}^2}{\mathrm{mW}}}{8}} \tag{3.1}$$

where I is the intensity of the field, for ^{87}Rb $\gamma_r = 2\pi \times 6$ MHz. For drive laser power 600 μW passing through beam with 7 mm diameter $\Omega_d = 0.44\gamma_r$.

We use several types of buffer gas in the atomic cell. For buffer Kr gas the dephasing rate (γ_{deph}) grows with buffer gas pressure according to Ottinger [141] as

$$\gamma_{deph} = 2\pi \times 1.72 \frac{\mathrm{MHz}}{\mathrm{Torr}} \tag{3.2}$$

and for Ne buffer gas

$$\gamma_{deph} = 2\pi \times 0.87 \frac{\mathrm{MHz}}{\mathrm{Torr}} \tag{3.3}$$

In the media with buffer gas beam with radius (r) and length of the cell (L), γ_{bc} is given by Vanier [142]

$$\gamma_{bc} = 2\pi \left(\frac{2.405^2}{r^2} + \frac{\pi^2}{L^2} \right) D_0 \frac{P_0}{P} \tag{3.4}$$

For Ne at $T = 67^o$C $D_0 = .48$ cm^{2}s^{-1} for Kr at $T = 47^o$C $D_0 = .16$ cm^{2}s^{-1}. So for 30 Torr Ne buffer gas in 1 cm long cell with laser beam diameter 7 mm we get

$\gamma_{bc} = 2\pi \times 692$ Hz.

For a cell without buffer gas we estimate γ_{bc} by the time of flight of an ^{87}Rb atom through the beam

$$\gamma_{bc} = 2\pi \times \frac{u}{2r} \tag{3.5}$$

so for beam with diameter 7 mm and taking $u = 400$ m/s we obtain $\gamma_{bc} = 2\pi \times 57$ kHz.

Density narrowing factor (discussed in following chapters) $\eta = 3N\lambda^2 L/8\pi^2$ taken for length of the cell $L = 1$ cm, density of ^{87}Rb atom $N = 10^{12}$ cm^{-3}, and wavelength of ^{87}Rb $\lambda = 794$ nm is

$$\eta = 240 \tag{3.6}$$

F. Cell used in experiments

Rb isotope	length, mm	diameter, mm	buffer gas	buffer gas pressure, Torr
^{87}Rb	10	15	N_2	3
^{87}Rb	25	25	N_2	30
^{87}Rb	10	13	Ne	1
^{87}Rb	25	22	Ne	30
^{87}Rb	10	21	Ne	100
^{87}Rb	53.5	30	Kr	.12
^{87}Rb	47.5	22	—	0

CHAPTER IV

PROPERTY OF EIT

A. Electromagnetically induced transparency

Using the fact that $\gamma = d^2/3\pi\hbar\varepsilon_0\lambda^3$ [3], and taking in account only resonance term from Eq. (2.14) we derive the probe field susceptibility

$$\chi = -\kappa\rho_{ab}/\Omega_p \tag{4.1}$$

where $\kappa = 3N\lambda^2\gamma_r/8\pi^2$.

The coherence ρ_{ab} is given by Eq. 2.51 which we rewrite here for convinience

$$\rho_{ab} = i\Omega_p \frac{(\rho_{bb} - \rho_{aa})(\Gamma^*_{ac}\Gamma_{cb} + |\Omega_p|^2) + |\Omega_d|^2(\rho_{aa} - \rho_{cc})}{\Gamma_{ab}\Gamma^*_{ac}\Gamma_{cb} + \Gamma^*_{ac}|\Omega_d|^2 + \Gamma_{ab}|\Omega_p|^2} \tag{4.2}$$

In the case where the drive field is strong, level $|c\rangle$ is depleted by drive field and level $|b\rangle$ is populated via decay of upper level $|a\rangle$. Eventually in this case

$$\rho_{aa} = \rho_{cc} = 0, \rho_{bb} = 1 \tag{4.3}$$

Then disregarding the term $\sim |\Omega_p|^2$ and keeping the above assumption in mind we obtain an expression for the susceptibility of the media to the probe field

$$\chi = \frac{i\kappa\Gamma_{cb}}{\Gamma_{ab}\Gamma_{cb} + |\Omega_d|^2} \tag{4.4}$$

recalling that $\Gamma_{ab} = \gamma + i(\Delta + \delta), \Gamma_{cb} = \gamma_{cb} + i\delta$

$$\chi = \frac{i\kappa}{\gamma + i(\Delta + \delta)} \left(1 - \frac{\frac{|\Omega_d|^2}{\gamma + i(\Delta+\delta)}}{\gamma_{cb} + \frac{|\Omega_d|^2}{\gamma + i(\Delta+\delta)} + i\delta}\right). \tag{4.5}$$

Assuming that $\Delta, \delta, \gamma_{cb} \ll \gamma$ so that $\Gamma_{ab} = \gamma$, we finally find

$$\chi = \frac{i\kappa}{\gamma}\left(1 - \frac{\frac{|\Omega_d|^2}{\gamma}}{\gamma_{cb} + \frac{|\Omega_d|^2}{\gamma} + i\delta}\right). \tag{4.6}$$

It is easy to see that in case of $\delta = 0$ and

$$|\Omega_d| \gg \sqrt{\gamma\gamma_{cb}} \tag{4.7}$$

that $\chi = 0$ this effect is called EIT . Since without drive field ($\Omega_d = 0$) there is strong absorption $\sim \chi'' = \kappa/\gamma$. In other words, in a Λ system of probe and strong drive fields under the condition of zero two-photon detuning, an otherwise opaque medium becomes transparent for a weak probe field.

The shape of the EIT resonance is described by a Lorentzian as can be seen from Eq. 4.6 with full width half maximum (FWHM)

$$\Gamma_{EIT} = 2\left(\gamma_{bc} + \frac{|\Omega_d|^2}{\gamma}\right) \tag{4.8}$$

The dependence of the absorption (χ'') as function of δ and Ω_d are shown in Figs. 9,10, 11, 12 and 13. We see that in the strong drive regime $\Omega_d \gg \gamma$ (Fig. 9) the width of the EIT resonance is proportional to Ω_d. We can see in this case that absorption curve consists of two Lorentzian peaks (so called Autler-Townes resonances [143]) separated by the distance equals to $2\Omega_d$.

In the case where $\Omega_d \leq \gamma$, the EIT resonance width is proportional to $|\Omega_d|^2$ according to our approximation (Eq. 4.8) as can be seen in Figs. 10,11, 12 and 13.

We can see that in case of weak drive ($\Omega_d \ll \sqrt{\gamma\gamma_{bc}}$), the absorption ($\chi''$) does not reach zero (see Fig. 13), so there is no total EIT regime. In other words, the transparency in this case is enhanced but does not reach 100%. In case of $\Omega_d = 0$, the amplitude of EIT resonance also is zero.

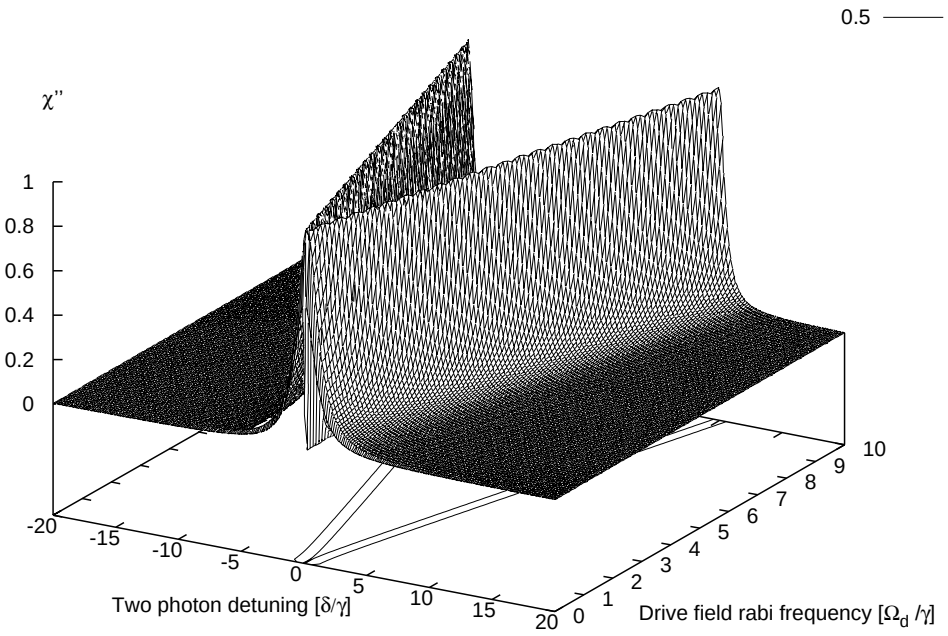

Fig. 9. χ'' vs probe laser two-photon detuning (δ) and drive Rabi frequency (Ω_d). Two-photon detuning δ and Ω_d are measured in units of γ. Lines at the bottom track the position of $\chi'' = .5$, thus the separation between the closest lines depicts the width of the EIT resonance (Γ_{EIT}). Parameters are $\gamma = 1, \Omega_p = 10^{-5}\gamma, \gamma_{cb} = 10^{-4}\gamma$

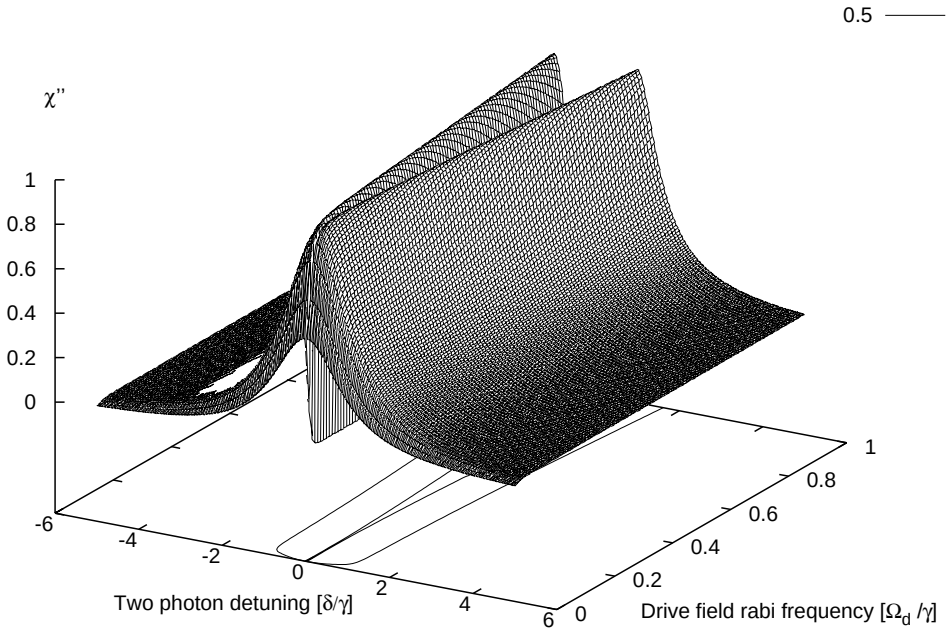

Fig. 10. χ'' vs probe laser two-photon detuning (δ) and drive Rabi frequency (Ω_d). Two-photon detuning δ and Ω_d are measured in units of γ. Lines at the bottom track the position of $\chi'' = .5$, thus the separation between the closest lines depicts the width of the EIT resonance (Γ_{EIT}). Parameters are $\gamma = 1, \Omega_p = 10^{-5}\gamma, \gamma_{cb} = 10^{-4}\gamma$

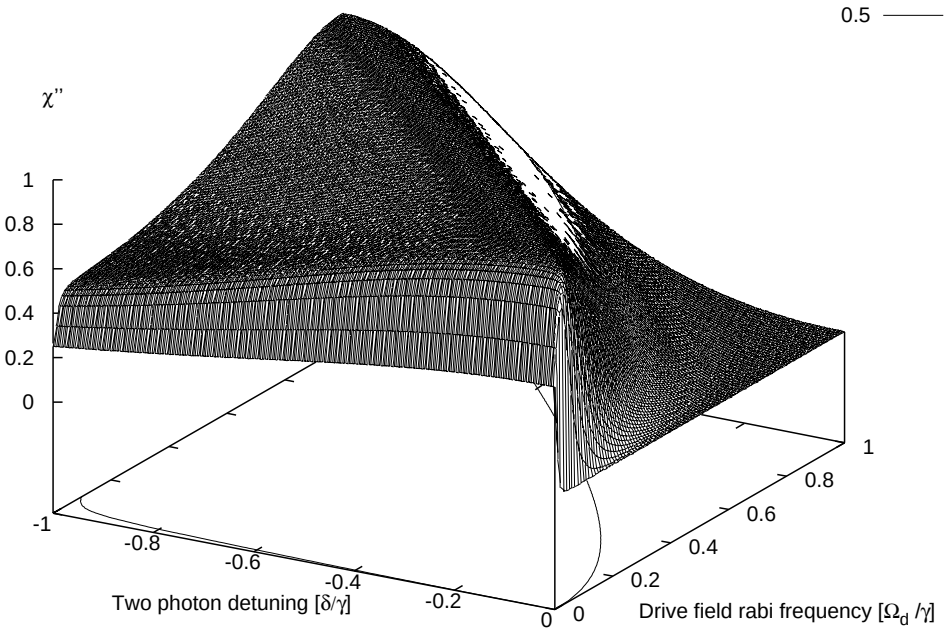

Fig. 11. χ'' vs probe laser two-photon detuning (δ) and drive Rabi frequency (Ω_d). Two-photon detuning δ and Ω_d are measured in units of γ. Lines at the bottom track the position of $\chi'' = .5$, thus the separation between the closest lines depicts the width of the EIT resonance (Γ_{EIT}). Parameters are $\gamma = 1, \Omega_p = 10^{-5}\gamma, \gamma_{cb} = 10^{-4}\gamma$

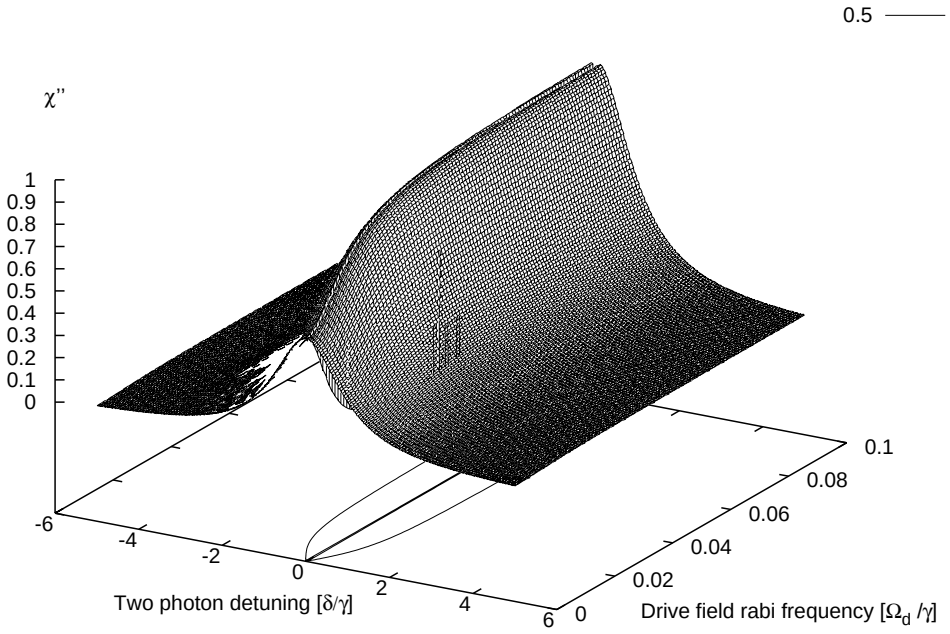

Fig. 12. χ'' vs probe laser two-photon detuning (δ) and drive Rabi frequency (Ω_d). Two-photon detuning δ and Ω_d are measured in units of γ. Lines at the bottom track the position of $\chi'' = .5$, thus the separation between the closest lines depicts the width of the EIT resonance (Γ_{EIT}). Parameters are $\gamma = 1, \Omega_p = 10^{-5}\gamma, \gamma_{cb} = 10^{-4}\gamma$

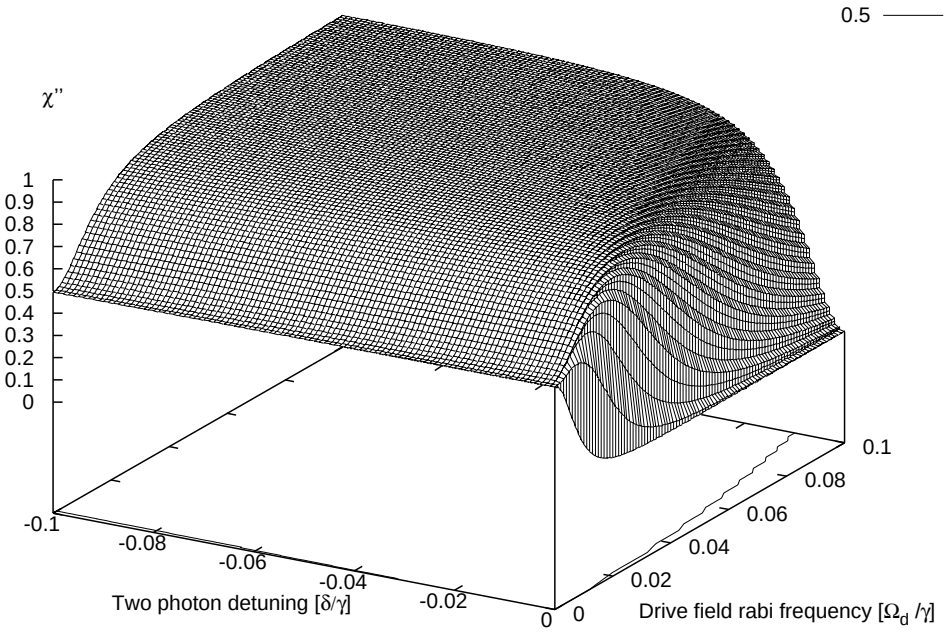

Fig. 13. χ'' vs probe laser two-photon detuning (δ) and drive Rabi frequency (Ω_d). Two-photon detuning δ and Ω_d are measured in units of γ. Lines at the bottom track the position of $\chi'' = .5$, thus the separation between the closest lines depicts the width of the EIT resonance (Γ_{EIT}). Parameters are $\gamma = 1, \Omega_p = 10^{-5}\gamma, \gamma_{cb} = 10^{-4}\gamma$

B. EIT in the case of strong probe

If $\gamma_{cb} \ll |\Omega_p|^2/\gamma \ll |\Omega_d|^2/\gamma$ we should keep term $\sim |\Omega_p|$ in denominator, then recalling that $\Gamma^*_{ac} = \gamma - i\Delta$

$$\chi = \frac{i\kappa}{\gamma + i(\Delta+\delta)} \left(1 - \frac{\frac{|\Omega_d|^2}{\gamma+i(\Delta+\delta)} + \frac{|\Omega_p|^2}{\gamma - i\Delta}}{\gamma_{cb} + \frac{|\Omega_d|^2}{\gamma+i(\Delta+\delta)} + \frac{|\Omega_p|^2}{\gamma-i\Delta} + i\delta} \right) \tag{4.9}$$

Again in case of $\Delta, \delta \ll \gamma$

$$\Gamma_{EIT} = 2\left(\gamma_{cb} + \frac{|\Omega_d|^2 + |\Omega_p|^2}{\gamma} \right) \tag{4.10}$$

The case a weak probe field that is not weak ($\Omega_p \sim \Omega_d$) is rather complicated for analytical discussion, since $\rho_{aa}, \rho_{bb}, \rho_{cc}$ are now functions of probe power. However numerical solution of density matrix equation is a simple procedure.

We can approximate the susceptibility of the medium as

$$\chi = \frac{i\kappa A(\Omega_p)}{\gamma + i(\Delta+\delta)} \left(1 - \frac{\gamma_{EIT}}{\gamma_{EIT} + i\delta} \right) \tag{4.11}$$

where $\gamma_{EIT} = \Gamma_{EIT}/2$ and $A \leq 1$ is the amplitudes of one-photon and two-photon absorption resonances. In the case of $|\Omega_p| \ll |\Omega_d|$, the amplitude of resonances $A = 1$.

Fig. 14 shows the absorption (χ'') as a function of two-photon detuning and probe Rabi frequency (Ω_p). We see that with increasing of Ω_p the EIT resonance width becomes wider with quadratic dependence on Ω_p for $\Omega_p \ll \Omega_d$ as we predict above, while at the same time the strength of the resonance becomes smaller, for large enough values of Ω_p the absorption will be nearly 0 due to power saturation effect. We can see the effect of power saturation (Fig. 15) as probe power grows from $\Omega_p = .01\gamma$ to $\Omega_p = .5\gamma$. For high enough probe power the absorption of the probe field is highly suppressed.

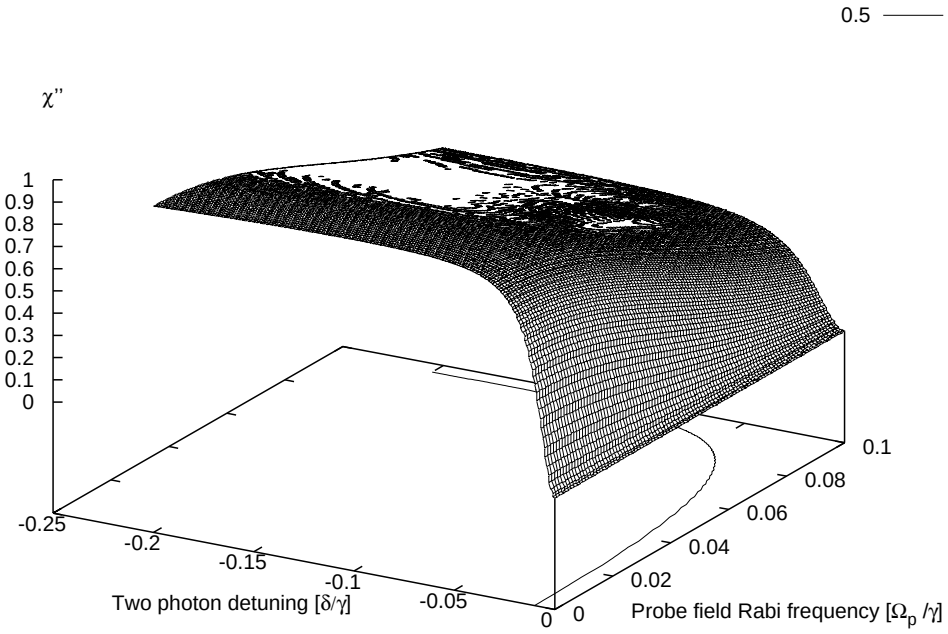

Fig. 14. χ'' vs probe laser two-photon detuning (δ) and probe Rabi frequency (Ω_p). Two-photon detuning δ and Ω_p are measured in units of γ. Lines at the bottom are track position of $\chi'' = .5$, thus separation between the closest line depict width of EIT resonance (Γ_{EIT}) Parameters are $\gamma = 1, \Omega_d = .1\gamma, \gamma_{cb} = 10^{-4}\gamma$

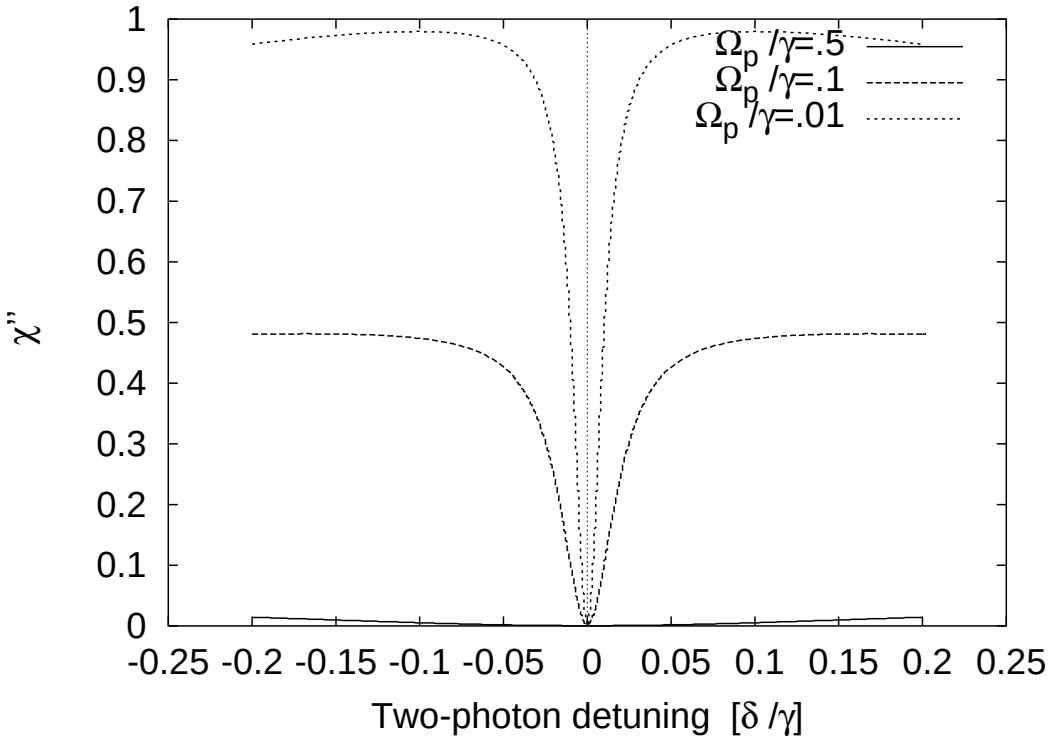

Fig. 15. χ'' vs probe laser two-photon detuning (δ) for different probe Rabi frequencies (Ω_p). Two-photon detuning δ and Rabi frequency Ω_p are measured in units of γ. Parameters are $\gamma = 1, \Omega_d = .1\gamma, \gamma_{cb} = 10^{-4}\gamma$

C. Real part of susceptibility

The real part of the susceptibility (χ') is responsible for the phase change of the electro-magnetic field during propagation through the medium. Also, the index of refraction (n) can be expressed through χ' in a following way [3] in case of $\chi' \ll 1$ (as it is in gases)

$$n = 1 + \frac{\chi'}{2} \tag{4.12}$$

In Fig. 16 we show χ' as function of probe two-photon detuning and Ω_d for condition similar to these in Fig. 9.

The dependence of χ' on probe two-photon detuning for different values of probe field power is shown in Fig. 17. Notice that as the probe field is increased, the dispersion slope at zero detuning decreases. This is crucial for our explanation of low group velocity experiments.

D. EIT in media with thermal velocity distribution

So far we have considered light interacting with a stationary atom. Moving atoms interact with a shifted frequency with respect to the one measured in the laboratory frame. This shift of frequency is called the Doppler shift. If ligth has a frequency ω in the laboratory frame then in the moving frame the frequency will be given by the following relation

$$\tilde{\omega} = \omega - \vec{k}\vec{v} = \omega\left(1 - \frac{v}{c}\right) \tag{4.13}$$

where ($\tilde{}$) denotes values measured in the moving frame, k is the wave vector, and v is the velocity of the atom. v is positive if the direction of vector k coincides with the direction of the atom's motion.

So all equation remains the same if we make the following substitution, with

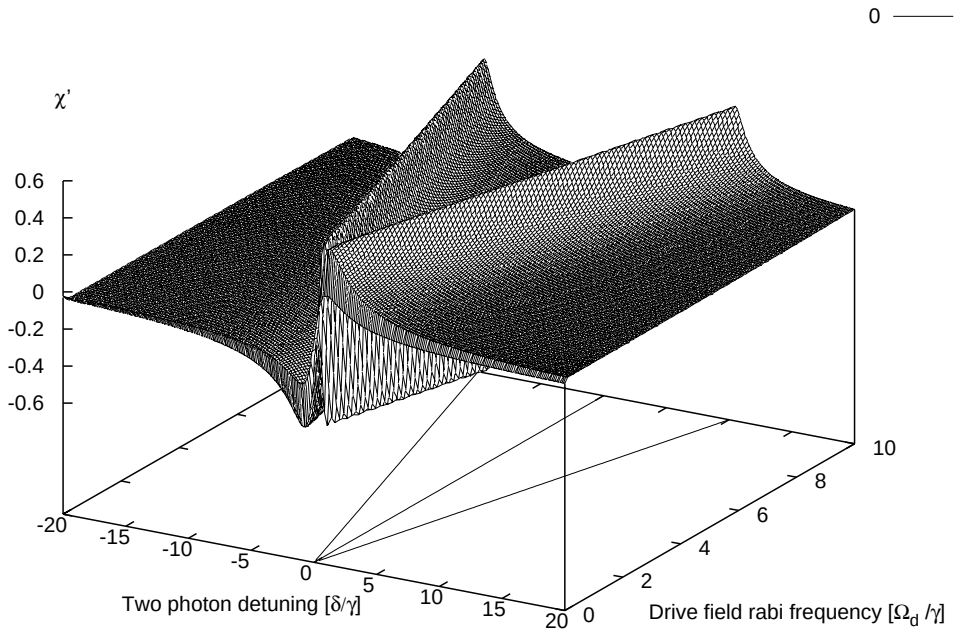

Fig. 16. χ' vs probe laser two-photon detuning (δ) and drive Rabi frequency (Ω_d). Two-photon detuning δ and Ω_d are measured in units of γ. Lines at the bottom track the position of $\chi'' = 0$. Parameters are $\gamma = 1, \Omega_p = 10^{-5}\gamma, \gamma_{cb} = 10^{-4}\gamma$

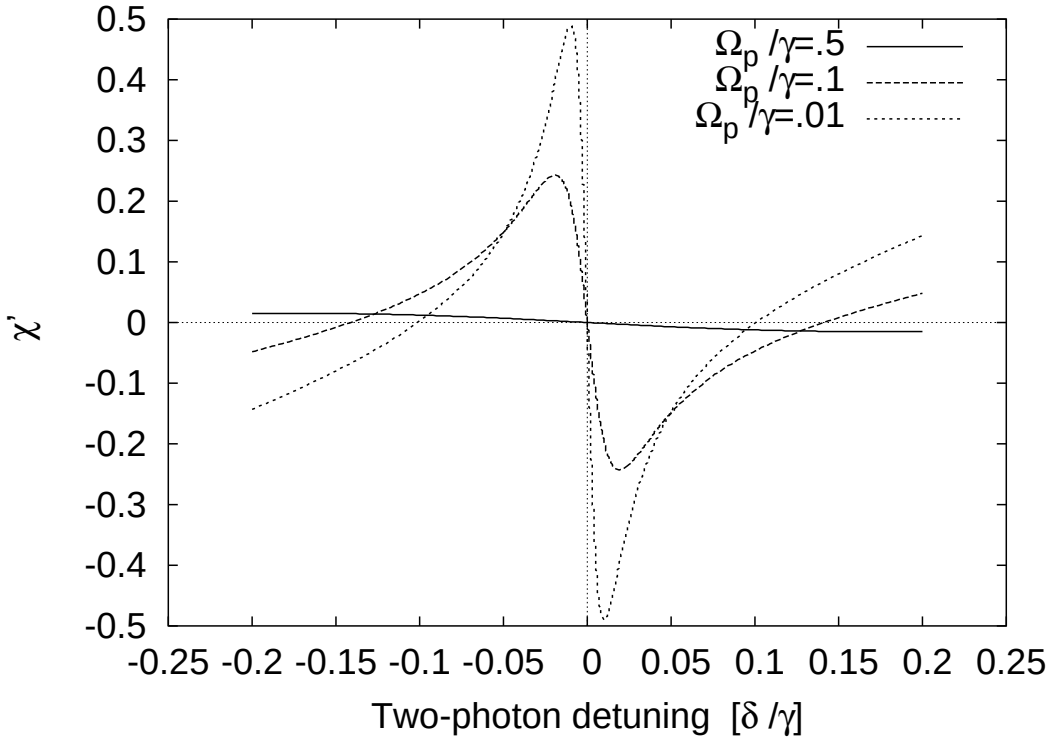

Fig. 17. χ' vs probe laser two-photon detuning (δ). Two-photon detuning δ and Ω_p are measured in units of γ. Parameters are similar to those in Fig. 15 $\gamma = 1, \Omega_d = .1\gamma, \gamma_{cb} = 10^{-4}\gamma$

the assumption that the probe and drive fields are copropagating along the Z axis: $\omega_d \rightarrow \omega_d - k_d v$, $\omega_p \rightarrow \omega_p - k_p v$, thus $\Delta \rightarrow \Delta - k_d v$, $\delta \rightarrow \delta - (k_p - k_d)v$, where k_d and k_p are the wave vectors of the drive and probe field correspondingly.

Now χ depends on v , so to find χ for the whole ensemble of moving atoms with thermal distribution $M_u(v) = \frac{1}{\sqrt{\pi}u} e^{-\frac{v^2}{u^2}}$

$$\chi = \int_{-\infty}^{\infty} \chi(v) M_u(v) dv \tag{4.14}$$

where $u = \sqrt{2k_b T/m}$ is most probable velocity of atom in ensemble, m is the mass of the atom, k_b is the Boltzmann constant, and T is the temperature of the medium.

It was shown [67, 144, 145] that in the limit of weak probe field and $\Delta = 0$, the width of the EIT resonance is

$$\Gamma_{EIT} = \begin{cases} \sqrt{\frac{2\gamma_{bc}}{\gamma}}\Omega_d & (x \ll 1) \\ \frac{\Omega_d^2}{W_D} & (x \gg 1) \end{cases} \tag{4.15}$$

where $2W_D$ is the FWHM of the width of the thermal distribution (in the references [67, 144, 145] Lorentzian velocity distribution was used), and $x = \Omega_d^2 \gamma / 2\gamma_{bc} W_D^2$.

Comparison of susceptibility for motionless atoms and a Doppler averaged ensemble is shown in Figs. 18 and 19 which show a non Doppler broaden atomic ensemble (ensemble of still atoms), and Figs. 20 and 21. We can see that area of large absorption for thermally distributed ensemble is broader, since its characteristic width is now determined by $W_D \sim k_p u$, but the width of the EIT resonance is narrower as it is predicted by the above formulas. It is important to note that the behavior of χ coincides with the behaviour given by Eq. (4.11) with an appropriately modified coefficient A and resonance width γ_{EIT}.

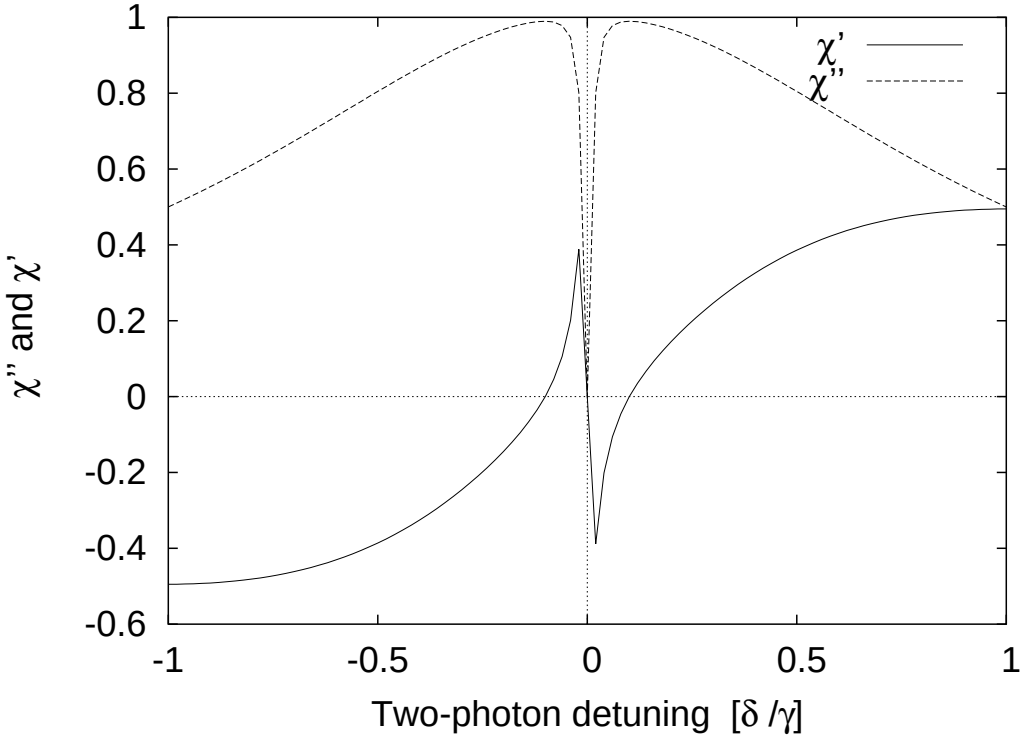

Fig. 18. Susceptibility of the media for motionless atoms vs two-photon probe detuning. Parameters are $\gamma = 1$, $\gamma_{cb} = 10^{-4}$, $\Omega_d = 0.1\gamma$, $\Omega_p = 10^{-5}\gamma$.

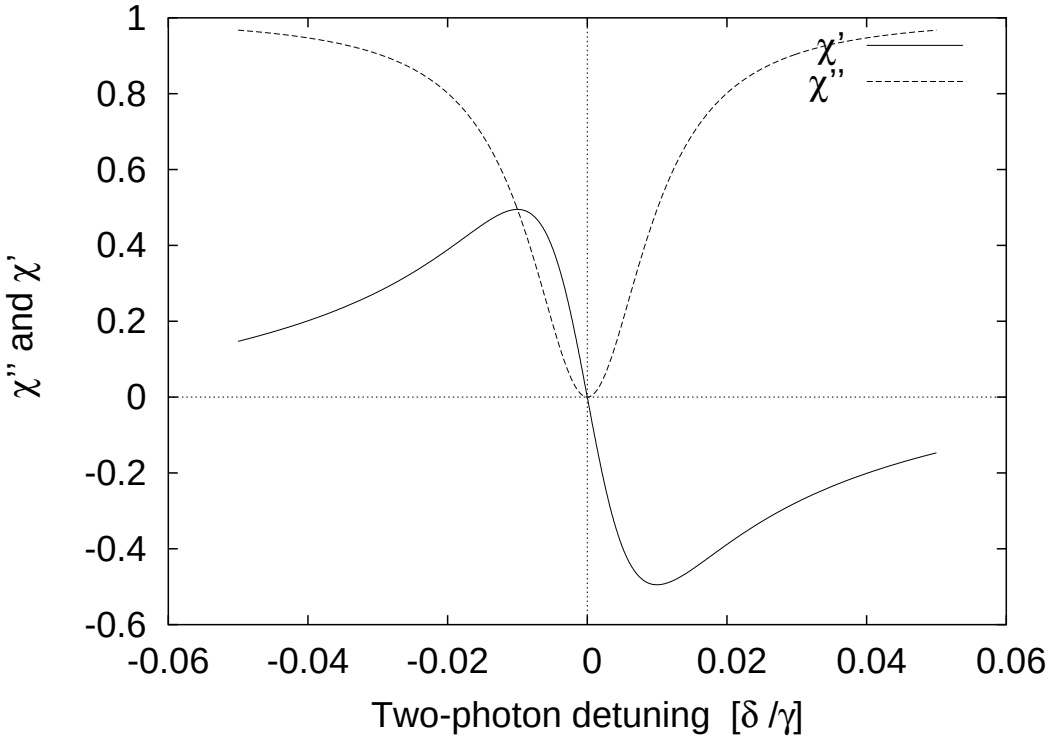

Fig. 19. Susceptibility of the media for motionless atoms vs two-photon probe detuning (zoomed version of Fig. 18). Parameters are $\gamma = 1$, $\gamma_{cb} = 10^{-4}$, $\Omega_d = 0.1\gamma$, $\Omega_p = 10^{-5}\gamma$.

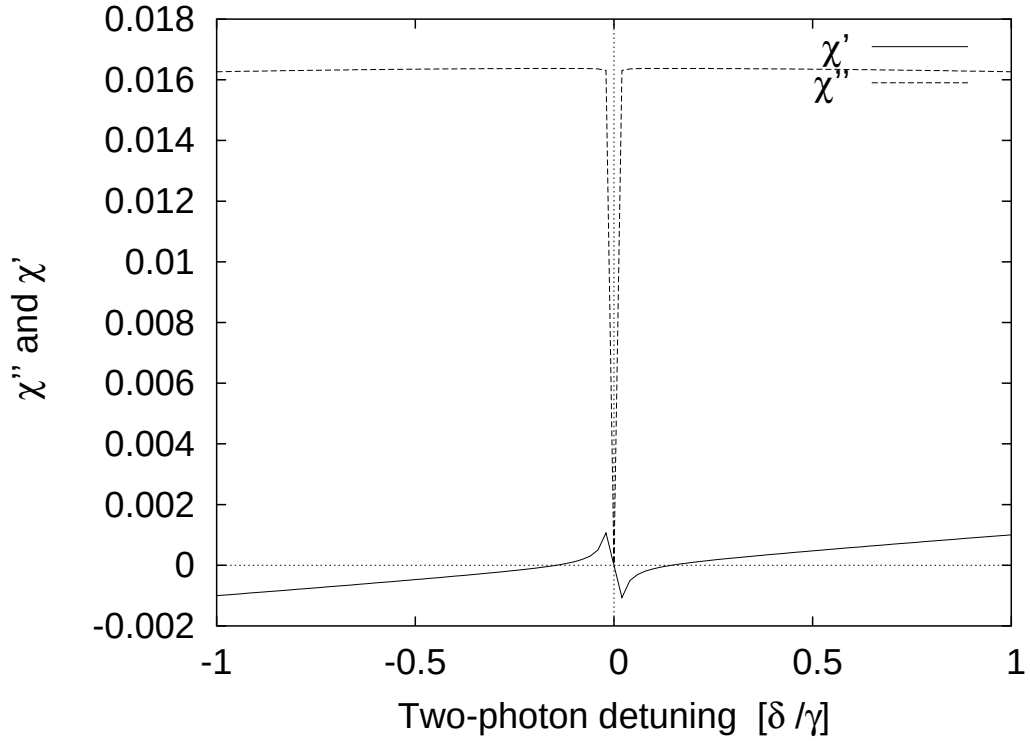

Fig. 20. Susceptibility of the media for thermally distributed ensemble vs two-photon probe detuning. Parameters are $\gamma = 1$, $\gamma_{cb} = 10^{-4}$, $\Omega_d = 0.1\gamma$, $\Omega_p = 10^{-5}\gamma$, $ku = 100\gamma$.

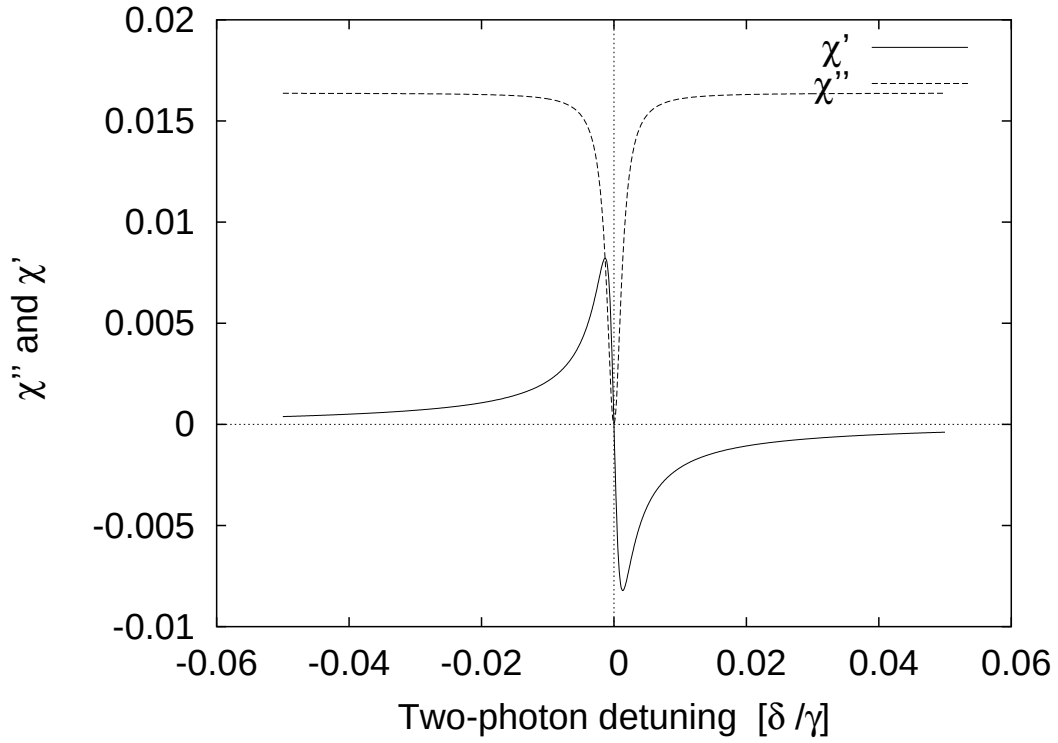

Fig. 21. Susceptibility of the media for thermally distributed ensemble vs two-photon probe detuning (zoomed version of Fig. 20). Parameters are $\gamma = 1$, $\gamma_{cb} = 10^{-4}$, $\Omega_d = 0.1\gamma$, $\Omega_p = 10^{-5}\gamma$, $ku = 100\gamma$.

E. EIT in optically dense media

When the light propagates through a dense medium we have to solve propagation equation Eq. (2.12). We can simplify this equation by rewriting it in terms of susceptibility and probe field Rabi frequency as

$$\frac{\partial \Omega_p(z)}{\partial z} = ik_p \chi \Omega_p. \tag{4.16}$$

Assuming that Ω_p is small compare to Ω_d, and the drive field propagates without significant absorption, we can treat χ as a constant with respect to coordinate z. We can express the transmission coefficient $T = \Omega_p(L)/\Omega_p(0) = \exp(-k_p \chi'' L)$.

It was predicted theoretically [64] and shown experimentally [146] that in optically thick media the width of the EIT resonance becomes narrower than the width of EIT under same the condition (same $\Omega_p, \Omega_d, \gamma, \gamma_{cb}$) in optically thin media. The resonance width gets narrower by a factor $\sqrt{\eta L}$, where $\eta = 3\lambda^2 N/8\pi^2$ where λ wavelength of the probe beam, N is density of atom, L is the length of the medium.

An accurate derivation of the EIT resonance width after the cell is given in a later chapter devoted to observation of absorption resonance. For now let us just show final result

$$\gamma_{EIT}(N, L) = \gamma_{EIT} \frac{1}{\sqrt{\eta L}} \tag{4.17}$$

where γ_{EIT} is the width of the resonance in the optically thin medium derived above.

CHAPTER V

FOUR-WAVE MIXING

A. Introduction

In media with high optical density, the generated Stokes fields introduce significant changes and must be taken in account. We have found that as a function of probe laser (anti-Stokes) frequency, the transmission linewidth of the generated Stokes field measured at the output of the cell is significantly broader than that of the probing anti-Stokes field. This result may be surprising in light of earlier work [64]. The study of Stokes harmonics properties, such as resonance width and dependence on drive laser power is the subject of this chapter.

B. Theory

Let us have a closer look at Eqs. (2.61-2.68) describing the four-wave mixing process

$$\begin{aligned}
\Gamma_{ab}\rho_{ab} &= in_{ba}\Omega_p + i\rho_{cb}\Omega_d \\
\Gamma'_{ab}\rho'_{ab} &= i\rho_{cb}\Omega_s + in_{ba}\Omega_p \\
\Gamma_{ca}\rho_{ca} &= in_{ac}\Omega_d^* - i\rho_{cb}\Omega_p^* \\
\Gamma'_{ca}\rho'_{ca} &= in_{ac}\Omega_s^* - i\rho_{cb}\Omega_d^* \\
\Gamma_{cb}\rho_{cb} &= i\rho'_{ab}\Omega_s^* - i\rho_{ca}\Omega_p + i\rho_{ab}\Omega_d^* - i\rho'_{ca}\Omega_d
\end{aligned} \tag{5.1}$$

where $n_{ba} = \rho_{bb} - \rho_{aa}$ and $n_{ac} = \rho_{aa} - \rho_{cc}$

A solution of the above equations is

$$\begin{aligned}
C\rho_{ab} &= \left(i\Gamma_{ca}\Gamma'_{ca}n_{ba}\Omega_p\Omega_s - i\Gamma_{ca}\Gamma'_{ca}n_{ba}\Omega_d\Omega_p + i\Gamma'_{ab}\Gamma_{ca}n_{ac}\Omega_d^2\right)\Omega_s^* \\
&\quad + i\Gamma'_{ab}\Gamma'_{ca}n_{ba}\Omega_p^2\Omega_p^* + \left(\left(i\Gamma'_{ab}\Gamma_{ca}n_{ba} + i\Gamma'_{ab}\Gamma'_{ca}n_{ac}\right)\Omega_d\Omega_d^* + i\Gamma'_{ab}\Gamma_{ca}\Gamma'_{ca}\Gamma_{cb}n_{ba}\right)\Omega_p
\end{aligned}$$

$$
\begin{aligned}
C\rho'_{ab} &= i\Gamma_{ab}\Gamma_{ca}n_{ac}\Omega_d\Omega_s\Omega_s^* + \left(i\Gamma_{ab}\Gamma'_{ca}n_{ac} - i\Gamma_{ca}\Gamma'_{ca}n_{ba}\right)\Omega_d^*\Omega_p\Omega_s \\
&\quad + i\Gamma_{ab}\Gamma'_{ca}n_{ba}\Omega_p^2\Omega_p^* + \left(\left(i\Gamma_{ca}\Gamma'_{ca} + i\Gamma_{ab}\Gamma_{ca}\right)n_{ba}\Omega_d\Omega_d^* + i\Gamma_{ab}\Gamma_{ca}\Gamma'_{ca}\Gamma_{cb}n_{ba}\right)\Omega_p \\
C\rho_{ca} &= \left(i\Gamma_{ab}\Gamma'_{ca}n_{ac}\Omega_d^*\Omega_s + \left(i\Gamma_{ab}\Gamma'_{ca}n_{ba}\Omega_p - i\Gamma_{ab}\Gamma'_{ab}n_{ac}\Omega_d\right)\Omega_p^*\right)\Omega_s^* \\
&\quad + i\Gamma'_{ab}\Gamma'_{ca}n_{ba}\Omega_d^*\Omega_p\Omega_p^* + \left(i\Gamma'_{ab}\Gamma'_{ca} + i\Gamma_{ab}\Gamma'_{ab}\right)n_{ac}\Omega_d\Omega_d^{*2} + i\Gamma_{ab}\Gamma'_{ab}\Gamma'_{ca}\Gamma_{cb}n_{ac}\Omega_d^* \\
C\rho'_{ca} &= i\Gamma_{ab}\Gamma_{ca}n_{ac}\Omega_s\Omega_s^{*2} + \left(i\Gamma'_{ab}\Gamma_{ca}n_{ba} - i\Gamma_{ab}\Gamma'_{ab}n_{ac}\right)\Omega_d^{*2}\Omega_p \\
&\quad + \left(i\Gamma_{ab}\Gamma'_{ab}n_{ac}\Omega_p\Omega_p^* + i\Gamma_{ab}\Gamma_{ca}n_{ba}\Omega_d^*\Omega_p\right)\Omega_s^* \\
&\quad + \left(i\Gamma'_{ab}\Gamma_{ca}n_{ac}\Omega_d\Omega_d^* + i\Gamma_{ab}\Gamma'_{ab}\Gamma_{ca}\Gamma_{cb}n_{ac}\right)\Omega_s^* \\
C\rho_{cb} &= -\left(\Gamma_{ab}\Gamma_{ca}\Gamma'_{ca}n_{ba}\Omega_p - \Gamma_{ab}\Gamma'_{ab}\Gamma_{ca}n_{ac}\Omega_d\right)\Omega_s^* \\
&\quad + \left(\Gamma'_{ab}\Gamma_{ca}\Gamma'_{ca}n_{ba} - \Gamma_{ab}\Gamma'_{ab}\Gamma'_{ca}n_{ac}\right)\Omega_d^*\Omega_p \\
C &= \Gamma_{ab}\Gamma_{ca}\Gamma'_{ca}\Omega_s\Omega_s^* + \Gamma_{ab}\Gamma'_{ab}\Gamma'_{ca}\Omega_p\Omega_p^* \\
&\quad + \left(\Gamma'_{ab}\Gamma_{ca}\Gamma'_{ca} + \Gamma_{ab}\Gamma'_{ab}\Gamma_{ca}\right)\Omega_d\Omega_d^* + \Gamma_{ab}\Gamma'_{ab}\Gamma_{ca}\Gamma'_{ca}\Gamma_{cb}
\end{aligned}
\tag{5.2}
$$

Assuming that the power of the probe and Stokes fields is small compared to the drive field, or $\Omega_p, \Omega_s \ll \Omega_d$, we obtain

$$
\begin{aligned}
\rho_{ab} &= \frac{\left(\left(in_{ba}\Omega_d^*\Gamma_{ca} + n_{ac}i\Gamma'_{ca}\Omega_d^*\right)\Omega_d + in_{ba}\Gamma_{cb}\Gamma'_{ca}\Gamma_{ca}\right)\Omega_p + n_{ac}i\Gamma_{ca}\Omega_d^2\Omega_s^*}{\left(\Omega_d^*\Gamma_{ca}\Gamma_{ab} + \Gamma'_{ca}\Omega_d^*\Gamma_{ca}\right)\Omega_d + \Gamma_{cb}\Gamma'_{ca}\Gamma_{ca}\Gamma_{ab}} + \cdots \\
\rho'_{ab} &= \frac{in_{ba}\Omega_p}{\Gamma'_{ab}} + \cdots \\
\rho_{ca} &= \frac{n_{ac}i\Omega_d^*}{\Gamma_{ca}} + \cdots \\
\rho'_{ca} &= -\frac{\left(n_{ac}i\Omega_d^{*2}\Gamma_{ab} - in_{ba}\Omega_d^{*2}\Gamma_{ca}\right)\Omega_p + \left(-n_{ac}i\Omega_d^*\Gamma_{ca}\Omega_d - n_{ac}i\Gamma_{cb}\Gamma_{ca}\Gamma_{ab}\right)\Omega_s^*}{\left(\Omega_d^*\Gamma_{ca}\Gamma_{ab} + \Gamma'_{ca}\Omega_d^*\Gamma_{ca}\right)\Omega_d + \Gamma_{cb}\Gamma'_{ca}\Gamma_{ca}\Gamma_{ab}} + \cdots \\
\rho_{cb} &= \frac{\left(n_{ac}\Gamma'_{ca}\Omega_d^*\Gamma_{ab} - n_{ba}\Gamma'_{ca}\Omega_d^*\Gamma_{ca}\right)\Omega_p + n_{ac}\Gamma_{ca}\Gamma_{ab}\Omega_d\Omega_s^*}{\left(\Omega_d^*\Gamma_{ca}\Gamma_{ab} + \Gamma'_{ca}\Omega_d^*\Gamma_{ca}\right)\Omega_d + \Gamma_{cb}\Gamma'_{ca}\Gamma_{ca}\Gamma_{ab}} + \cdots
\end{aligned}
\tag{5.3}
$$

Taking in account the propagation equation

$$
\begin{aligned}
\frac{\partial\Omega_p}{\partial z} &= i\eta\rho_{ab} = \eta(\alpha_p\Omega_p + \beta_p\Omega_s^*) \\
\frac{\partial\Omega_s^*}{\partial z} &= i\eta\rho'_{ca} = \eta(\alpha_s\Omega_p + \beta_s\Omega_s^*)
\end{aligned}
\tag{5.4}
$$

where $\eta = 3\lambda^2 N/8\pi$ we find

$$\begin{aligned}
\alpha_p &= -\frac{(n_{ba}\Gamma_{ca} + n_{ac}\Gamma'_{ca})\,|\Omega_d|^2 + n_{ba}\Gamma_{cb}\Gamma'_{ca}\Gamma_{ca}}{D} \\
\beta_p &= -\frac{n_{ac}\Gamma_{ca}\Omega_d^2}{D} \\
\alpha_s &= \frac{(n_{ac}\Gamma_{ab} - n_{ba}\Gamma_{ca})\Omega_d^{*2}}{D} \\
\beta_s &= -\frac{n_{ac}\Gamma_{ca}|\Omega_d|^2 + n_{ac}\Gamma_{cb}\Gamma_{ca}\Gamma_{ab}}{D} \\
D &= (\Gamma_{ca}\Gamma_{ab} + \Gamma'_{ca}\Gamma_{ca})\,|\Omega_d|^2 + \Gamma_{cb}\Gamma'_{ca}\Gamma_{ca}\Gamma_{ab}
\end{aligned} \tag{5.5}$$

We see that Ω_p and Ω_s are coupled together and even if the Stokes Rabi frequency $\Omega_s = 0$ at $z = 0$, it will be generated during propagation through the media.

We can change $z \to \xi$ where $\xi = \eta z$ is a dimensionless length, leading to the following propagation equations

$$\begin{aligned}
\frac{\partial \Omega_p}{\partial \xi} &= \alpha_p \Omega_p + \beta_p \Omega_s^* \\
\frac{\partial \Omega_s^*}{\partial \xi} &= \alpha_s \Omega_p + \beta_s \Omega_s^*
\end{aligned} \tag{5.6}$$

C. Generation of Stokes component

Due to high non-linear interaction of the electro-magnetic field with a coherently prepared medium even without any Stokes field component at the entrance of the cell, we observe a signal corresponding to the Stokes component at the output of the cell. This effect was briefly mentioned in [89]. Here we present a more extensive study of this effect.

According to Eq. 5.6, even if the power of the Stokes component is zero ($E_s = 0$)

$$\frac{\partial \Omega_s^*}{\partial \xi} = \alpha_s \Omega_p \tag{5.7}$$

in other words during propagation through the coherent medium, the Stokes field will

be generated.

We compare the signal (amplitude of corresponding two-photon resonance) of the transmitted probe and Stokes field for various probe and drive laser powers (see Figs. 22 and 23). We see that the transmitted signal grows with drive power as well as with probe laser power. For high enough probe laser intensities, we see that the signal does not grow linearly with probe power as it does for small intensities. This behaviour is not explained by the simple low probe power approximation described in the theory sections, since the probe power is just several times smaller then drive power, ($\Omega_p = 50\ \mu$W $\sim \Omega_d = 310\ \mu$W; recall that the approximation is developed for $\Omega_p \ll \Omega_d$). The Stokes component shows linear grows with power of the drive laser since $\alpha_s \sim \Omega_d^2$ as shown in Eq. (5.4).

We find significant improvement of Stokes field generation for non zero probe field. Fig. 22 shows that coherently prepared media is more favorable to generation of new field than the to usual Raman scattering process where no such coherence is prepared ($\Omega_p = 0$).

Also it is interesting to see that according to the data shown in Fig. 23, there is a region of drive power less than 160 μW where the signal of the generated Stokes field should be bigger than the transmitted signal of probe field. So there is a region of weak drive power when it is more useful to detect the generated Stokes field than the probe field.

D. Width

During the experiment, we utilize the setup described in section III.A. We have measured the difference in the resonance width of the probe and new field. Representative data is shown in Fig. 24. The new field transmission resonance width was noticeably

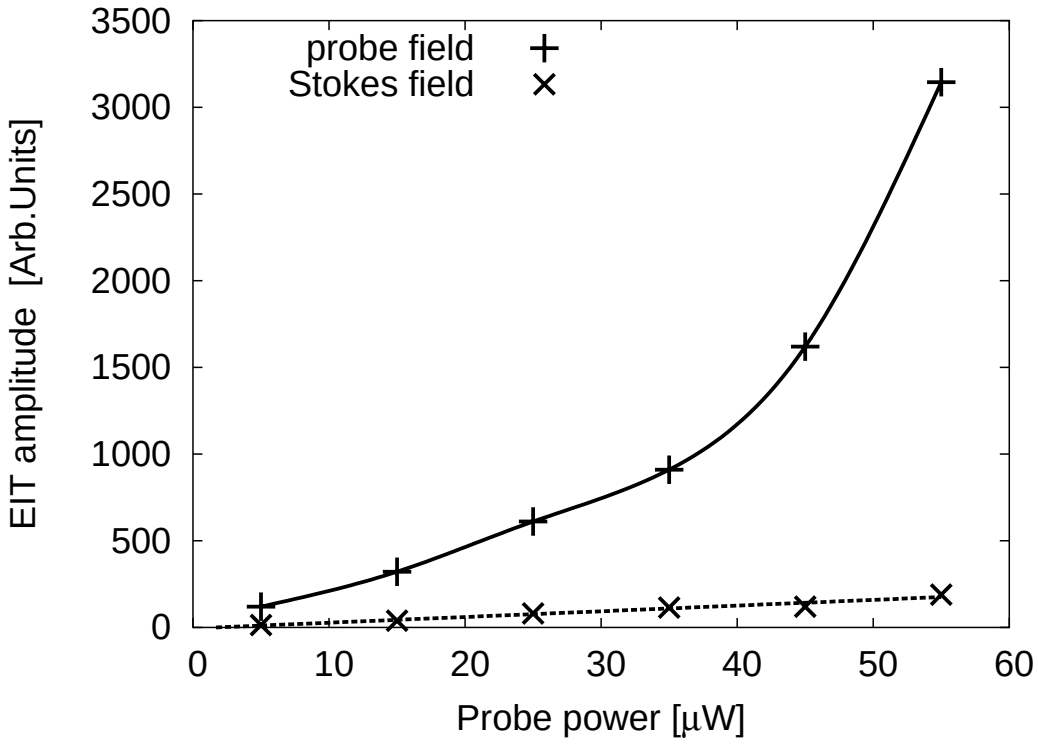

Fig. 22. Amplitude of transmitted signal for probe and generated Stokes component vs probe laser power. Temperature is 89.6^{o}C. Density $2.4 \cdot 10^{12}$ cm^{-3}. Drive power is 310 μW. 1 cm long cell with isotopically enhanced ^{87}Rb and 3 Torr N_2 buffer gas.

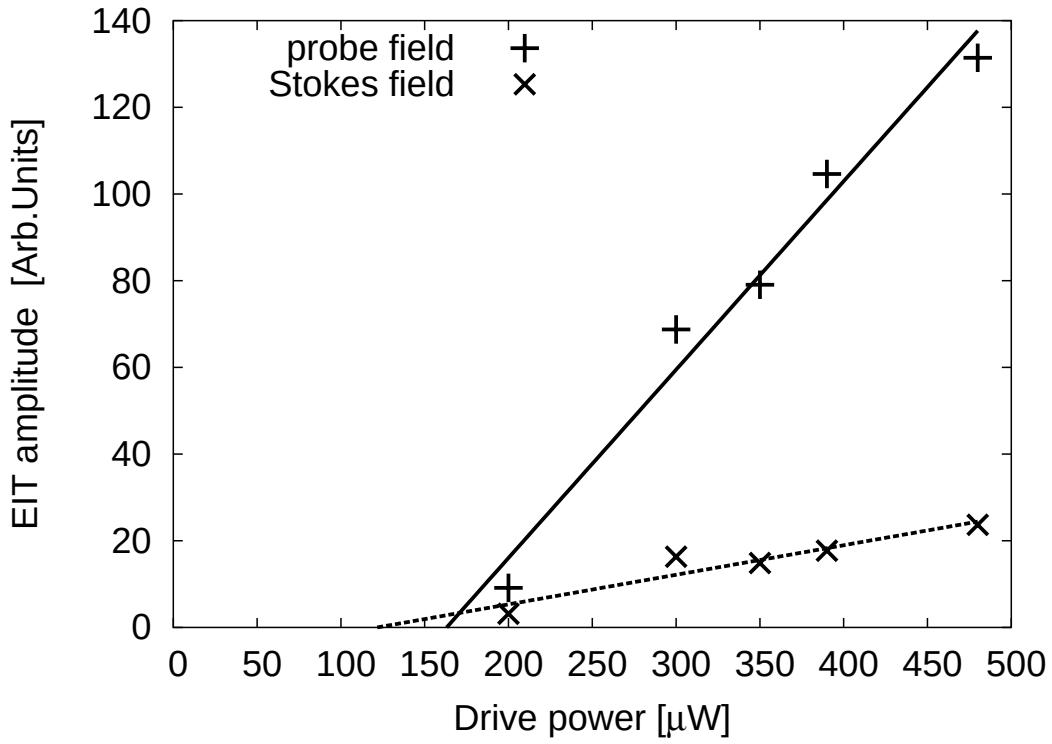

Fig. 23. Amplitude of transmitted signal for probe and generated Stokes component vs drive laser power. Temperature is 89.6^{o}C. Density $2.4 \cdot 10^{12}$ cm^{-3}. Probe power is 3 μW. 1 cm long cell with isotopically enhanced ^{87}Rb and 3 Torr N_2 buffer gas.

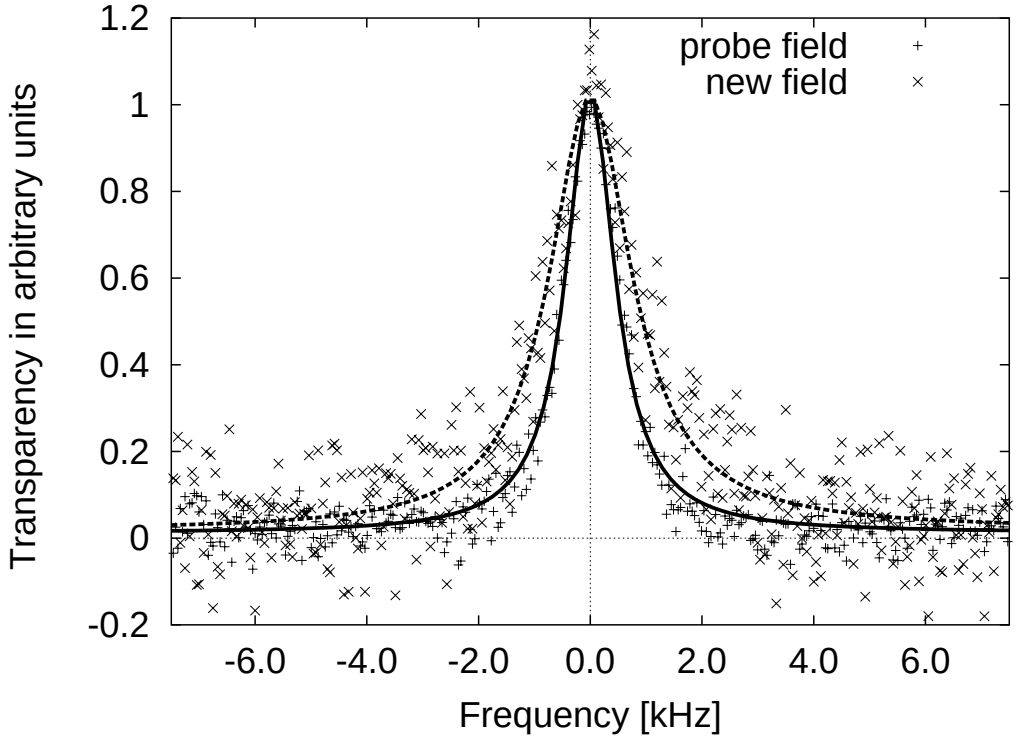

Fig. 24. Representative data showing the shape of the EIT resonance for probe and new fields. Temperature is 89.6^{o}C. Density $2.4 \cdot 10^{12}$ cm^{-3}. Probe power is 3 μW.

greater than the EIT resonance width of the probe field. Also we find linear growth of the resonance width with increasing drive field power for constant probe field. These data are shown in Fig. 25. Similarly, we observe linear increase of the resonance width with increasing probe field power when the drive laser power is held constant, as seen in Fig. 26.

Since the driving field has circular polarization, it transfers most population of the magnetic sublevels to the one with maximal value of m_F. Thus, effectively, the population ends up in the one state. A simple model to describe this physical situation is a three-level Λ-system obtained from the real one (see in Fig. 2) by neglecting the

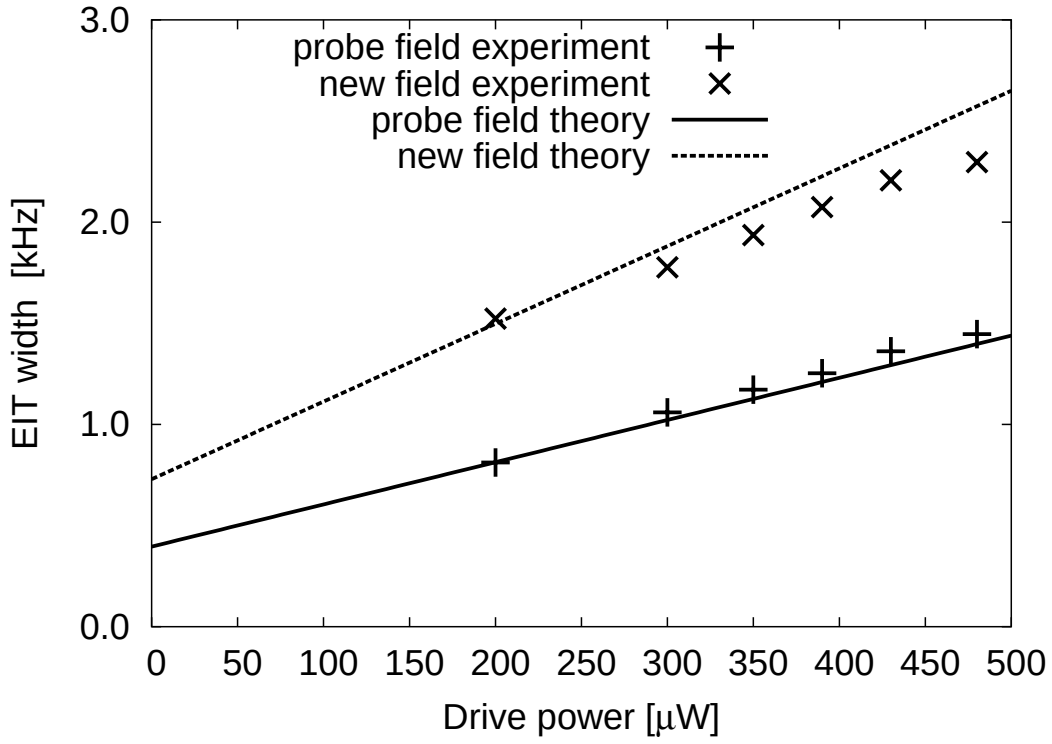

Fig. 25. Data showing dependence of EIT width versus drive power for probe and new fields. Temperature is 89.6^{o}C. Density $2.4 \cdot 10^{12}$ cm^{-3}. Beam diameter is 5 mm. Probe power is 3 μW.

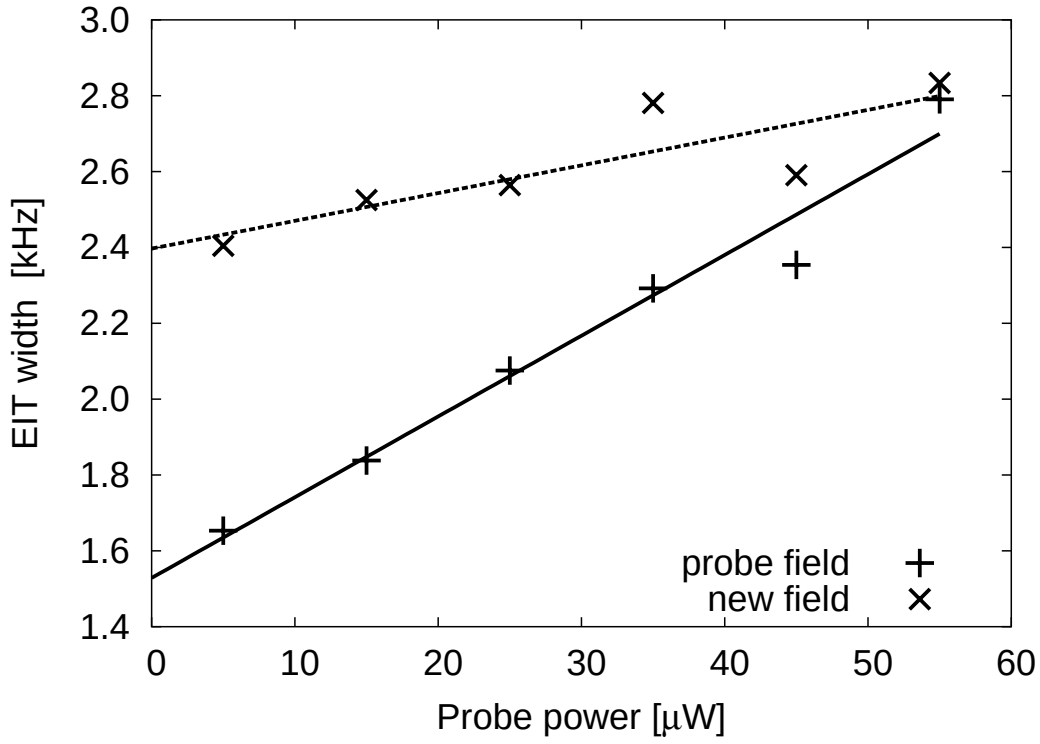

Fig. 26. Data showing dependence of EIT width versus probe power for probe and new fields. Temperature is 77.7^{o}C. Density $1.0 \cdot 10^{12}$ cm^{-3}. Beam diameter is 5 mm. Drive power is 300 μW.

magnetic sublevels that are mostly emptied by optical pumping.

We calculate the fields after propagation through a dense medium. At the frequency of two-photon resonance, the probe and drive fields acting together induce low-frequency atomic coherence ρ_{cb} that plays a crucial role in establishing EIT. Increasing the two-photon detuning decreases the coherence ρ_{cb} and increases absorption of the probe field. Thus, the probe field has a narrow window at the vicinity of two-photon resonance, with a width that depends on the rate of coherence relaxation and power broadening. On the other hand, the low-frequency coherence ρ_{cb} is also responsible for a new field generation, and the intensity of the new field has a similar resonance behavior as the transparency of the probe field. The important difference is that the new field has a large detuning from one-photon resonance and, consequently, has practically no absorption.

Our numerical calculation shows a similar dependence for the width of the resonance versus drive laser power (see Fig. 25). The simulation are in good agreement with the experimentally observed data, because the experimental range of driving field intensities are in the range for which the simplest theory developed above is valid. From the simple theory we can see that the difference in the widths of EIT window and new field generated in the cell appears from the propagation. Increasing the probe field intensity leads to a redistribution of population between levels b and c which changes the effective power broadening of the EIT window, while the change of the width of the generated new field is not that strong (see in Fig. 26).

We have shown that the transmission resonance for the Stokes component is wider than the resonance for the low power anti-Stokes (probe) field. Also we report that both resonance widths of the Stokes component resonance and the probe field transmission have linear dependences on the drive and probe laser power when the power of the second laser (probe and drive correspondingly) is kept constant.

E. Propagation of field corresponding to Stokes component

Here we consider propagation of Stokes field through the coherent medium in the case where both probe and Stokes field are present at the entrance of the cell. The setup of the experiment is described in section III.C. Due to method of generation of probe and Stokes component fields as sidebands of t he drive field, both probe and Stokes components are equal in power and have phase opposite each other (phase of probe = - phase of Stokes field).

We tune the drive to exact one-photon resonance of the $F = 2 \rightarrow F' = 2$ transition of ^{87}Rb . Then we scan the two-photon detuning by changing the frequency modulation of the EOM in the vicinity of the two-photon transition (ground level hiperfine splitting 6.835 GHz).

Typical transmission spectra of probe and Stokes fields are shown in Fig. 27 and Fig. 28 correspondingly. The slight asymmetry of the probe field EIT resonance is due to residual magnetic field inside magnetic shield.

As far as we can see there is no noticeable effect of the Stokes component on the shape of the probe field resonance. However, compared to the case when we have zero Stokes component at the entrance to the cell (see Fig. 24) we see that transmission spectrum for the Stokes component is dramatically different (see Fig. 28). Namely instead of Lorentz shape, we obtain a dispersion-like shape for the transmission signal. In the absence of EIT, the probe field is totally absorbed and the input Stokes field is totally transmitted. Thus, we observe the EIT resonance on zero background, but we observe changes in the Stokes field transmission on the 100% transmitted background. This s completely clear since the Stokes field propagates off resonance, and the four-wave mixing process is just a small correction to zero absorption coefficient.

The dispersion-like form of the Stokes field transmission spectrum can be ob-

tained from the following consideration. As we show in theory section Eq. (2.78), the absorption coefficient for the Stokes field mimics the behavior of the susceptibility of the refractive part of the probe field, which is dispersion-like (with a correction introduced by the Stokes field of order of $1/\omega_g$, which is small). We support this argument by fitting the probe field transmission spectra by a Lorentz profile

$$L(\delta) = A\frac{\delta^2}{\gamma_{EIT}^2/4 + \delta^2} \tag{5.8}$$

and Stokes field spectra profile by a dispersion-like function

$$D(\delta) = B\frac{\gamma_s\delta}{\gamma_s^2/4 + \delta^2} \tag{5.9}$$

where A and B are fitting parameter, γ_{EIT} is width of EIT resonance, γ_s is width of dispersion curve of Stokes field profile. For data shown in Figs. 27 and 28 $\gamma_{EIT} =$ 6.9 kHz and $\gamma_s = 11.4$ kHz. Such a narrower width for the EIT resonance is explained by similar arguments as in previous sections. Namely probe field propagates in an optically thick medium and thus experiences density narrowing, but the Stokes field is off resonant and is not narrowed during propagation (optically thin medium case).

F. Density dependent transmission

The dimensionless length ξ is proportional to Nz. Thus, increasing the density of atoms is esentially similar to increasing the length of the interaction medium or the cell length. So we have easy tool to study propagation of the probe and Stokes field in the cell by varying the atomic density of ^{87}Rb .

To study this we use the one-laser setup described in section III.C. Esentially we have a drive field, and equal in power probe and Stokes fields entering the cell. All have circular polarizations at the entrance. Then we vary the temperature of the

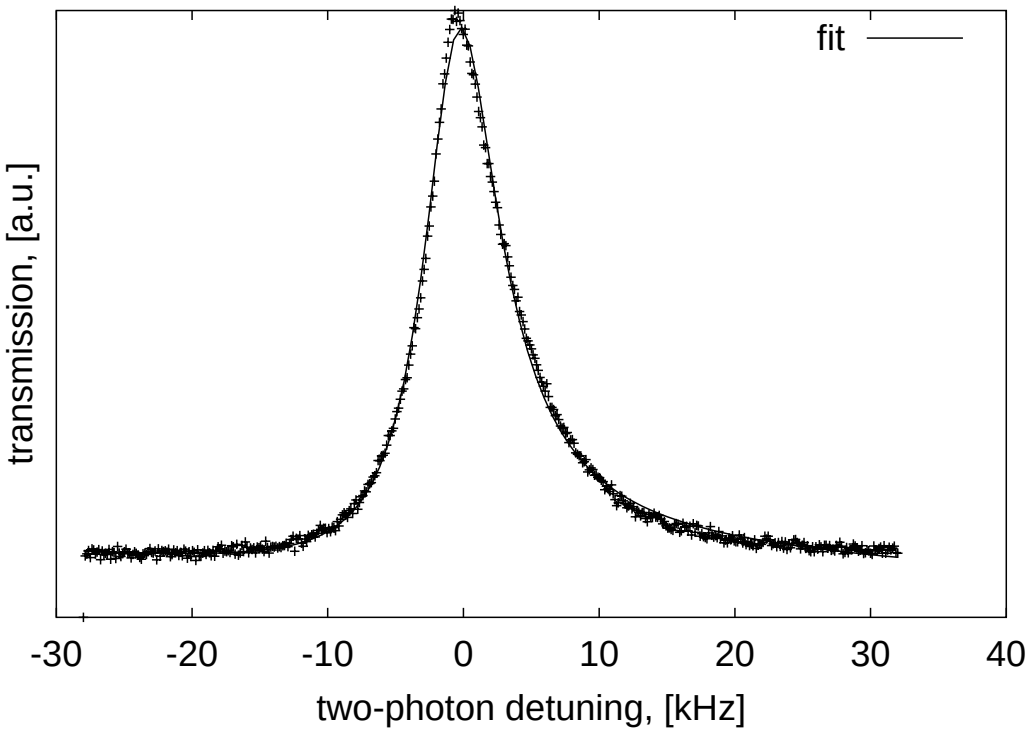

Fig. 27. Two photon resonance shape example for probe field. Cell length is 1 cm. Cell is filled with isotopically enhanced ^{87}Rb and 1 Torr of Ne as a buffer gas. Total field power is 650 μW. Temperature is 73.6^o C. Density $0.74 \cdot 10^{12}$ cm^{-3}.

cell, which changes density of ^{87}Rb atoms in the vapor. We detect the transmission signal of the probe and Stokes field and its dependence on density of atoms.

Due to four-wave mixing in the coherent medium, power is redistributed between the probe and Stokes component. The output signal depends not only on the coupling coefficients β_p, α_s, but also on the density of the atoms or dimensionless length ξ.

Typical transmission signal vs density of atoms shown in Figs. 29 and 30.

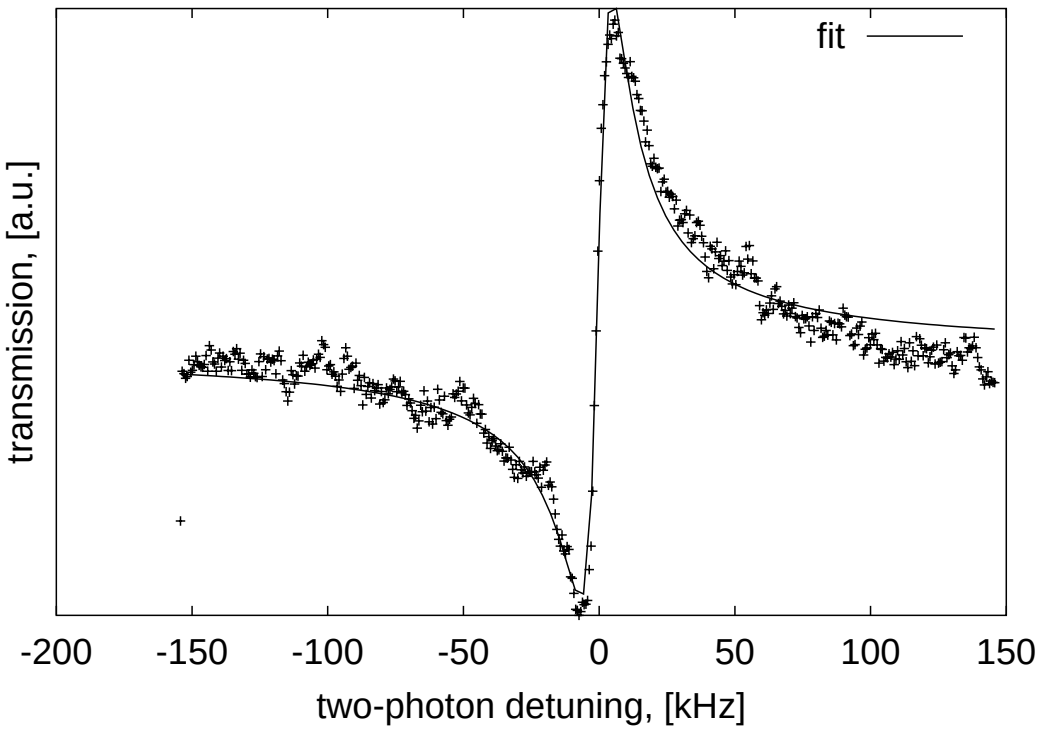

Fig. 28. Two photon resonance shape example for Stokes field. Cell length is 1 cm. Cell is filled with isotopically enhanced ^{87}Rb and 1 Torr of Ne as a buffer gas. Total field power is 650 μW. Temperature is 73.6^o C. Density $0.74 \cdot 10^{12}$ cm^{-3}.

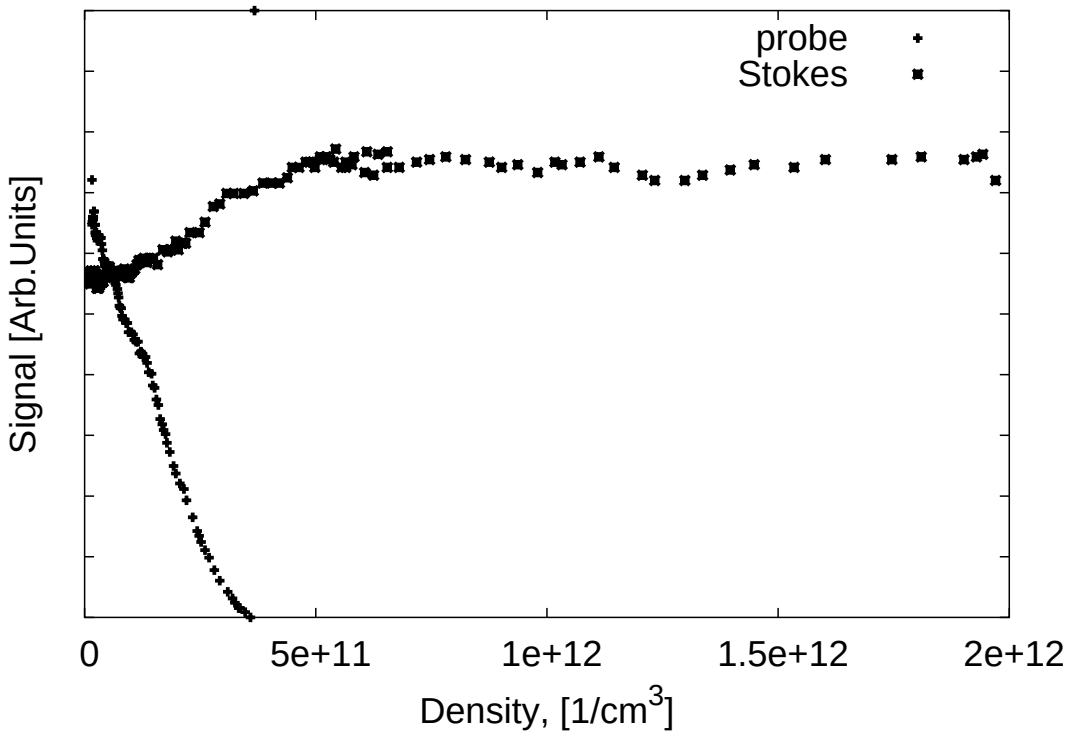

Fig. 29. Transmission signal for probe and Stokes field vs density of ^{87}Rb atoms. 5.35 cm long cell filled with .12 Torr of Kr. Total power in 1520 μW.

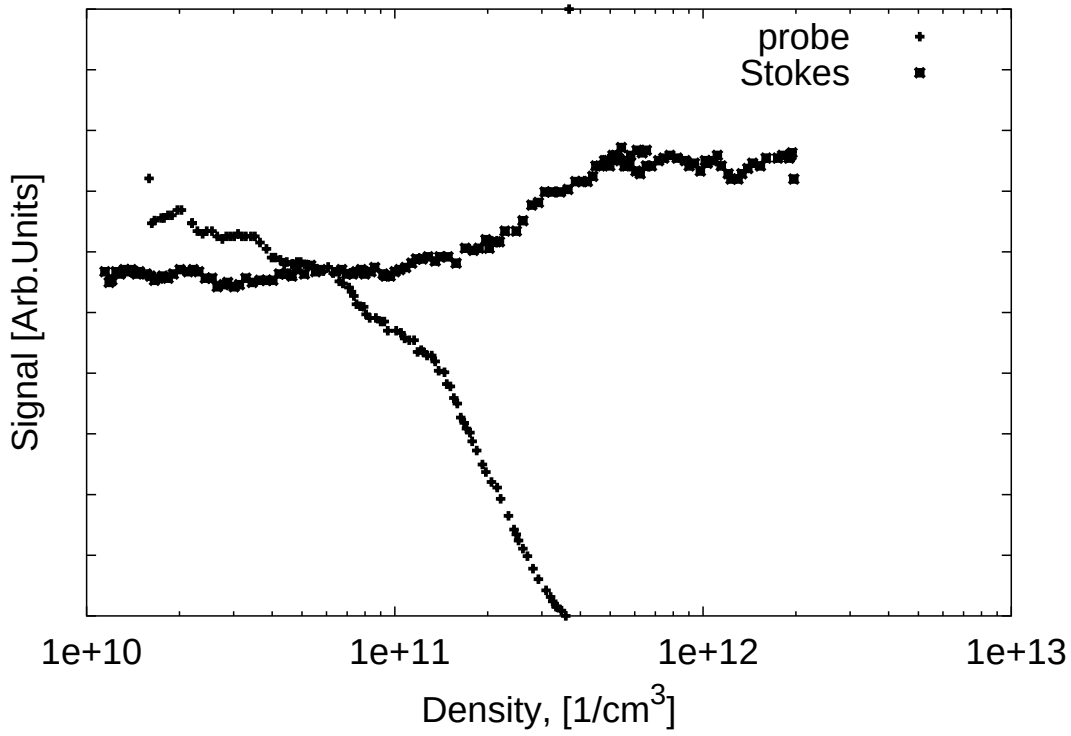

Fig. 30. Transmission signal for probe and Stokes field vs density of ^{87}Rb atoms. 5.35 cm long cell filled with .12 Torr of Kr. Total power in 1520 μW. Density shown in log scale.

CHAPTER VI

SLOW LIGHT

A. Introduction

The group velocity of light in media can be expressed as [147]

$$v_g = \frac{d\omega}{dk} = \frac{c - \omega\frac{\partial n(\omega,k)}{\partial k}}{n(\omega,k) + \omega\frac{\partial n(\omega,k)}{\partial \omega}} = \tilde{v}_g - v_s \tag{6.1}$$

where c is the speed of light in vacuum, ω is the frequency of the field, n is the index of refraction in the medium, k is the vacuum wave number, and we have defined

$$\tilde{v}_g = \frac{c}{n(\omega,k) + \omega\frac{\partial n(\omega,k)}{\partial \omega}} \tag{6.2}$$

and

$$v_s = \frac{\omega\frac{\partial n(\omega,k)}{\partial k}}{n(\omega,k) + \omega\frac{\partial n(\omega,k)}{\partial \omega}} \ . \tag{6.3}$$

Here and below we use the convention that terms with a tilde ($\tilde{}$) denote values in the moving reference frame and terms with no tilde denote values in the laboratory frame.

The first term, $\tilde{v}_g$, is due to frequency dispersion and the second term, v_s, is due to spatial dispersion. Because of spatial dispersion, the group velocity is different for atoms with different speeds v_a. This is easily seen because in the moving frame $\tilde{\omega} = \omega - kv_a$ (we take v_a positive for an atom moving in the same direction as the light propagation), from which we see that $v_g = \frac{d\omega}{dk} = \tilde{v}_g + v_a$. This is just just the Galilean transformation from the moving frame of the atoms to the laboratory frame. Thus, a mono-velocity atomic beam moving in the opposite direction from the light propagation direction slows the group velocity.

In a dense Doppler broadened medium, it is possible to obtain slower or even zero

group velocity [147, 148] for the probe field in a Λ configuration of strong drive and weak probe fields when both are red detuned but maintain the two-photon resonance condition. The following conditions on the power of the drive field must be satisfied

$$\Omega \gg \sqrt{\gamma\gamma_{cb}} \tag{6.4}$$

$$\Omega \ll k_d v_T \sqrt{\frac{\gamma_{cb}}{\gamma}} \tag{6.5}$$

where Ω is the Rabi frequency of the drive laser and k_d is its wave vector, v_T is the average thermal velocity, γ is the decay rate of the upper level, and γ_{cb} is the decay rate of coherence between the lower (ground) levels.

Equation (6.4) is just the usual condition for EIT for individual atoms. Equation (6.5) is applicable only for the case where the drive field is weak enough that EIT occurs only for a narrow spread of atomic velocities. In this case, the intensity of the drive field is not large enough to pump all atomic velocity subgroups into the dark state. This means that the optical pumping rate $|\Omega|^2\gamma/\Delta^2$, for atoms having one-photon detuning Δ, is less than the relaxation rate γ_{bc} between levels b and c. Therefore, $|\Omega|^2\gamma/\Delta^2 < \gamma_{bc}$ implies that EIT does not occur for all moving atoms and the light interacts with a quasi atomic beam. When these conditions are satisfied, one can choose a velocity sub-group of atoms with a particular average velocity (in the direction of light propagation) and narrow velocity spread $\Delta v \approx \frac{\Omega}{k_d}\sqrt{\gamma_{cb}/\gamma}$. This is accomplished by changing the one-photon detuning of the drive laser field while maintaining two-photon resonance. In this case, the center of the quasi-beam of moving atoms is determined by the simple Doppler relation

$$v_a = c\frac{\Delta}{\omega_d} \tag{6.6}$$

where ω_d is the drive laser frequency. Naturally we would expect atoms moving

with the atomic quasi-beam to increase the group velocity, and atoms moving in the opposite direction to "drag" light with them, or decrease the total group velocity.

The intuitive picture described above is quantified rigorously in Ref. [147]. In this chapter, we experimentally study these theoretical predictions by measuring the dependence of the group velocity on probe-field one-photon detuning for different experimental conditions.

A common method of increasing the dispersion in an EIT medium is to lengthen the ground-state coherence lifetime, thereby decreasing the linewidth of the EIT resonance. The coherence lifetime is often limited by the interaction time of the atoms with the lasers. Common methods for increasing this lifetime are by introducing a buffer gas to confine the atoms [61, 63, 69, 149], using wall coatings in the cell so that coherence is preserved between successive interactions of the atoms and the lasers [70, 150–154], and by cooling and trapping the atoms [155, 156].

We have found that for EIT conditions in a sample with buffer gas (with linewidth on the order of several kHz and group velocity on the order of a few tens to hundreds of meters/sec) the probe field has a slower group velocity when it is blue detuned with respect to resonance and higher group velocity for red detuning. This result is opposite to the intuitive picture described above, and to that of Kocharovskaya *et al.* in [147].

1. Setup

A schematic of the experimental setup is shown in Figs. 31 and 32. One external cavity diode laser (ECDL) is used as the source of a strong driving field and another as a weak probe. The drive and probe lasers are combined and pass through a cell containing isotopically enhanced ^{87}Rb vapor. The ^{87}Rb density is varied by changing the temperature of the cell. A three layer magnetic shield (MS) screens out the

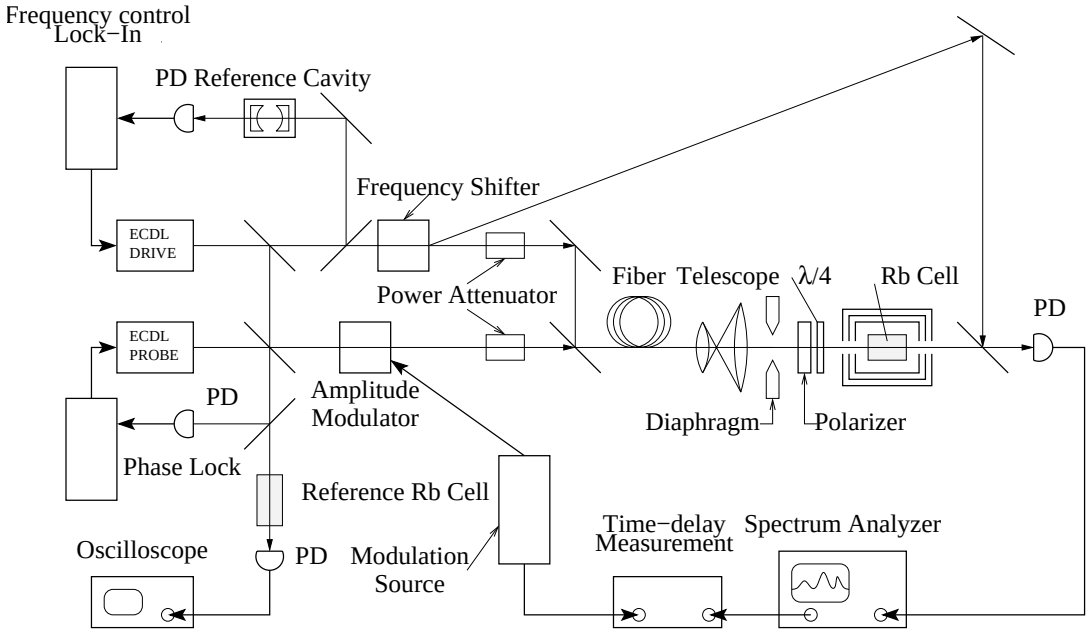

Fig. 31. Detailed group velocity measurement setup with two lasers.

laboratory magnetic field.

The lasers are phase locked to each other with a frequency offset that is tunable about the ground level hyperfine splitting of ^{87}Rb (6835 MHz). The drive laser is tuned to the $5S_{1/2}(F = 2) \rightarrow 5P_{1/2}(F' = 2)$ transition of ^{87}Rb and the probe laser is tuned to the $5S_{1/2}(F = 1) \rightarrow 5P_{1/2}(F' = 2)$ transition as shown in Fig. 33.

The configuration of drive and probe lasers shown in Fig. 33 is called a Λ configuration. In this case, the lasers optically pump all atoms in the desired velocity subgroup into a dark state superposition of the ground levels, giving rise to strong coherence between these lower levels. Scattering of the drive field on this coherence results in the generation of a fairly strong Stokes component (new field) in the medium (shown in Fig. 33). The generation of this new field near two-photon resonance of the drive and probe field is described in Ref. [64, 89, 157] and in chapter V.

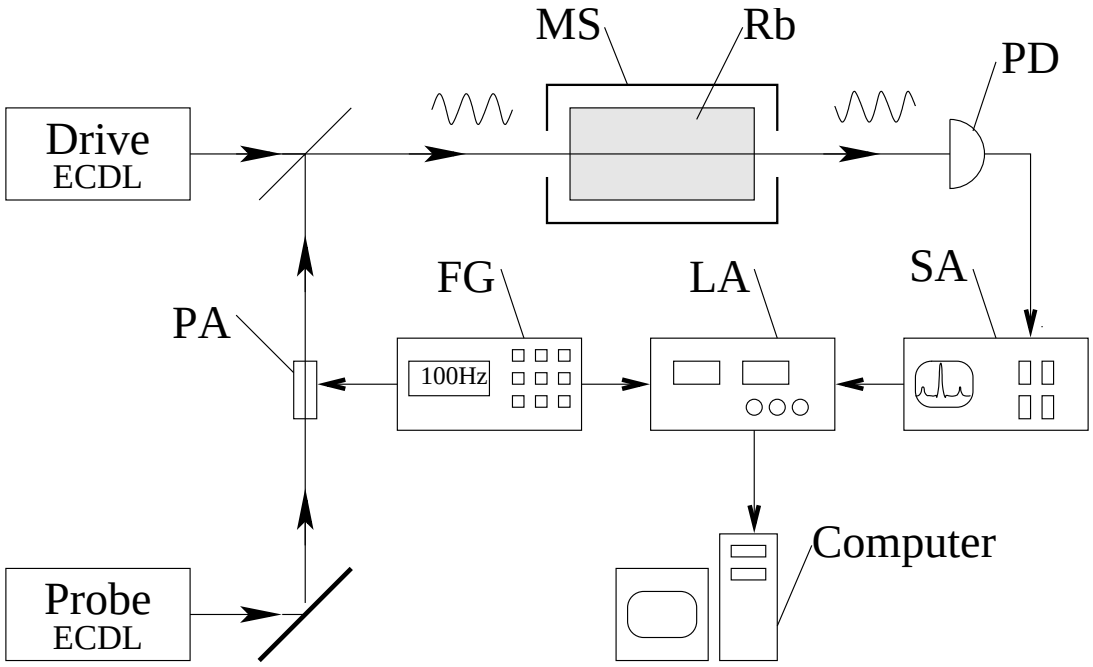

Fig. 32. Schematic of the experimental setup. MS is magnetic shield, PD is fast photo diode, PA is power attenuator, FG is frequency generator, LA is lock-in amplifier, SA is spectrum analyzer.

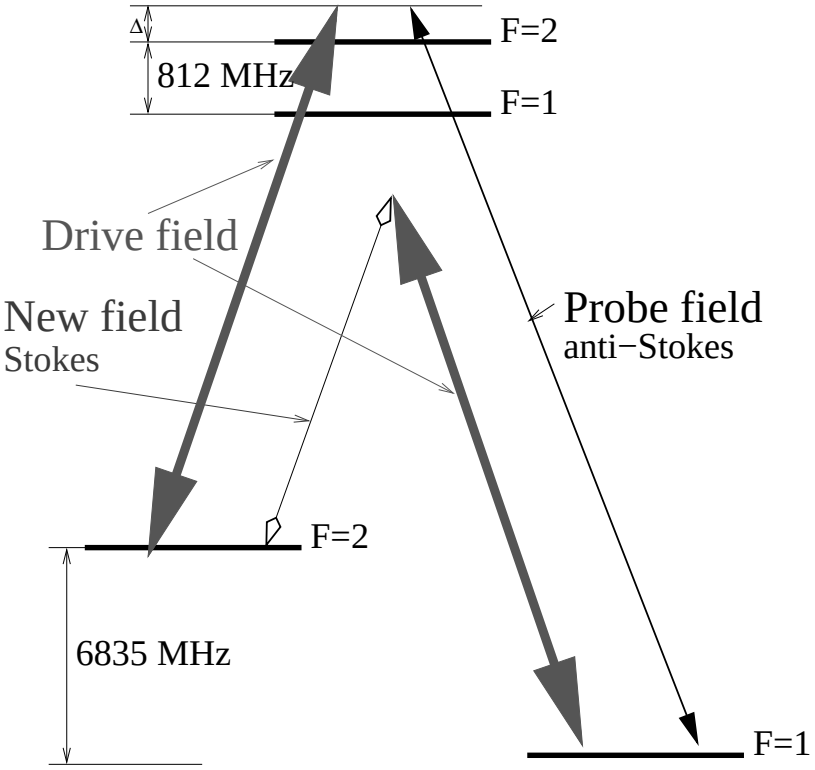

Fig. 33. Relevant levels in ^{87}Rb.

The transmitted drive and probe fields and the generated Stokes field are detected separately by heterodyne detection on a fast photo detector. This is done by splitting off part of the drive field from the main beam before entering the cell. This component is shifted up in frequency by a small amount (60 MHz), and combined with the beams exiting the cell before the photo-detector. The photo-current thus contains beat signals at various RF frequencies, separated by 60 MHz, in the vicinity of the 6835 MHz separation of the drive and probe. By separately analyzing these components with a spectrum analyzer (SA), we extract the transmitted probe and generated new fields independently. This technique is described in Ref. [89, 157].

2. Time delay and group velocity measurement procedure

We extract the group velocity in the medium by modulating the intensity of the probe field before the cell, and observing the time delay before this modulation is observed in the transmitted field. Experiments have been conducted with gaussian shaped (temporal) pulses and with sinusoidal modulation.

In Fig. 34 we see how a probe field Gaussian pulse is delayed in the ^{87}Rb medium. The two upper pictures are taken under the same conditions but with different pulse duration. The lowest picture is taken for significantly higher probe and drive field power, and demonstrate a smaller delay time or larger group velocity because of the power broadening process as described above in chapter IV section B.

We find that the delay time is independent of the probe field modulation technique as long as the bandwidth of the modulation does not exceed the transmission linewidth of the EIT resonance.

The modulation is generated by use of a frequency generator (FG) which drives an acousto-optical (AO) modulator in the probe laser. The deflected beam from the AO is blocked, so the AO serves as a programmable probe power attenuator (PA in

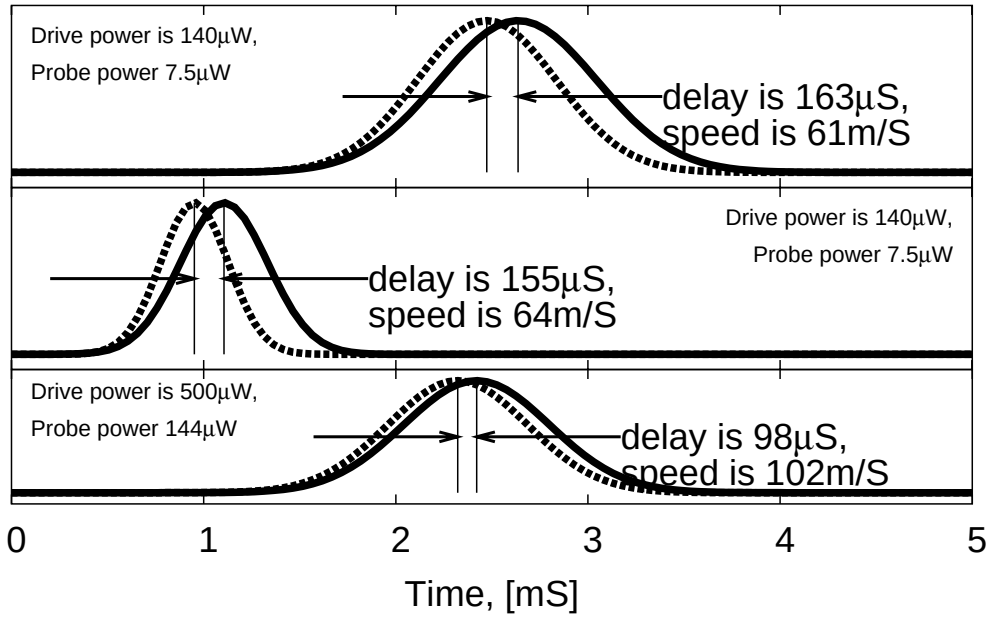

Fig. 34. Probe field Gaussian pulse delay in 1 cm long cell.

Fig. 32). We also measure the time delay of the generated new field.

With a sinusoidal modulation of the probe, lock-in detection of the transmitted probe field provides a sensitive measure of the time delay due to the medium. When using lock-in detection in this way, we obtain the time delay from the phase shift of the transmitted probe field intensity relative to the probe intensity before the cell. For a sine wave of frequency f, this phase shift is given by

$$\psi = 2\pi\tau_d f - \psi_0 \,, \tag{6.7}$$

where τ_d is the time delay introduced by the atoms and ψ_0 is a phase shift introduced by electronics. To eliminate the unknown ψ_0 we measure the phase shift for several different modulation frequencies. The phase shift increases linearly with frequency f and the slope of this line is $2\pi\tau_d$. We extract τ_d with a least squares fit. We then find the group velocity v_g by setting $v_g = L/\tau_d$ where L is the length of the cell. ($L \approx 1$ cm for our experiment.)

Another experimental technique to simplify the group velocity measurement is to replace the second laser and phase-lock circuitry with an electro-optic modulator (EOM) in the drive laser beam. This technique is described in chapter III section C. By applying a narrow tunable microwave signal to the EOM, upper and lower sidebands are generated at the microwave frequency, which we choose to match the 6.835 GHz ground state hyperfine splitting. We tune the laser to the drive transition, so that the upper sideband drives the probe transition and the lower sideband is off resonance. We choose the microwave amplitude to generate a sideband with power that is 1/10 of the drive power. A careful comparison of the two methods (two phased locked lasers versus one modulated laser) shows no difference in the group velocity measurements. We note that a similar technique is to modulate the laser current, which directly creates sidebands on the laser. This has also been successfully

employed [158].

B. Power dependent group velocity

1. Simplified theoretical group velocity dependence on resonance width

Index of refraction in case of $\chi' \ll 1$ (which is common case in gas media) is expressed as following [3]

$$n \approx 1 + \chi'/2 \tag{6.8}$$

If $\omega\frac{\partial n(\omega,k)}{\partial\omega} \gg 1$ we can disregard $n \approx 1$ in gas, then group velocity is given by simplified Eq. 6.1 as

$$v_g = \frac{d\omega}{dk} = \frac{c - \omega\frac{\partial n}{\partial k}}{\omega\frac{\partial\chi'(\omega,k)/2}{\partial\omega}} \tag{6.9}$$

Using Eq. (4.11) we can rewrite the susceptibility in the case $|\Omega|^2 \gg \gamma\gamma_{cb}$ as

$$\chi = \frac{i\kappa A(\Omega_p)}{\gamma}\left(1 - \frac{\gamma_{EIT}(\gamma_{EIT} - i\delta)}{\gamma_{EIT}^2 + \delta^2}\right) \tag{6.10}$$

so

$$\begin{aligned}\chi' &= -\frac{\kappa A}{\gamma}\frac{\gamma_{EIT}\delta}{\gamma_{EIT}^2 + \delta^2} \\ \chi'' &= \frac{\kappa A}{\gamma}\left(1 - \frac{\gamma_{EIT}^2}{\gamma_{EIT}^2 + \delta^2}\right)\end{aligned} \tag{6.11}$$

Then

$$\frac{\partial\chi'}{\partial w_p} = \frac{\partial\chi''}{\partial\delta} = -\frac{\kappa A}{\gamma}\left(\frac{\gamma_{EIT}}{\gamma_{EIT}^2 + \delta^2} - \frac{2\gamma_{EIT}\delta^2}{\gamma_{EIT}^2 + \delta^2}\right) \tag{6.12}$$

In case of $\delta = 0$ we obtain that

$$v_g \approx \frac{\gamma_{EIT}}{A} \tag{6.13}$$

where $\omega\kappa A/(2(c - \omega\frac{\partial n}{\partial k})) \to A$. It is important to note that A is proportional to the strength of resonance.

So we see that a narrowing the EIT resonance leads to smaller group velocity,

and the relation between group velocity and the width of the EIT resonance should be linear if other factors remain the same.

2. Experimental data

To illustrate Eq. 6.13 where group velocity depends linearly on resonance width, we vary the resonance width by modifying the probe intensity for several constant values of the drive laser intensity. As we know from the previous chapter, the EIT resonance width of the probe as well as the resonance width of the generated Stokes component depends linearly on probe power. So we have a tool for modifying resonance width. During group velocity measurements we keep the one-photon detuning constant and equal to zero ($\Delta = 0$) as well as two-photon detuning ($\delta = 0$).

Measured dependences of probe and Stokes fields on corresponding resonance width are shown in Fig. 35. The width is changed by varying the probe field power while the drive power is kept constant. As predicted by the simple theory above, the group velocity is proportional to the resonance width. The change of coefficient A with probe power can be neglected in the region of small probe power. However, A depends on drive power, so we see a set of lines corresponding to different drive power.

The resonance width depends linearly on drive or probe power (power broadening). Thus, the linear dependence of group velocity on laser power shown in Figs. 36 and 37 is not a surprise. Power broadening leads to growth of the resonance width which leads to the growth of group velocity.

It is interesting to note that the slope of the group velocity dependence on probe power is different from the slope of dependence on drive power (see Fig. 36) when they should be the same according to weak probe approximation. However, this approximation is not valid in our case when the probe power is just several times

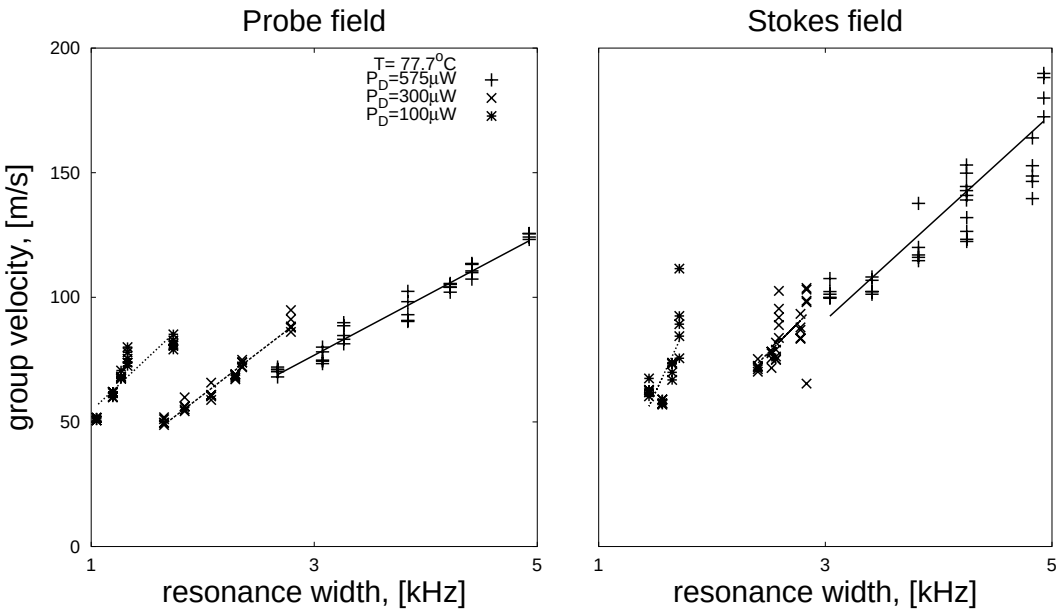

Fig. 35. Group velocity of probe and Stokes (new) field vs width of the EIT resonance for different drive power. 1 cm long cell with isotopically pure ^{87}Rb and 3 Torr of N_2 as buffer gas. Temperature of the cell is 77.7^o C Density of ^{87}Rb atoms is $1.0 \cdot 10^{12}$ cm^{-3}.

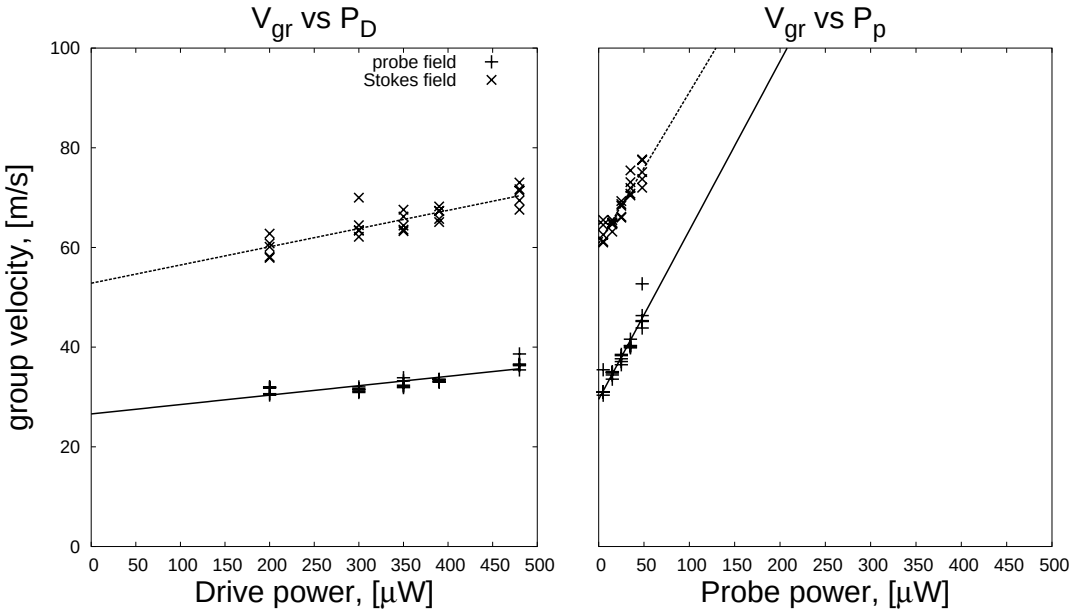

Fig. 36. Group velocity of probe and Stokes (new) field vs probe and drive power. 1 cm long cell with isotopically pure ^{87}Rb and 3 Torr of N_2 as buffer gas. Temperature of the cell is 77.7^o C Density of ^{87}Rb atoms is $1.0 \cdot 10^{12}$ cm^{-3}.

smaller than the drive power. In this case it is practically impossibile to get a simple analytical expression for the resonance width (γ_{EIT}) and amplitude (A). However as we see in Figs. 14 and 15, for large probe power the resonance amplitude (A) decreases with increasing probe power. Thus, the dependence of group velocity on probe power is steeper.

We also compare group velocity dependence for probe and generated Stokes field. We find out that the Stokes field group velocity grows linearly with probe power (see Fig. 37) since the resonance width grows linearly with power as well, due too power broadening.

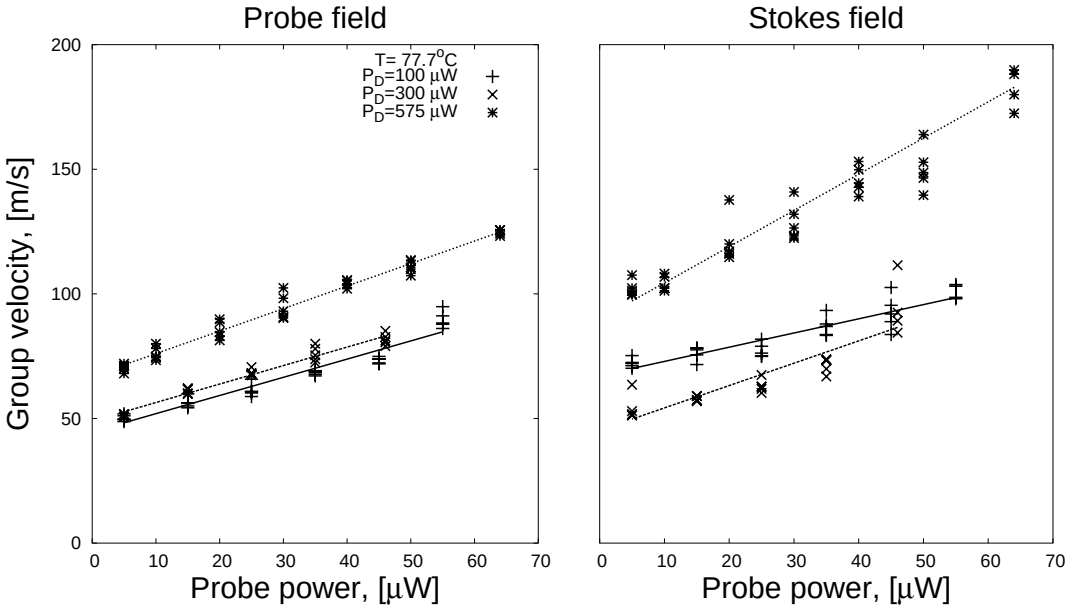

Fig. 37. Group velocity of probe and Stokes (new) field vs probe power. 1 cm long cell with isotopically pure ^{87}Rb and 3 Torr of N_2 as buffer gas. Temperature of the cell is 89.6^o C Density of ^{87}Rb atoms is $2.4 \cdot 10^{12}$ cm^{-3}.

C. Dependence on one-photon detuning (Δ)

We measure the dependence of v_g on one-photon laser detuning $\Delta = \omega_d - \omega_{22}$, where ω_d is the frequency of the drive laser and ω_{22} is the frequency of the $F = 2 \rightarrow F' = 2$ transition. During each such measurement, the frequency difference of the probe and drive lasers is kept constant and equal to the ground level splitting (6.835 GHz). The drive laser power is $300\mu W$, and probe power is $3\mu W$. These measurements may then be repeated for different ^{87}Rb densities (different temperatures of the cell).

We first consider the case where no buffer gas is used, and the ground-state coherence lifetime is limited by the free-flight transit time of the thermal rubidium atoms through the laser beam. In our experiment, the EIT transmission linewidth is 30 kHz and the resulting group velocity on the order of 10 km/s. Figure 38 shows the dependence of the group velocity as a function of the drive laser frequency in the vicinity of the drive resonance. The group velocity is too large to observe the spatial dispersion effect described in the introduction. Another way to see this is to note that the group velocity is much higher than the mean thermal speed of the atoms. In Fig. 38 the drive detuning spans the full range of the upper-state hyperfine splitting, and the small feature on the left of the spectrum is the result of generating EIT on the upper $F' = 1$ level (see Fig. 33).

Next we narrow the transmission linewidth with a buffer gas. This increases the dispersion considerably, resulting in reduced group velocity. Figure 39 shows the group velocity as a function of drive laser detuning for similar conditions as Fig. 38 but with the addition of 3 torr of N_2 buffer gas. The EIT transmission linewidth is only a few kHz and we see that the group velocity has fallen to below 100 m/s. We also see that increasing the laser beam diameter increases the dispersion and reduces the group velocity as expected.

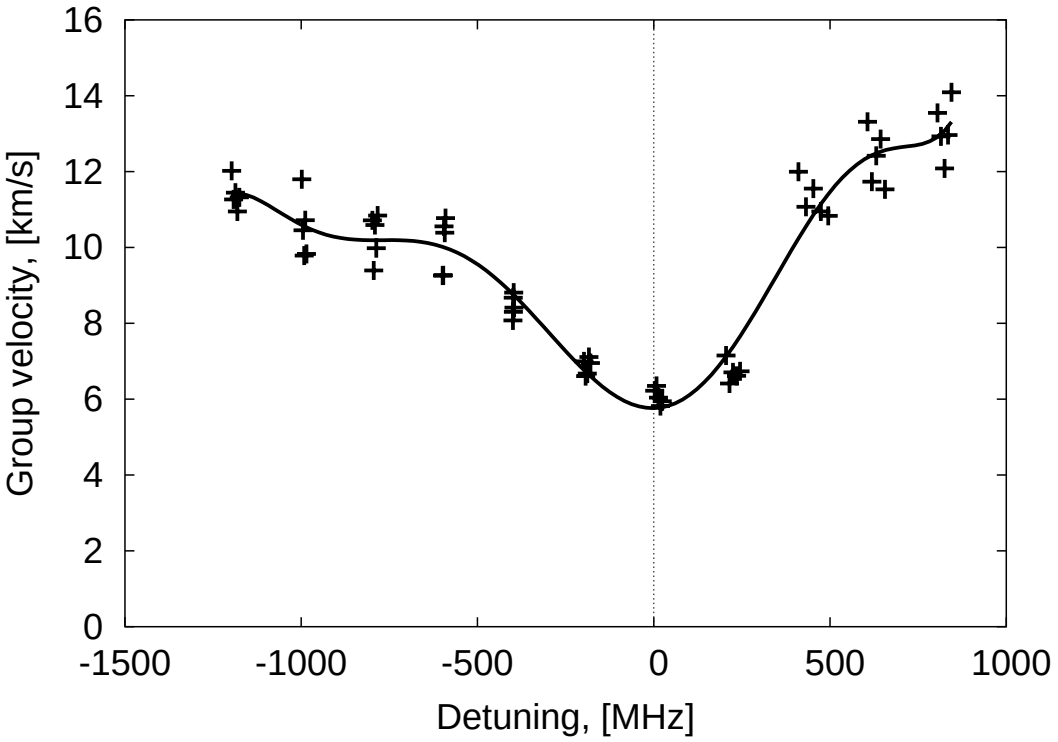

Fig. 38. Group velocity vs detuning of ^{87}Rb atoms for probe field in cell with no buffer gas. Cell length $L = 47.5$ mm and the density is 3.6×10^{11} cm^{-3}. Drive power input to the cell is $1310\mu W$, and transmitted drive power is $741\mu W$. Data points are shown by a +. The solid curve is a seventh-order polynomial fit to the data points and is shown only as a guide for the eye.

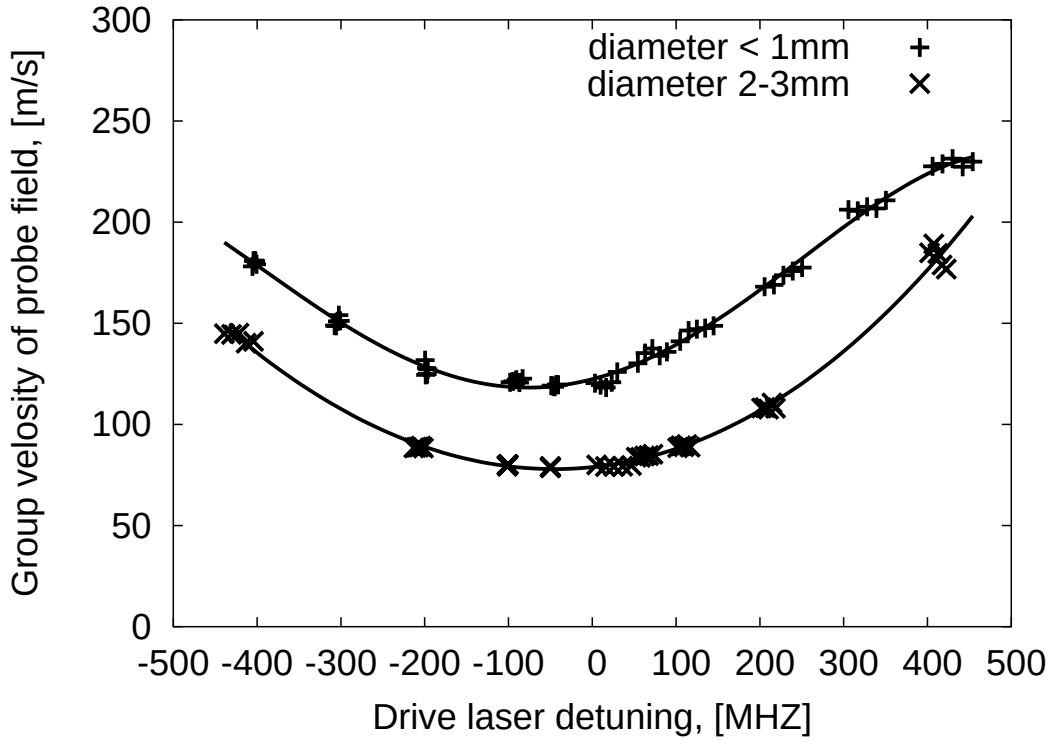

Fig. 39. Probe field group velocity vs drive laser one-photon detuning in a cell with 3 torr of N_2 buffer gas. Cell length $L = 10$ mm and the density is 8.7×10^{11} cm^{-3}. The two curves are for beam diameters of 1 and 3 mm respectively.

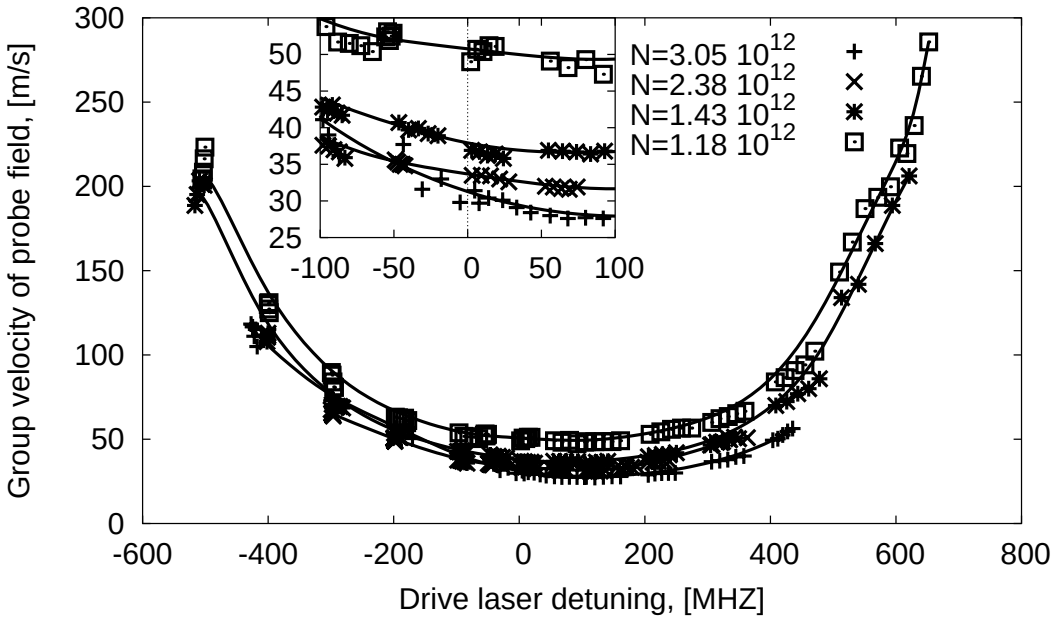

Fig. 40. Probe field group velocity vs drive laser one-photon detuning, for the same cell as in Fig. 39. Drive power is $300\mu W$ and probe power $3\mu W$. Curves are shown for different atomic density, measured in cm^{-3}. Inset: blow-up of the data in the vicinity of resonance, showing an increase to the red and decrease to the blue of resonance.

Figure 40 shows how the group velocity depends on drive laser detuning for increasing atomic density. We observe a lowering of the group velocity for higher density, but in no case do we observe a lowering of the group velocity as the drive laser is detuned red of resonance, which we would expect based on the prediction of dragging slow light by atoms moving opposite to the laser propagation direction [147]. On the contrary, we see the group velocity increase for negative drive laser detuning, and a minimum group for one-photon detuning about 100 MHz blue of one-photon resonance (see Fig. 40).

The explanation of this effect is still not clear, but it is plausible that this counter-

intuitive behavior is caused by velocity changing collisions in the presence of the buffer gas. We note that when the beam diameter decreases, the group velocity dependence versus one-photon detuning becomes more shifted to the side of negative detuning (see Fig. 39). In other words, the behavior becomes less counter-intuitive. We explain this by noting that for a very narrow beam, fewer velocity changing collisions take place before the atom leaves the laser beam. In any case, it is clear that the discussion of Ref. [147] about a quasi mono-velocity beam is not applicable in the case with a buffer gas, since all velocity groups are mixed by velocity changing collisions.

When the density of ^{87}Rb atoms is increased ($\approx 10^{12}$ cm^{-3}) highly nonlinear interaction of the drive and probe fields leads to very efficient generation of a Stokes component, or new field [64, 89]. We can measure the intensity of the generated field as a function of two-photon detuning and find the width to be greater than the transmission width of the EIT resonance of the probe field. (Under the conditions in our experiment it is roughly a factor of two wider [157].) Correspondingly, we also measure the time delay between modulation of the probe field before the cell and the resulting modulation of the new field after the cell. For the rubidium cell with buffer gas, this delay time is smaller than for the probe field, meaning that the group velocity of the new field (v_n) is greater than the group velocity of the probe field (v_p). This is no great surprise since the new field is propagating far from one-photon resonance.

As discussed above, as the rubidium density is increased the probe field group velocity decreases. Similar behavior occurs for the generated new field for low density. However, for large atomic density the group velocity for the new field starts to increase with density. These results are shown in Fig. 41. This dependence is connected with a propagation effect. The effective generation of new field occurs in the part of the cell where the group velocity is small. As the light propagates through the cell, the

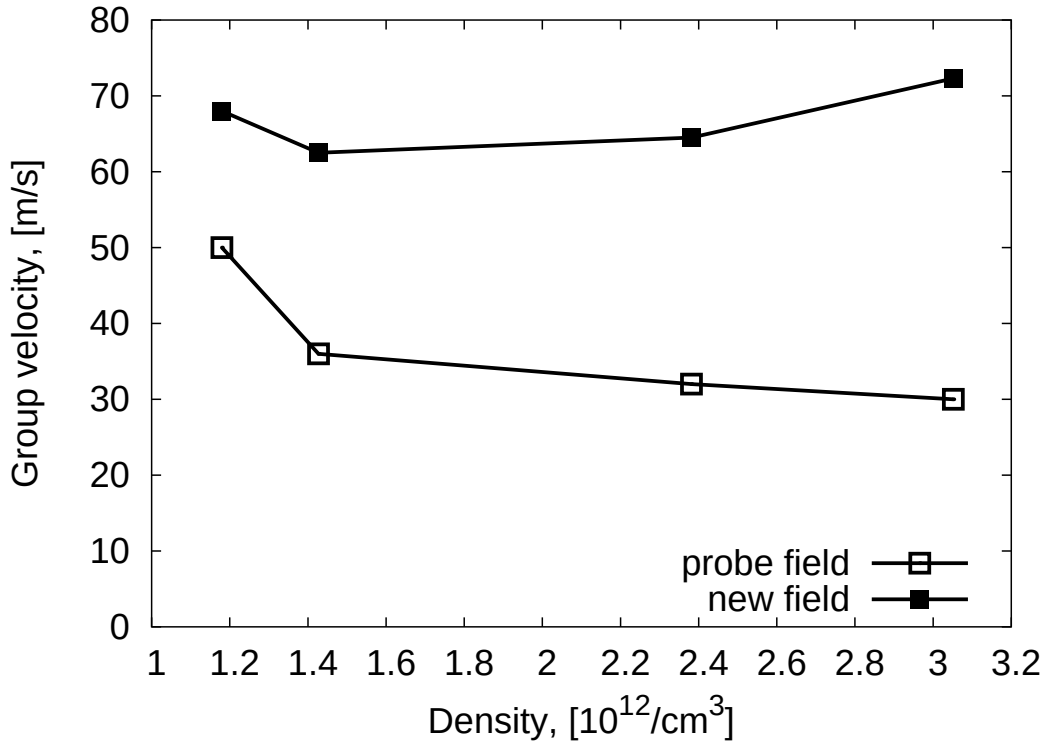

Fig. 41. Group velocity vs density of ^{87}Rb atoms for probe and new fields, for the same cell as in Fig. 39. Drive power is $300\mu W$, and probe power is $3\mu W$.

drive field intensity decreases until the new field is decoupled from the probe. After this point, the new field propagates at nearly the vacuum speed of light. Thus the observed average speed of new field increases with atomic density.

We can also measure the new-field group velocity as a function of drive laser detuning. The results are shown in Fig. 42. We find that the the group velocity is smaller for negative one-photon detuning than for positive detuning in vicinity of resonance. This behavior follows the intuitive predictions of Ref. [147].

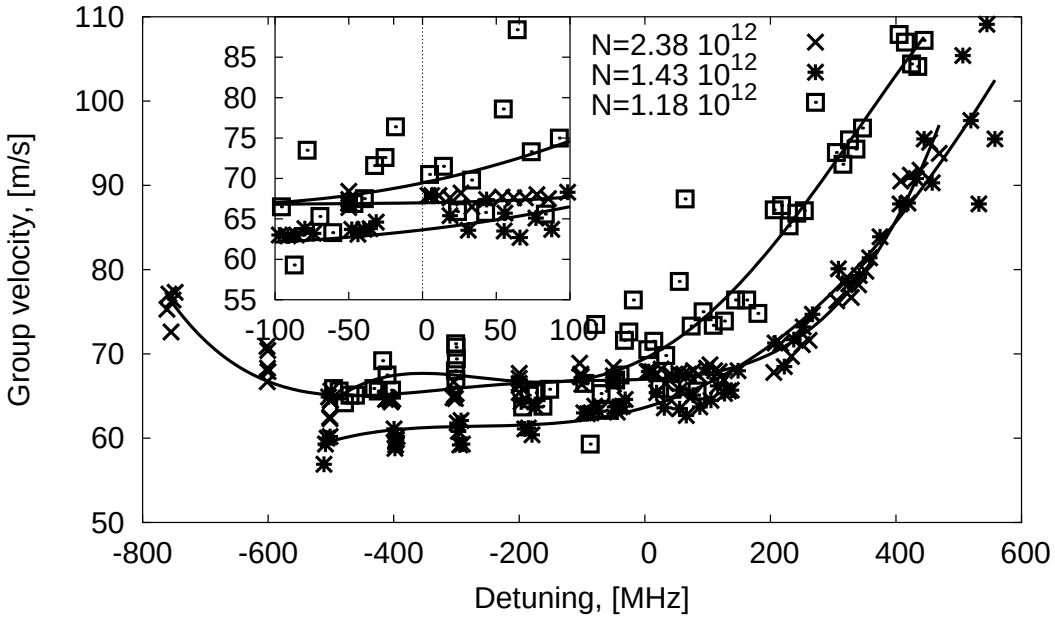

Fig. 42. New field group velocity vs drive laser one-photon detuning, for the same cell as in Fig. 39. Drive power is $300\mu W$ and probe power $3\mu W$. Curves are shown for different atomic density, measured in cm^{-3}. Inset: blow-up of the data in the vicinity of resonance, showing an increase to the red and decrease to the blue of resonance.

D. Summary

We observe a counter-intuitive dependence of the probe field group velocity versus drive field one-photon detuning for different densities (temperatures) of ^{87}Rb (see Fig. 40). The group velocity decreases slightly for blue-detuned drive fields and increases slightly for red-detuned fields. We conclude that the the predictions of Ref. [147] cannot be applied to the case where the EIT linewidth is reduced with a buffer gas, since all velocities are constantly mixing via velocity changing collisions. Unfortunately, without a buffer gas we cannot achieve narrow enough EIT resonances to reach the amount of dispersion needed to get group velocities low enough to observe the effect of dragging the light by atoms.

We find that the group velocity is higher for the generated Stokes field, and that the behavior as a function of detuning is opposite that of the probe field.

CHAPTER VII

ABSORPTION RESONANCES

A. Introduction

The addition of a buffer gas (inert atoms, N_2, CO_2, CH_4, etc.) to the atomic vapor is a common method for obtaining narrow EIT resonances. Because of the extremely low spin-exchange cross-section, the collisions between rubidium and buffer gas atoms or molecules do not destroy the quantum coherence of the internal states of the atoms, but effectively prolong the time they stay inside the laser beam(s). The processes of decoherence and redistribution of atomic population have been extensively studied in optical pumping experiments [62, 159, 160]. Substantial narrowing of the dark resonance linewidth is reported in [61, 63, 69, 149].

In this chapter we experimentally demonstrate that, in the presence of buffer gas, the transmission peaks corresponding to EIT can be transformed into enhanced absorption peaks for proper laser detuning. We observe this effect in a two-field configuration, where strong and weak laser fields form a Λ scheme on two ground-state hyperfine sublevels (Fig. 43). It is important to emphasize that in this case the atoms are prepared in a coherent superposition of levels (hyperfine states), and that no absorption is observed (that is, EIT is preserved) in the absence of buffer gas. A related effect has been reported by Affolderbach *et al.* [161]. In that work the enhanced absorption is observed in a bichromatic standing wave as a result of atomic motion. Because of large Doppler shifts, moving atoms effectively interact with a double-Λ level configuration, which may result in both suppression or enhancement of absorption, depending on the relative phases of the fields. This theory, however, cannot be applied to the present experimental data, since our experiments are carried

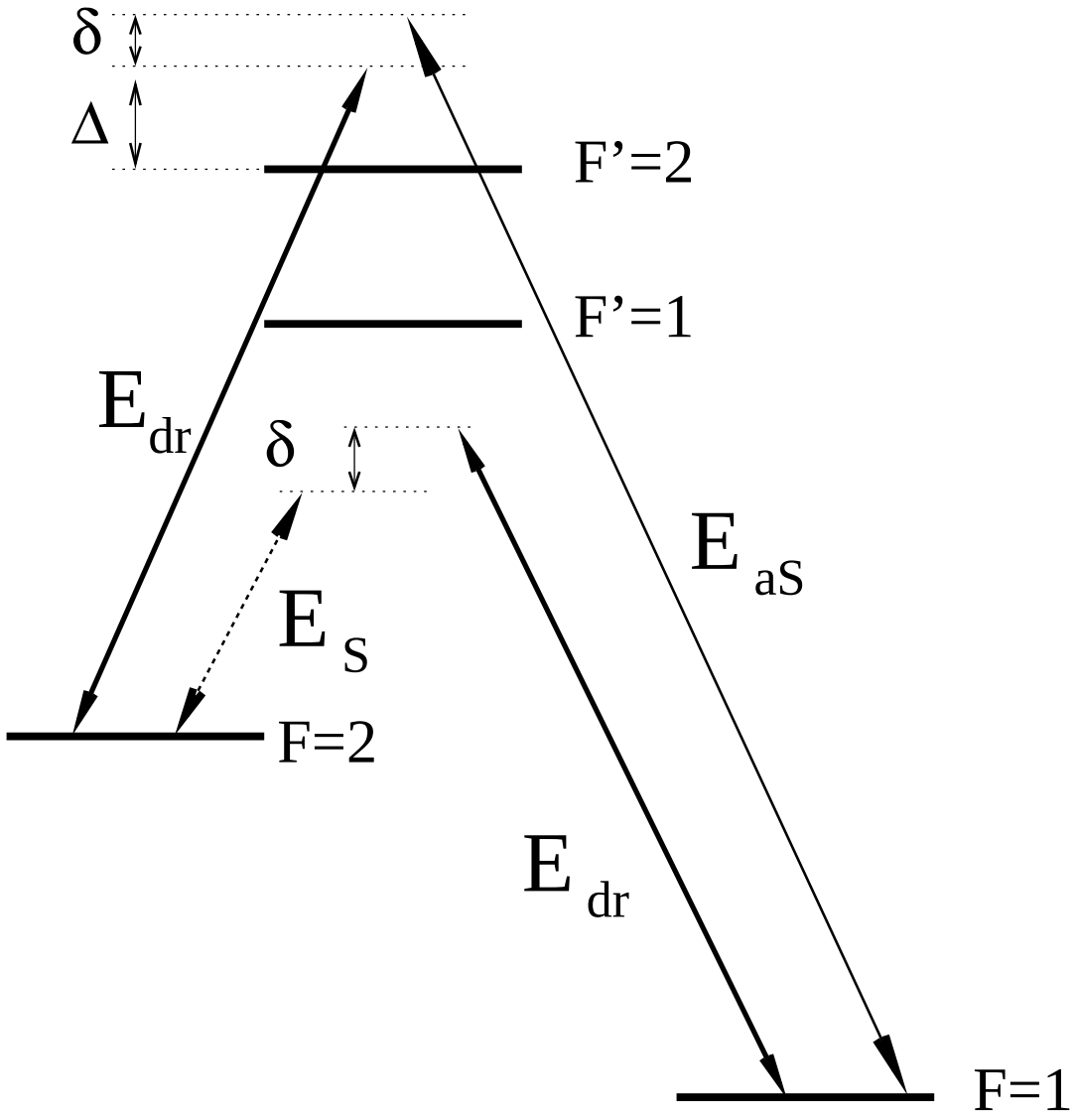

Fig. 43. Three-level interaction scheme of three laser fields with ^{87}Rb atoms: the long-lived coherence is created on hyperfine ground-state sublevels with strong driving field E_d and weak probe (anti-Stokes) field E_p; the probe and Stokes field E_s are generated by electro-optic modulation. Δ is the one-photon detuning of the drive laser from atomic resonance, and δ is the two-photon detuning due to frequency mismatch.

out with running waves.

The effect reported here is also different from Electromagnetically Induced Absorption (EIA) [66, 107, 108, 162–165], or the closely related enhanced absorption Hanle effect [166–170]. In those cases, a narrow peak is observed in the absorption of the probe field interacting with a quasi-degenerate two-level system. However, it is a general requirement in both of those cases that the degeneracy of the ground state must be lower than that of the excited state, i.e. $F < F'$. When that requirement is met, the dark state does not exist and narrow EIA resonances are due to the spontaneous coherence transfer from the excited states of the atoms [107, 164, 171]. In addition, the experimental arrangements for traditional EIA experiments involve laser fields resonant with the corresponding atomic transitions, whereas the narrow absorption resonances, discussed in this paper appear for far-detuned laser fields.

B. Experimental setup

We utilize the setup described in the section III.C. A schematic of the experimental setup is shown in Fig. 44. An external cavity diode laser is tuned to the $5S_{1/2} \rightarrow 5P_{1/2}$ (D_1) line of ^{87}Rb . The probe field (and and additional Stokes field) are produced by an electro-optic modulator (EOM) driven by a narrow stable microwave generator tuned to the 6.835 GHz ground-state hyperfine frequency. The microwave frequency is tunable about this resonance, which allows for tuning of the probe field. The probe and Stokes field have equal intensities of approximately 10% of that of the drive field. After the EOM all fields pass through a single-mode optical fiber to create a clean spatial mode with a Gaussian intensity distribution and to increase the diameter of the output beam to 7 mm. The fields are circularly polarized with a quarter-wave plate placed after the fiber.

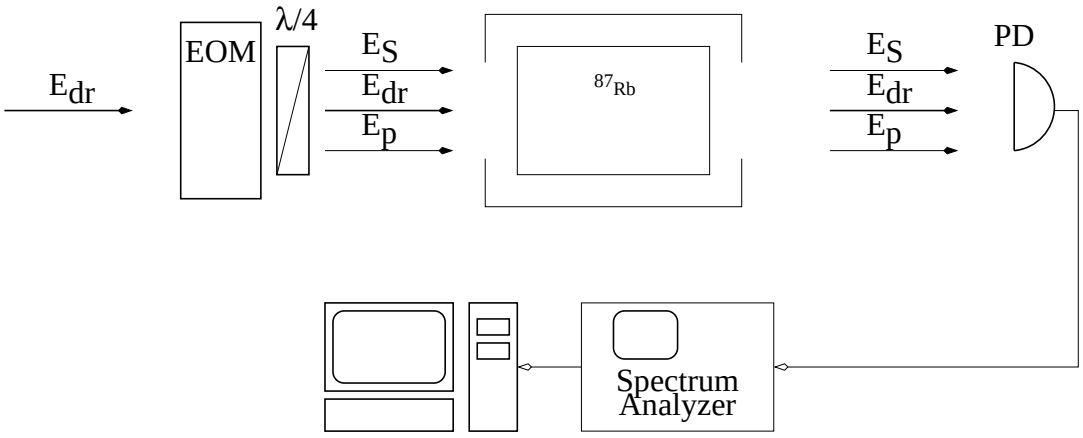

Fig. 44. Schematic of the experimental setup.

In this experiment we use several glass cells filled with isotopically enhanced ^{87}Rb and various pressures and types (Ne, Kr) of buffer gas. The cell is placed inside a 3-layer magnetic shield to screen the laboratory magnetic field from the system. The cell is heated to 60^o C to increase density of the ^{87}Rb vapor to approximately 2.5×10^{11} cm^{-3}. After traversing the cell all three fields are mixed on a fast photodiode with an additional field shifted by 60 MHz with respect to the driving field. The resulting photo-current is measured with a spectrum analyzer to separate the transmission signals of the probe and Stokes components (see Fig. 44).

C. Enhanced absorption due to buffer gas in hyperfine Λ scheme

In a Λ configuration, the drive field couples the ground-state $5S_{1/2}F = 2$ level to the excited $5P_{1/2}F' = 2$ level. The probe field couples the ground-state $5S_{1/2}F = 1$ level to the same excited state. This is shown in Fig. 43a. When both of these fields are on resonance, the atoms are optically pumped into a dark state under the combined action of the strong drive and weak probe, and an EIT resonance is observed in

the transmission of the probe field. This is shown in the bottom curves in Fig. 45. Simultaneously, a second Λ scheme is formed with the drive field and the Stokes field that is also generated by the EOM. However this second Λ system is far detuned from both excited levels, so its influence on the ground-state coherence is negligible.

Figure 45 shows that for zero one-photon detuning all EIT resonances are symmetric, which is in agreement with theoretical predictions [67, 172] and our numerical simulations. The main difference between the cells with different amount of buffer gas is the width of the EIT peaks.

The shape of the transmission resonances changes, however, as we tune the lasers from one-photon resonance, and the character of this change depends strongly on the presence of the buffer gas in the atomic cell. If there is no buffer gas present, the EIT peak stays symmetric for all values of Δ. However, the behavior is very different in cells with buffer gas. As the one-photon detuning increases, the EIT resonance becomes asymmetric, and then gradually transforms into a narrow absorption resonance.

Let us emphasize here some of the important properties of these resonances, looking for example, at the cell with 30 Torr of Ne (Fig. 45). First note that the amplitude of the enhanced absorption peak, observed for large detuning ($\Delta = 1$ – 2 GHz) is comparable to, and sometimes larger than, that of the EIT peak at $\Delta = 0$, and its width is narrower. Second, the range of laser detuning for which the absorption resonance is observed (> 3 GHz) is much wider than the linewidth of the one-photon absorption determined by the Doppler width. Thus, the enhanced absorption peaks appears on top of 100% transmission of the probe field.

It is important to note here that the asymmetry in the EIT resonances for nonzero one-photon detuning of the laser fields has been observed by Knappe *et al.* [135]; however, the modification of the resonance lineshape is significantly weaker than that

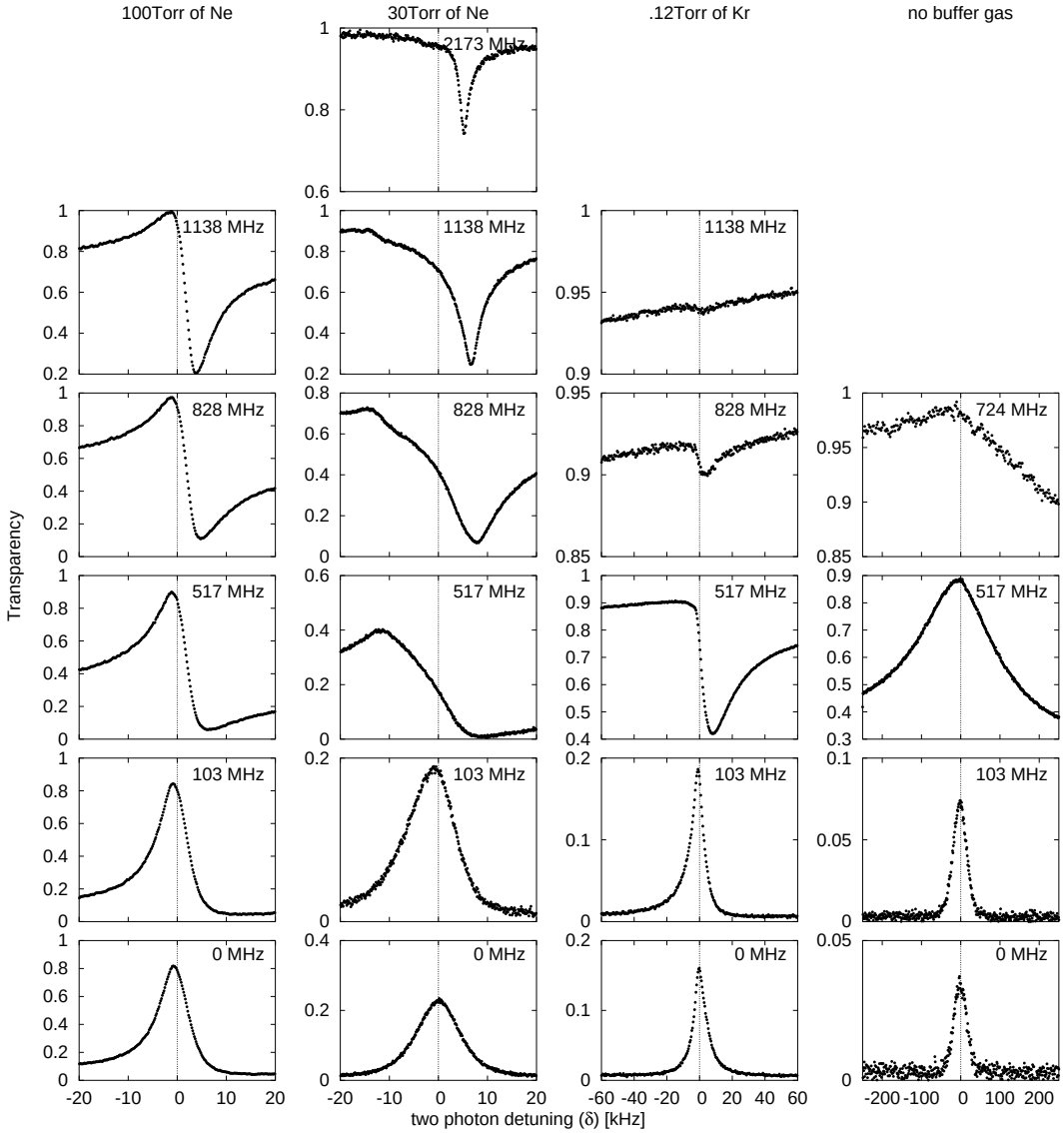

Fig. 45. Transmission of the probe field as a function of two-photon detuning δ for various one-photon detunings Δ (shown on the upper left corner for each graph). These data are recorded in the presence of 30 Torr of Ne (left column), 0.12 Torr of Kr (center column), and no buffer gas (right column). The vertical scale is arbitrary but the same for all graphs. The auto-scaled data are also shown for some graphs to show the resonance features not visible at large scale. The asymmetry of the resonance curves for $\Delta = 828$ and 1138 MHz in the cell with 0.12 Torr Kr, and for $\Delta = 517$ and 740 MHz in the vacuum cell are due to the slope of the one-photon absorption contour.

reported here. They also suggested an empirical expression for the resonance lineshape, which was later derived theoretically by Taichenachev *et al.* [134] in the limit of weak interaction fields (perturbation approach) (the derivation of this expression for the case of strong laser field is given in the next Section):

$$f(\delta) = \gamma_{EIT} \frac{A\gamma_{EIT} + B(\delta - \delta_0)}{\gamma_{EIT}^2 + (\delta - \delta_0)^2} + C \tag{7.1}$$

Here δ is the two-photon detuning, γ_{EIT} is the effective width of the coherent resonance, A, B, C are fitting parameters which functions of the one-photon detuning Δ. We introduce a shift of the resonance position from the resonant conditions δ_0 to reproduce the experimental data. One can see that this expression consists of symmetric and anti-symmetric in δ Lorentzian functions with the amplitudes A, and B respectively. Parameter C reflects the absorption of the electromagnetic field, which is determined by incoherent processes.

It is convenient to write the coefficients A and B in following form:

$$A = D\cos(\phi), B = D\sin(\phi), \tag{7.2}$$

so that the Eq. (7.1) can be written as:

$$f(\delta) = \Re\left\{ D(\Delta) e^{i\phi(\Delta)} \frac{\gamma_{EIT}}{\gamma_{EIT} + i(\delta - \delta_0)} \right\} + C. \tag{7.3}$$

In this case, parameter D characterizes the amplitude of the resonance, and the angle ϕ expresses the ratio between the symmetric and anti-symmetric components in Eq. (7.1). For example, $\phi = 0$ represents a symmetric peak of enhanced transmission, $\phi = \pi$ corresponds to a symmetric peak of enhanced absorption, and $\phi = \pm\pi/2$ corresponds to a pure dispersion-like lineshape.

These parameters are shown as functions of one-photon detuning in different cells in Figs. 46 and 47. We note that no deviation from the Lorentzian form is

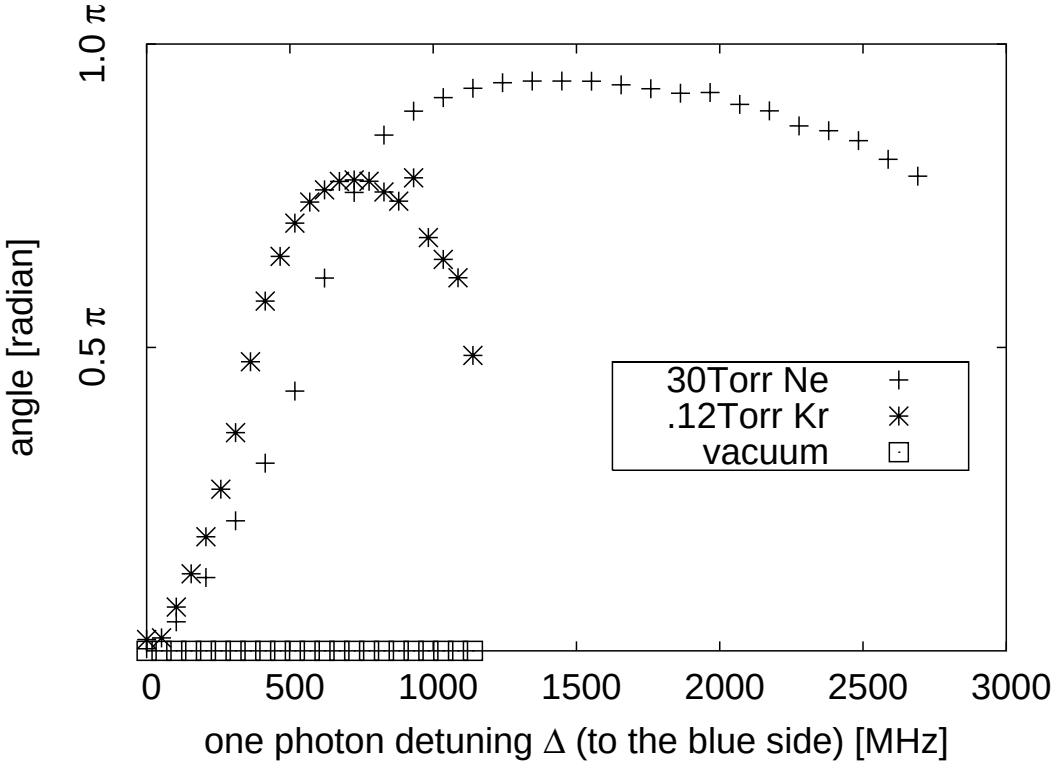

Fig. 46. Angle ϕ of two photon resonance for probe field for ^{87}Rb cells with different amount of a buffer gas.

observed for the EIT resonance in a vacuum cell ($\phi = 0$ for all detunings). However, buffered cells show the change from a symmetric transmission resonance (for $\Delta = 0$) to almost symmetric absorption resonance for $\Delta \approx 700$ MHz for 0.12 Torr buffer gas pressure and $\Delta \approx 1.4$ GHz for 30 Torr buffer gas pressure. Note that the highest "angle" is achieved in the cell with largest amount of the buffer gas. After reaching its maximum, the angle starts to decline again, although we never observe the recovery of the symmetric EIT peak for larger detunings.

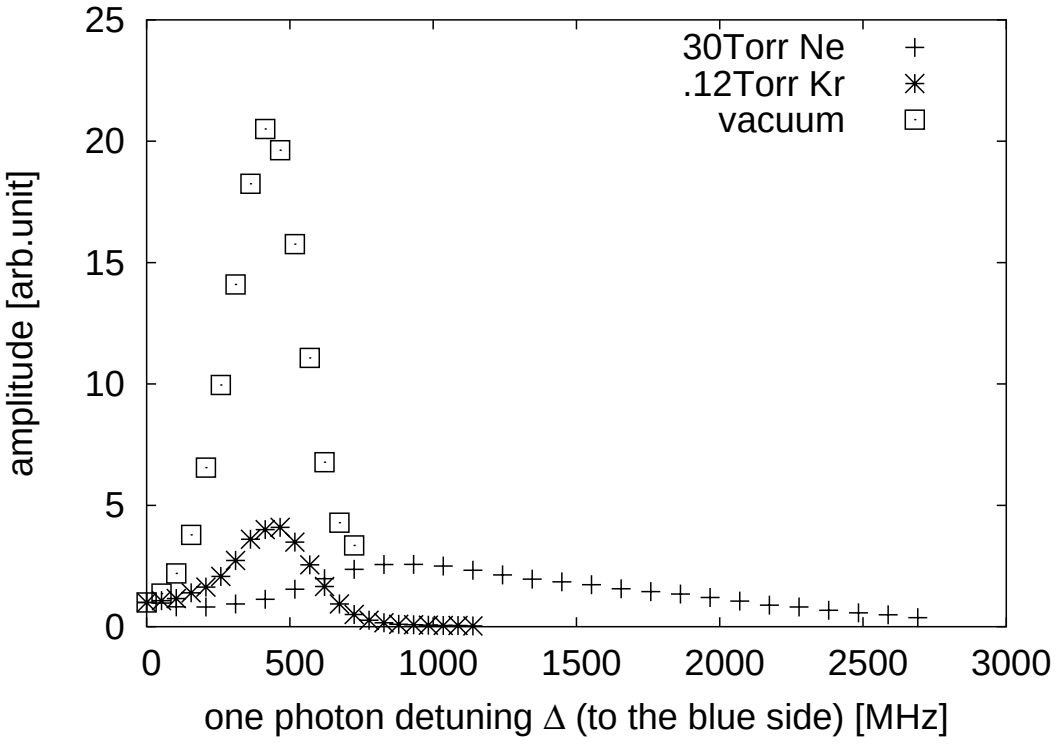

Fig. 47. Amplitude D of the two-photon resonance for probe field. For easier comparison, the values of D are normalized to the resonance amplitude at zero detuning.

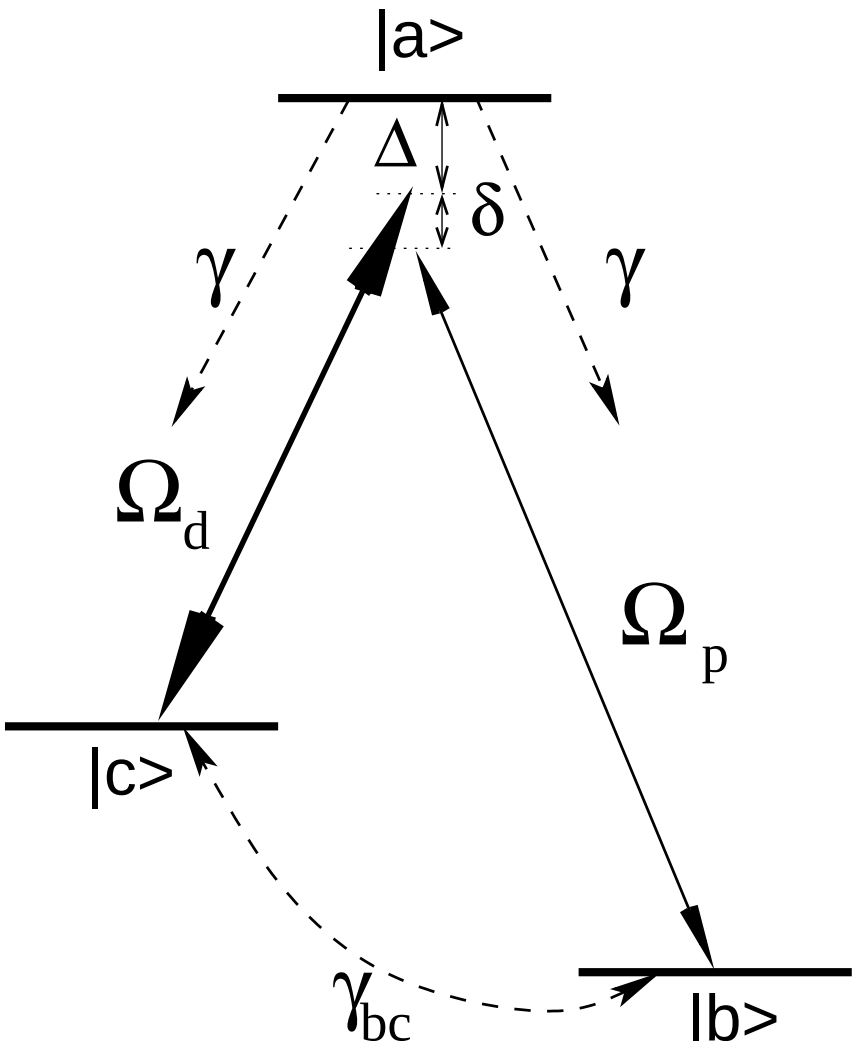

Fig. 48. Three-level Λ system.

D. Theoretical analysis

We now derive an expression for the absorption coefficient of a weak probe field in a closed three-level Λ-scheme as shown in Fig. 48. In this case, the time-evolution equations for the density matrix elements are the following (see, e.g. [172]):

$$\dot{\rho}_{bb} = i\Omega_p^*\rho_{ab} - i\Omega_p\rho_{ba} + \gamma_r\rho_{aa} - \gamma_{bc}\rho_{bb} + \gamma_{bc}\rho_{cc} \tag{7.4}$$

$$\dot{\rho}_{cc} = i\Omega_d^*\rho_{ac} - i\Omega_d\rho_{ca} + \gamma_r\rho_{aa} - \gamma_{bc}\rho_{cc} + \gamma_{bc}\rho_{bb} \tag{7.5}$$

$$\dot{\rho}_{ab} = -\Gamma_{ab}\rho_{ab} + i\Omega_p(\rho_{bb} - \rho_{aa}) + i\Omega_d\rho_{cb} \tag{7.6}$$

$$\dot{\rho}_{ca} = -\Gamma_{ca}\rho_{ca} + i\Omega_d^*(\rho_{aa} - \rho_{cc}) - i\Omega_p^*\rho_{cb} \tag{7.7}$$

$$\dot{\rho}_{cb} = -\Gamma_{cb}\rho_{cb} - i\Omega_p\rho_{ca} + i\Omega_d^*\rho_{ab} \tag{7.8}$$

where $\Omega_d = \wp_{ac}\mathrm{E_p}/\hbar$ and $\Omega_p = \wp_{ab}\mathrm{E_d}/\hbar$ are the Rabi frequencies of the drive and probe fields. The generalized decay rates are defined as:

$$\Gamma_{ab} = \gamma + i(\Delta + \delta), \tag{7.9}$$

$$\Gamma_{ac} = \gamma + i\Delta, \tag{7.10}$$

$$\Gamma_{cb} = \gamma_{bc} + i\delta. \tag{7.11}$$

Here $\gamma = \gamma_r + \gamma_{deph}$ is the polarization decay rate, γ_r is the radiative decay rate of the excited state, γ_{deph} is dephasing rate, and γ_{bc} is the inverse lifetime of the coherence between ground states $|b\rangle$ and $|c\rangle$. Here we recall that the presence of the buffer gas affects values of both γ_{bc} and γ. On one hand, as mentioned above, it allows preservation of the ground-state coherence longer, but on the other hand it broadens the optical transition, since $\gamma_{deph} = 0$ grows linearly with buffer gas pressure [142].

Solving these equations in the steady state regime and assuming $|\Omega_p| \ll |\Omega_d|$, we obtain the following expression for the linear susceptibility of the probe field:

$$\chi = -\kappa \frac{\Gamma_{cb}(\rho_{aa}^{(0)} - \rho_{bb}^{(0)}) + \dfrac{|\Omega_d|^2}{\Gamma_{ca}}(\rho_{aa}^{(0)} - \rho_{cc}^{(0)})}{\Gamma_{ab}\Gamma_{cb} + |\Omega_d|^2}, \tag{7.12}$$

Where $\kappa = \frac{3}{8\pi} N\lambda^2\gamma_r$, N is the ^{87}Rb density and λ is the wavelength of the probe field.

The atomic population differences in the approximation of strong driving field ($|\Omega_d|^2 \gg \gamma_{bc}\gamma$) are:

$$(\rho_{aa}^{(0)} - \rho_{bb}^{(0)}) \simeq -\frac{\gamma_{bc}\Delta^2 + \gamma|\Omega_d|^2}{2\gamma_{bc}\Delta^2 + \gamma|\Omega_d|^2} \tag{7.13}$$

$$(\rho_{aa}^{(0)} - \rho_{cc}^{(0)}) \simeq -\frac{\gamma_{bc}(\Delta^2 + \gamma^2)}{2\gamma_{bc}\Delta^2 + \gamma|\Omega_d|^2}. \tag{7.14}$$

By substituting these expressions into Eq. (7.12), we find the absorption coefficient α as a function of two-photon detuning δ:

$$\alpha = \frac{\kappa}{\gamma^2 + \Delta^2} \frac{\gamma_{bc}\Delta^2 + \gamma|\Omega_d|^2}{2\gamma_{bc}\Delta^2 + \gamma|\Omega_d|^2} \frac{\gamma_{bc}|\Omega_d|^2 + \gamma\delta^2}{\gamma_{EIT}^2 + (\delta - \delta_0)^2}, \tag{7.15}$$

where

$$\delta_0 = |\Omega_d|^2 \frac{\Delta}{\gamma^2 + \Delta^2} \tag{7.16}$$

is the ac-Stark shift of the excited state, and

$$\gamma_{EIT} = \frac{\sqrt{\gamma^2|\Omega_d|^4 + \gamma_{bc}^2\Delta^2(\gamma^2 + \Delta^2)}}{\gamma^2 + \Delta^2} \tag{7.17}$$

is the effective width of the two-photon transmission resonance.

Using Eq. (7.15) for the absorption coefficient we can now find expressions for the coefficients A, B, and C in Eq. (7.1) which describe the line-shape of the two-photon resonance for the probe field propagating through a medium of length L. For the moment we restrict ourselves to the case of optically thin media, so $I_{out} = I_{in}\ e^{-\alpha} \simeq$

$I_{in}(1-\alpha L)$:

$$A = \kappa L\eta \frac{|\Omega_d|^2}{\gamma^2+\Delta^2} \frac{\gamma|\Omega_d|^2(\gamma^2-\Delta^2)-\gamma_{bc}(\gamma^2+\Delta^2)^2}{\gamma^2|\Omega_d|^4+\gamma_{bc}^2\Delta^2(\gamma^2+\Delta^2)} \quad (7.18)$$

$$B = -\kappa L\eta \frac{\Delta}{\gamma^2+\Delta^2} \quad (7.19)$$

$$C = 1-\kappa L\eta \frac{\gamma}{\gamma^2+\Delta^2} \quad (7.20)$$

$$\eta = \frac{\gamma_{bc}\Delta^2+\gamma|\Omega_d|^2}{2\gamma_{bc}\Delta^2+\gamma|\Omega_d|^2} \quad (7.21)$$

It is easy to see that the coefficient C, which is determined by incoherent absorption processes in this approximation, coincides with the absorption of a weak field in a two-level scheme. The only difference is the coefficient η which represents the redistribution of the atomic population between ground levels: $\eta = 1$ when the one-photon detuning is small ($\Delta \ll \sqrt{\frac{\gamma}{\gamma_{bc}}}|\Omega_d|$) means all atomic population is optically pumped into a dark state, and $\eta = \frac{1}{2}$ if the laser is far-detuned, and the populations of the levels $|b\rangle$ and $|c\rangle$ are almost the same.

Coefficient A is a symmetric function of the one-photon detuning. Its sign changes as Δ gets larger: A is positive for small detunings, then at $\Delta \approx \gamma - 2\gamma_{bc}\gamma^2/|\Omega_d|^2$ it disappears, and for larger Δ the amplitude of the symmetric component of the resonance becomes negative (i.e. absorptive). Coefficient B is an odd function of Δ, and exactly zero on resonance.

Thus it is clear why there is no distortion of the symmetric Lorentzian line-shape observed for the cell without buffer gas. In this case the inhomogeneous broadening of the transitions is much larger that the radiative decay rate of the excited state, so the resulting shape of the EIT resonance should be an average over the Doppler distribution, so that the anti-symmetric part of Eq.(7.1) effectively cancels. At the same time, the simplified theoretical model described above should also be applicable for the case of high buffer gas pressure, for which the collisional broadening of the

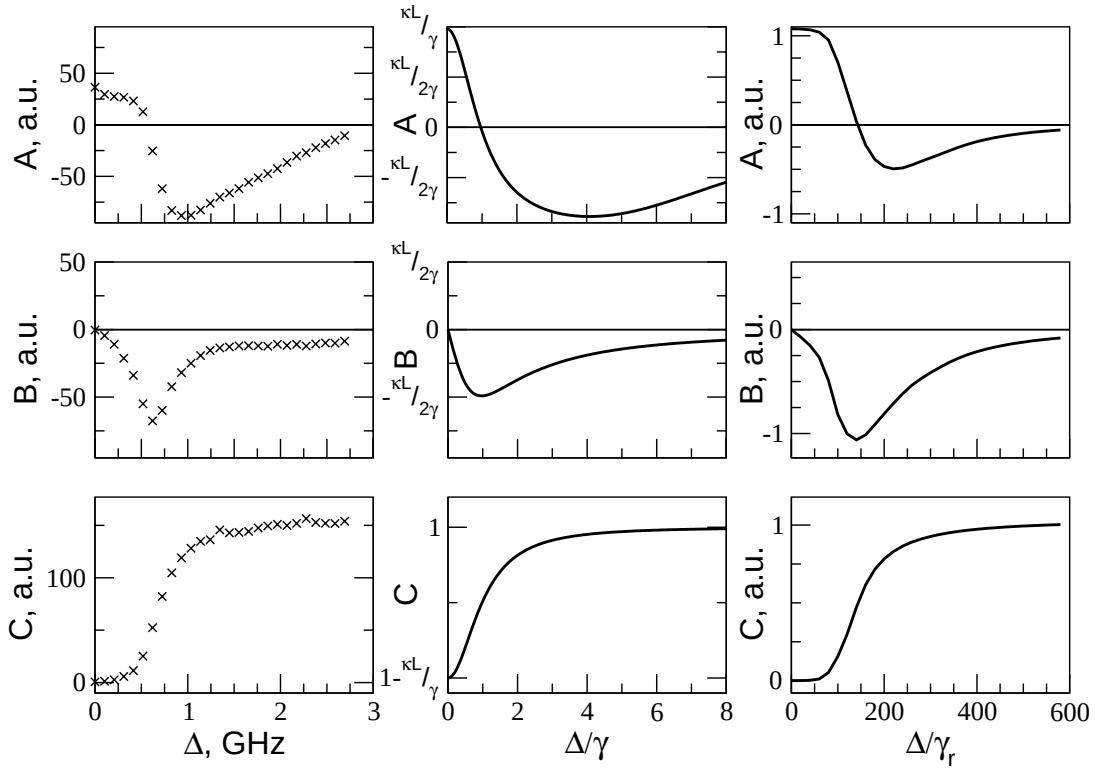

Fig. 49. Coefficients A, B, and C describing the line-shape of the coherent resonance Eq. (7.1): extracted from the experimental data for ^{87}Rb cell with 30 Torr (left column), calculated using Eqs. (7.18–7.20) (middle column), and obtained by numerical modelling (right column).

excited state exceeds the Doppler broadening. A comparison of the coefficients A, B, and C given by Eqs. (7.18–7.20), with those, obtained by fitting the experimental data for the Rb cell with 30 Torr of Ne is given in Fig. 49. One can immediately see that the theoretical formulae qualitatively describe the dependence of the coefficients as functions of one-photon detuning, although they are not accurate enough for a quantitative analysis. There are several reasons for this. On one hand, the collisional broadening created by a Ne pressure of 30 Torr is still smaller than the Doppler broadening, so that averaging over the velocity distribution can still significantly

affect the shape of the resonance. First, for simplicity we assumed that the medium is optically thin and there is no absorption of the drive field, which is not the case for the experimental conditions. One of the consequences of this effect is the density narrowing of the coherent resonances which will be discussed in the following Section.

To analyze the effects of propagation through the optically thick medium and thermal velocity distribution of the Rb atoms, we perform a numerical simulation of the interaction of the drive and probe field with the three-level Λ system, considered above. In this case we take into the account the attenuation of the probe intensity as the fields propagate through the optically thick medium. In addition, since atoms with different velocities "see" an electromagnetic fields at a shifted frequency, the final susceptibility has to be averaged over the Maxwell velocity distribution:

$$\chi(\Delta) = \frac{1}{\sqrt{\pi}ku} \int_{-\infty}^{+\infty} \chi(\Delta - kv) e^{-\frac{(kv)^2}{(ku)^2}} d(kv), \tag{7.22}$$

where $k = \nu_d/c$ is the drive field wave-vector, and $u = \sqrt{2k_BT/M}$ is the most probable thermal speed (here T is the temperature of the vapor, M is the mass of Rb atom and k_B is the Boltzmann constant). In general, this problem is straightforward but extremely cumbersome and can be solved only numerically.

To model best the experimental data obtained in the Rb cell with 30 Torr of Ne we use following parameters: $\gamma_{deph} = 10\gamma_r$, $\gamma_{bc} = 5 \times 10^{-4}\gamma_r$, $ku = 50\gamma_r$, $\Omega_d = 0.4\gamma_r$, $\Omega_p = 0.1\gamma_r$. The values of Rabi frequencies for the actual fields are $\Omega_d = 0.38\gamma_r$ ($I_d \simeq 1.2$ mW/cm^2) and $\Omega_p = 0.13\gamma_r$ ($I_d \simeq 0.13$ mW/cm^2). The small deviation between these values can be attributed to the nonuniform spatial distribution of the laser intensity. For the vacuum cell the only differences appear in the value of $\gamma_{bc} = 10^{-2}\gamma_r$ and zero γ_{deph}.

Although the results of the numerical simulation do not provide an exact coincidence with the experimental data, as it is seen in Fig. 49, they allow better un-

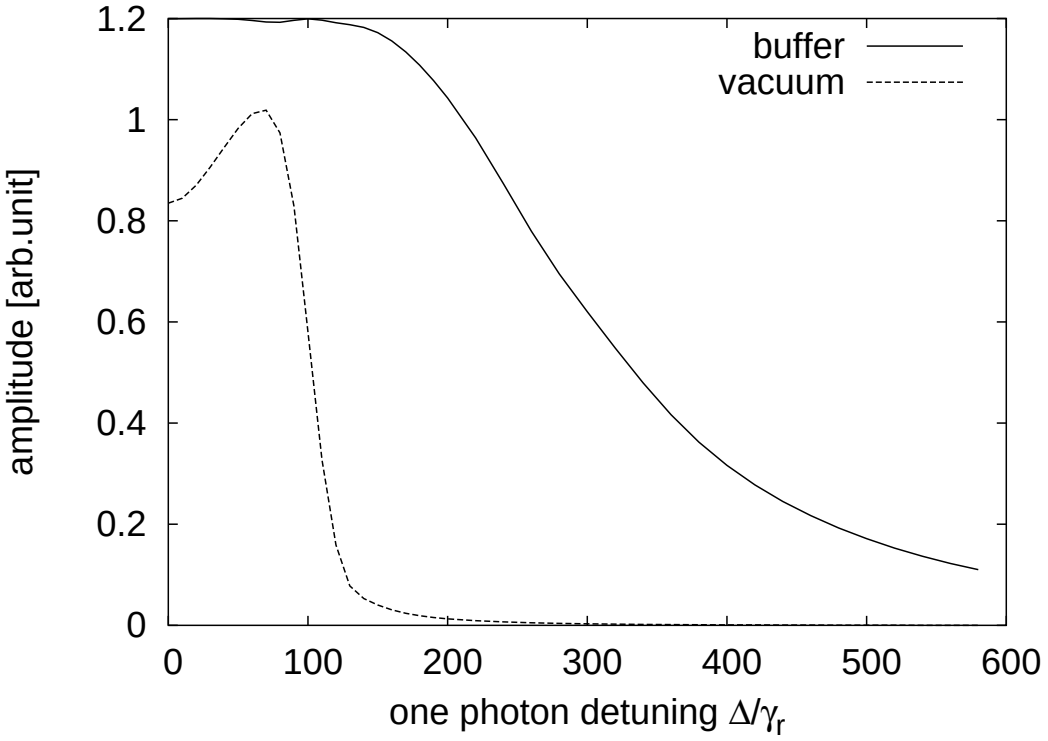

Fig. 50. Numerical calculation of resonance strength (D) vs one-photon detuning for probe field propagating in medium with buffer gas and vacuum. One-photon detuning and resonance width is given in units of γ_r.

derstanding of why no absorption resonances are observed in the cell with no buffer gas. The calculated values of the resonance amplitude D and the ratio ϕ are shown in Figs. 50 and 51. As one can see that the inversion of the EIT resonance occurs in the cell with buffer gas, when in the cell without buffer gas, no absorption resonances ever appear. However, the noticeable asymmetry of the resonance is expected for the values of the laser detuning ($\Delta > 100\gamma_r$) for which the amplitude of the resonances is very small and hardly detectable.

The importance of the Doppler averaging is also observed in the two-photon

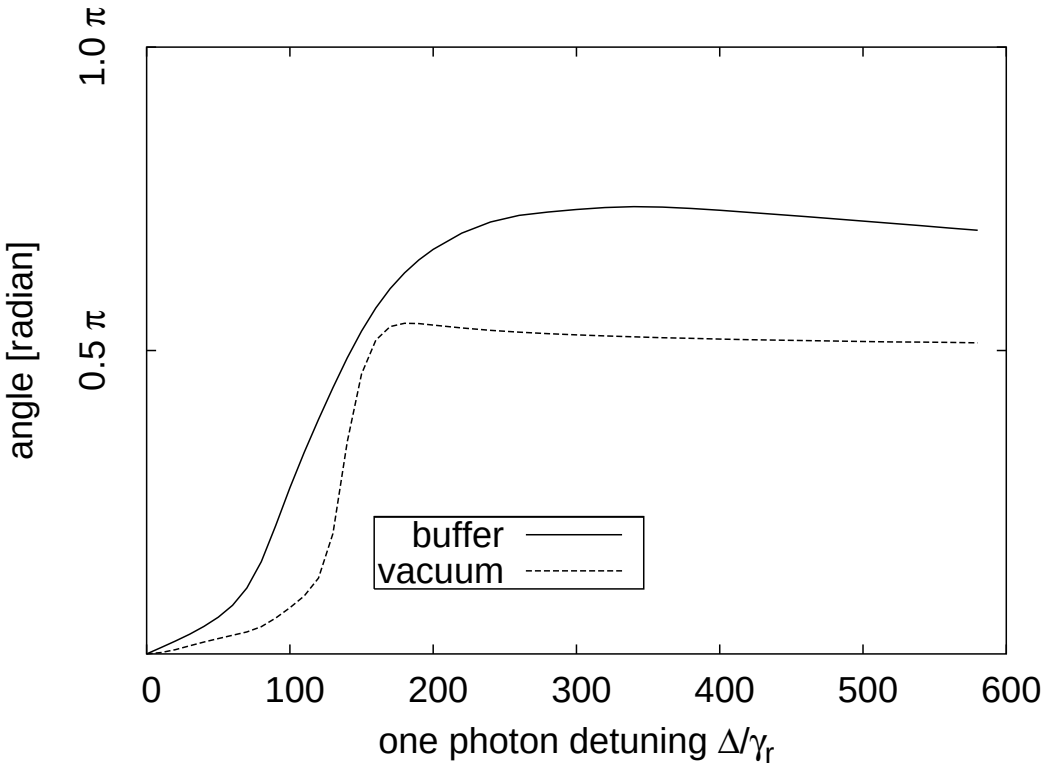

Fig. 51. Numerical calculation of angle (ϕ) vs one-photon detuning for probe field propagating in medium with buffer gas and vacuum. One-photon detuning and resonance width is given in units of γ_r.

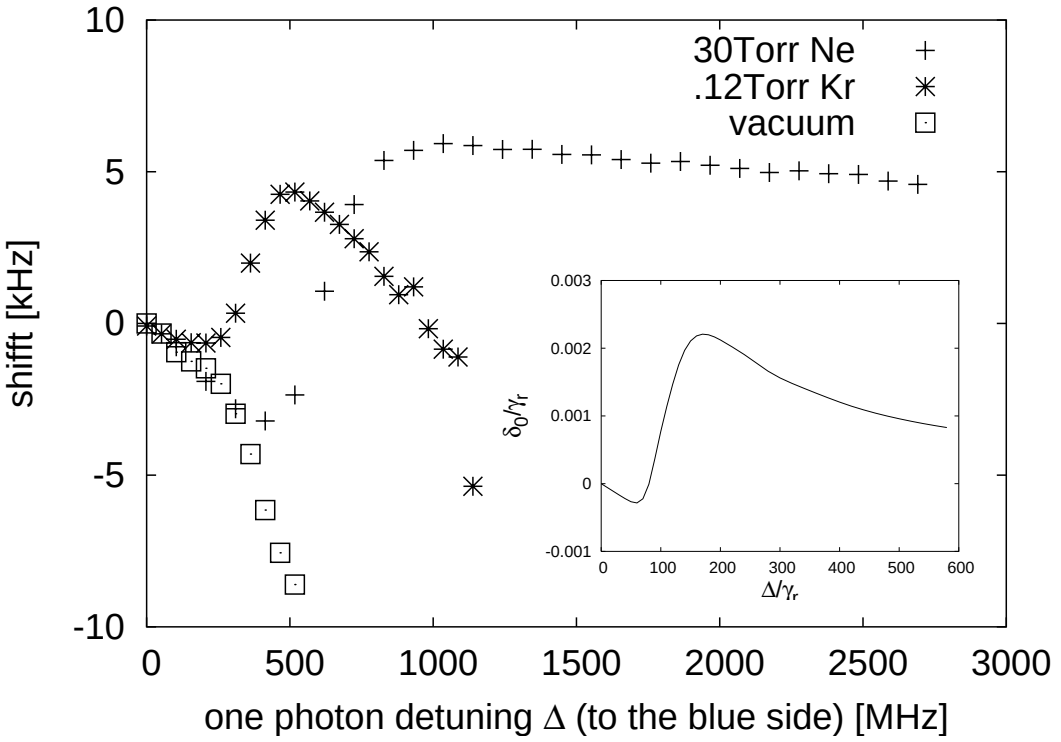

Fig. 52. Two photon resonance shift (δ_0) as a function of one-photon detuning for the vacuum cell (squares), cell with 0.12 Torr of Kr (stars) and with 30 Torr of Ne (crosses).*Inset:* the result of the numerical simulation for 30 Torr cell.

resonance shift δ_0. It is easy to notice in Fig. 45 that for non-zero detuning Δ the centers of both EIT and buffer-gas induced absorption resonances are shifted from zero two-photon detuning. One of the reasons of this effect is a light shift of the atomic levels, as it is shown by Eq.(7.16). However, this dependence on the laser detuning differs significantly from the behavior of the resonance shift, measured experimentally (Fig. 52). However, more realistic resonance shift as a function of laser detuning is obtained by numerical simulation if Doppler averaging is performed (Fig. 52, inset).

It has to be noted, however, that both the prediction of the theoretical model and the result of the numerical simulation developed above for three-level Λ system

provide only qualitative agreement with the experimental results. There are several major effects which are not considered here. For example, neither hyperfine structure of the excited state nor Zeeman substructure of all states is taken into consideration, although it may have a profound effect on the coherent interaction. In addition, no influence of four-wave mixing processes and the generation of the Stokes field is taken into account.

We numerically compare the case of large detuning ($\Delta = 250\gamma_r$) for the case of cell with buffer and vacuum. And find out that absorption resonance appear only for large enough drive laser power in the cell with buffer when in the cell without buffer gas resonance remains dispersion like ($\phi \approx \pi/2$) (see Fig. 53).

E. Influence of the buffer gas on four-wave mixing

Many previous publications [89, 115, 173, 174] have shown that dense coherent media contribute to significant enhancement of nonlinear processes. In particular, under the conditions of our experiment this leads to strong four-wave mixing: the drive field applied to $F = 1$ level, is scattered by the ground-state coherence, which leads to the generation of a coherent Stokes field. This process does not require the presence of a seed field, and is initiated by spontaneous photons [157].

The amplitude and the angle ϕ for the generated Stokes field in the cell with 30 Torr of Ne are shown in Fig. 54. One can see that the shape of this resonance also changes as the laser is detuned from the atomic transition: at resonance, the new field has a dispersion-like form, and is transformed into a symmetric transmission peak as Δ increases.

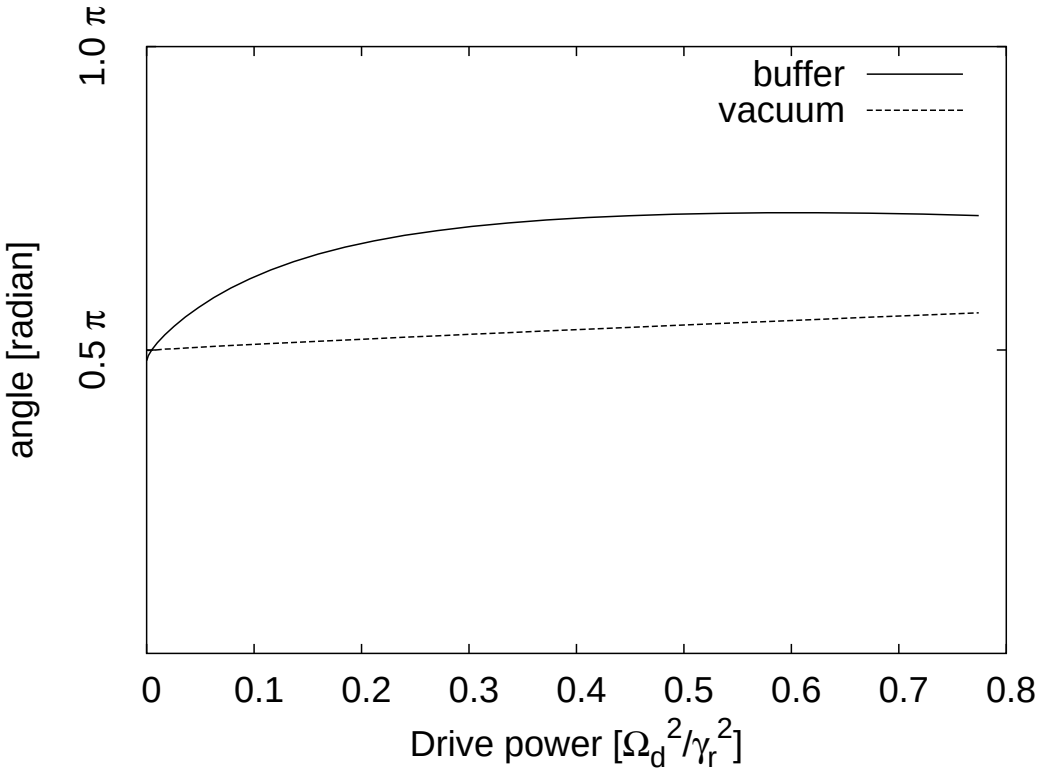

Fig. 53. Numerical calculation of angle (ϕ) vs drive power for probe field propagating in medium with buffer gas and vacuum.

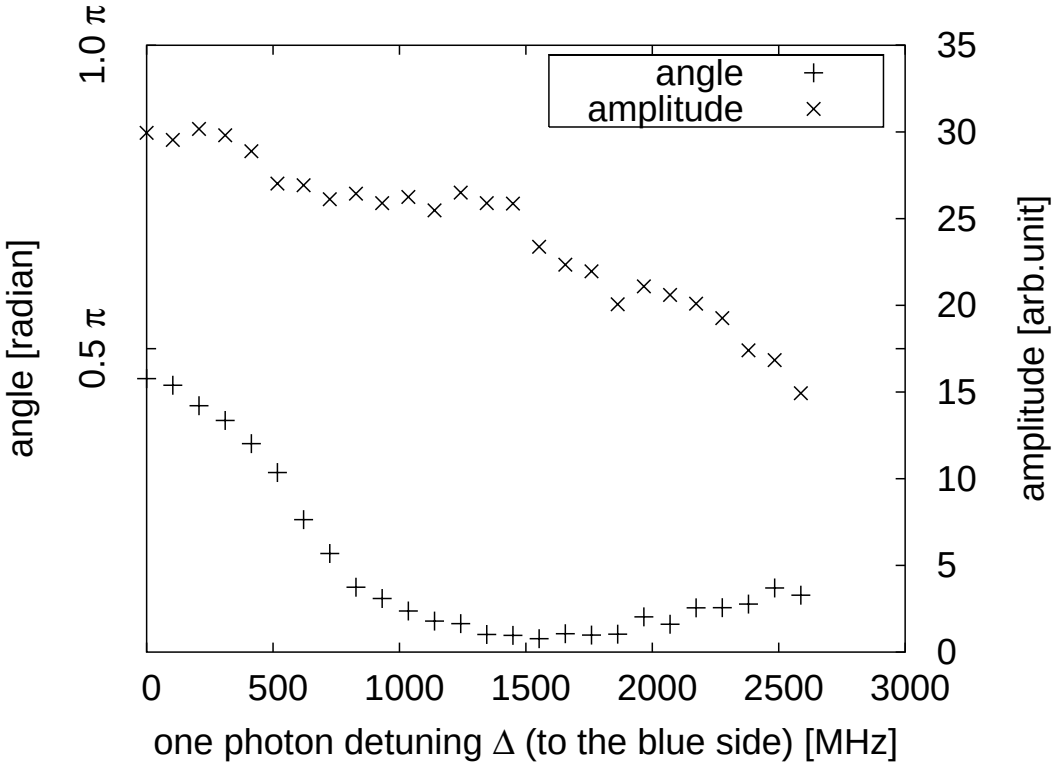

Fig. 54. Angle (ϕ) and amplitude (D) of the two photon resonance for the generated Stokes field.

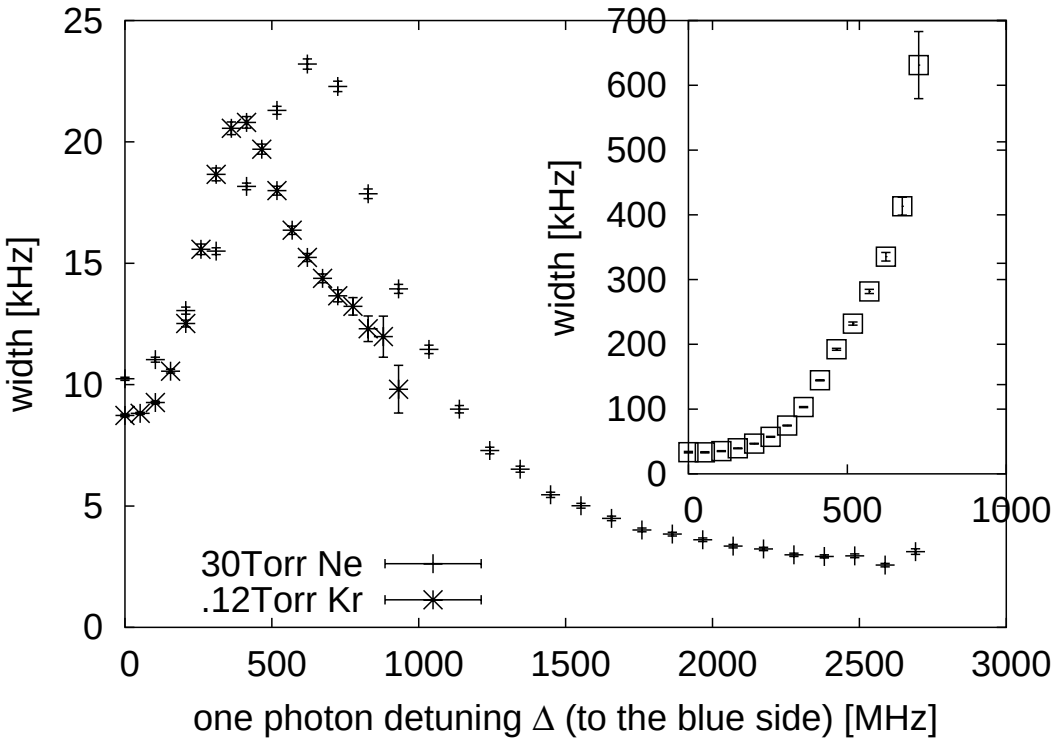

Fig. 55. Width of the two photon resonance $2\gamma_{EIT}$ as a function of one-photon detuning Δ for ^{87}Rb cell with 30 Torr of Ne (cross), 0.12 Torr of Kr (x), and without buffer gas (squares, inset). The minimum width of the EIT resonance in the vacuum cell with no buffer gas is $2\gamma_{EIT}(\Delta = 0) = 17$kHz.

F. Width of the probe and Stokes resonances

The measured widths of the two-photon resonance γ_{EIT} as functions of the one-photon detuning Δ are shown in Fig. 55 for the cells with different buffer gas pressure. Here we see again the difference between the cells with and without buffer gas: in the letter case the width of the EIT resonance increases significantly with one-photon detuning. For the buffered cells, however, the width increases only near the atomic resonance, but for a larger detuning the resonance start getting narrower.

Again, the numerical simulations (Fig. 56) show that there is no principle difference between the cell with or without buffer gas. Even in the vacuum cell there should be the narrowing of the resonance; however, this corresponds to the detuning of extremely low resonance amplitudes (compare with Fig. 50).

Narrow resonances with good signal-to-noise ratio are important for many applications. For example, narrow EIT resonances are used for precision metrology [69, 175, 176] and atomic clocks [177, 178]. Our experiments demonstrate that the coherent absorption resonances, observed for the far-detuned Λ system may have more attractive characteristics in terms of the resonance width and amplitude than the EIT resonances observed for the zero detuning. For example, in the cell with 30 Torr of Ne the amplitude of the absorption resonance for $\Delta = 1.2 - 2$ GHz is larger than that of the EIT resonance, while its width is narrower (for example, $\gamma_{EIT}(0)/\gamma_{EIT}(2GHz) \approx 3.3$).

To understand the behavior of the resonance width, we will use the theoretical expression for the width of the two-photon resonance Eq. (7.17) obtained in Section D. According to that, in the strong laser field limit ($|\Omega_d|^2 \gg \gamma_{bc}\gamma$) the width of the EIT resonance for small Δ does not depend on the ground-state coherence decay rate and is determined by power broadening: $\gamma_{EIT} \approx |\Omega_d|^2/\gamma$, which coincides with previous

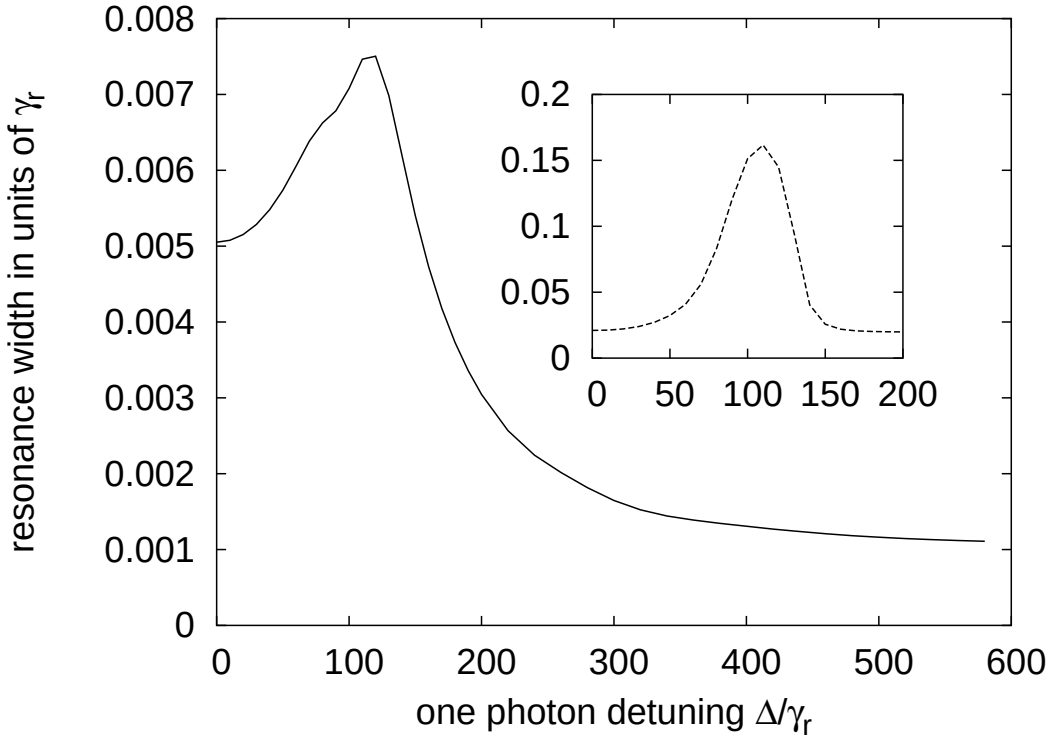

Fig. 56. Numerical calculation of resonance width (2 γ_{EIT}) vs one-photon detuning for probe field propagating in medium with buffer gas and vacuum.

studies [67]. Then the resonance width decreases with one-photon detuning, and for $\Delta \gg \gamma$ it drops as $1/\Delta^2$. Ultimately for $\Delta \gg |\Omega_d|\sqrt{\gamma/\gamma_{bc}}$, the width of the resonance is determined by the coherence decay rate γ_{bc}.

We would like to point out two effects that limit the accuracy of our analysis. First, we have not taken into account the velocity distribution of the thermal Rb atoms. Second, propagation through the Rb vapor becomes important for optically thick media. In this case the shape of the coherent resonance may change; in particular, its width can be greatly reduced. This effect is known as density narrowing of the EIT resonances [64, 179].

We note that both the above effects are not very important for the case of far-detuned laser frequency $\Delta \gg \gamma, ku$, since the absorption of the medium is small, and the parameters describing the resonance lineshape do not change noticeably within the Doppler contour. Thus, for large detuning $1/\Delta^2$ the dependence of the resonance width predicted from Eq. (7.17) is in good agreement with the experimental points, as shown in Fig. 57.

To fully understand how the resonance width behaves as a function of one-photon detuning for small Δ we should take both propagation and Doppler averaging into account. Since it is virtually impossible to do that exactly, we make a few simplifying assumptions that allow us to roughly predict the functional form of the resonance width on one-photon detuning. First, we assume that the main contribution to the resonance lineshape is due to the resonant velocity subgroup for which $\Delta - kv \simeq 0$. Then, the only consequence of the detuning the laser is the reduction of the number of atoms in this velocity group:

$$N(\Delta) \propto N e^{-\frac{\Delta^2}{(ku)^2}}. \tag{7.23}$$

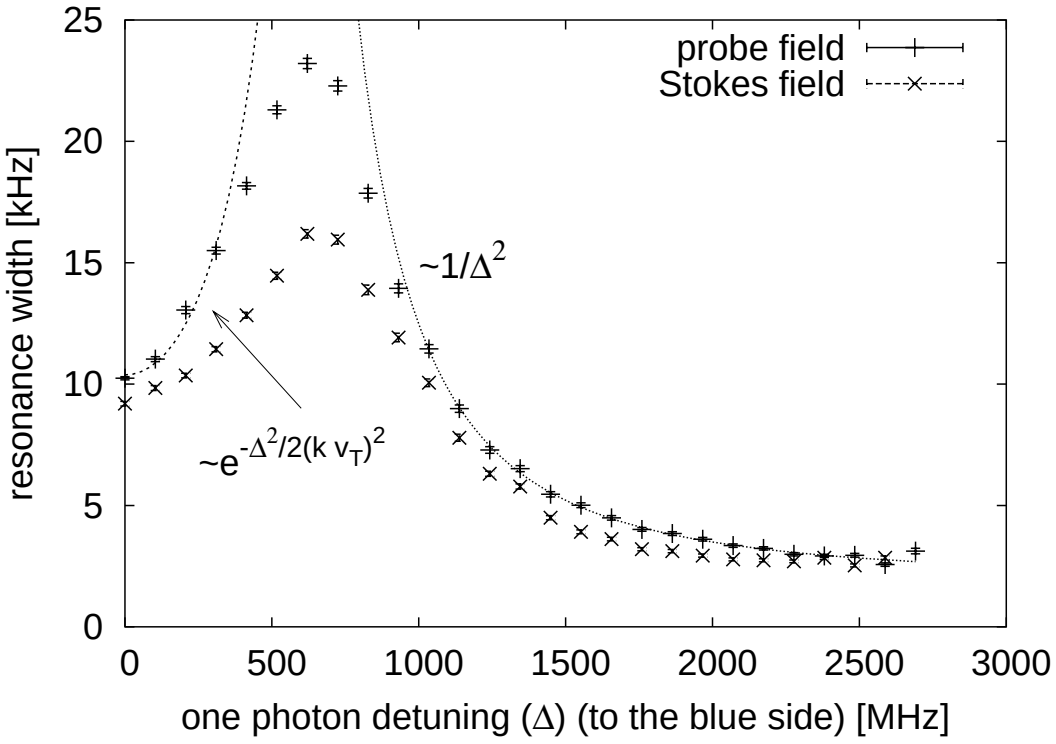

Fig. 57. Width of two photon resonance (γ) for the probe and generated Stokes field.

The output intensity I_{out} is then given by

$$I_{out} \simeq I_{in} e^{-\kappa L \frac{\gamma_{bc}}{|\Omega_d|^2}} e^{-\kappa L \frac{\gamma \delta^2}{|\Omega_d|^4}}. \tag{7.24}$$

In this expression the first term represents the residual absorption under EIT conditions, and the second one describes the shape of the peak as a function of two-photon detuning. It is easy to see that the width of the resonance in this case is inversely proportional to the atomic density [64]:

$$\gamma_{EIT\,D}(N) \simeq \frac{|\Omega_d|^2}{\sqrt{\gamma \gamma_r}} \left(\frac{3}{8\pi} N \lambda^2 L \right)^{-1/2}. \tag{7.25}$$

We use the expression for the density of the resonant velocity subgroup as a function of laser detuning given by Eq. (7.23) to obtain the width of the resonance:

$$\gamma_{EIT\,D}(\Delta) \propto \frac{|\Omega_d|^2}{\sqrt{\gamma \gamma_r}} \frac{1}{\sqrt{NL}} e^{\frac{\Delta^2}{2(ku)^2}}. \tag{7.26}$$

It is easy to see that this formula works only for a small frequency region in the vicinity of one-photon resonance where the resonance is nearly symmetric and deviates for larger Δ. This is consistent with the assumptions made in the derivations of Eq. (7.26).

The width of the Stokes field resonance is also shown in Fig. 57. It has approximately the same shape as the curve for the probe field, but it is worth mentioning that its width can be narrower than that for the probe field while having a similar resonance amplitude.

G. Summary

We demonstrate significant changes of the EIT resonance lineshape in a medium with buffer gas. We show that this shape changes from transparency-like to dispersion-like

and then to absorption-like shape with increasing of one-photon detuning. We also show that for large enough detuning, the resonance width is limited by the amount of ground level decay rate (γ_{bc}). Also we demonstrate that there is a region one-photon detunings when our signal is higher than for zero one-photon detuning (traditional way to observe EIT resonance) while the width of the resonance is narrower. Observation of absorption-like resonance is power dependent and takes place only for high enough drive power. We compared the behavior of the probe and Stokes field for large one-photon detuning, find that resonance width of these two fields behaves similarly, while the shapes of the resonances are different.

CHAPTER VIII

FAST LIGHT

A. Introduction

Under the condition of EIA , negative delay time was observed [106]. Negative delay was also observed in gain-assisted cesium gas [105], ultra high negative delay in the order of -400 μs has been observed in systems with atomic coherence induced by microwave emission by Godone *et al.* [91].

This chapter is devoted to the study of the dependences of the delay time of a probe pulse in a hot ^{87}Rb medium with buffer gas. Corresponding to the transformation of an EIT resonance for zero one-photon detuning to absorption-like resonance for large enough one-photon detuning, we demonstrate the transformation of positive delay time to negative delay by changing the one-photon detuning. Also we measure the dependence of delay time on laser power in the case of an EIT resonance as well as for non zero one-photon detuning where an absorption resonance is observed.

B. Experimental setup

The simplified experimental setup is shown in Fig. 58b. In our experiment we used an extended cavity diode laser tuned to the D_1 line of the ^{87}Rb transition $5S_{1/2}F = 2 \rightarrow 5P_{3/2}F = 2$ (drive field) (see Fig. 58a). An EOM driven in the vicinity of the ground level hyperfine splitting frequency (6.835GHz) is used to generate a sideband at the frequency of the transition $5S_{1/2}F = 1 \rightarrow 5P_{3/2}F = 1$ (probe field). This way, the drive and probe fields form a Λ system. The probe and drive fields pass through a single-mode fiber which results in a Gaussian spatial distribution of laser field intensity. We expand the beam diameter to approximately 7 mm. Power attenuation

is provided by two crossed polarizers. The polarization of the electric field is changed to circular with a $\lambda/4$ wave plate placed just before a cell of length 2.5 cm filled with a mix of isotopically enhanced ^{87}Rb and 30 Torr of Ne buffer gas. The addition of buffer gas to the cell is a common tool for decreasing the ground level coherence decay rate (γ_{bc}) [61, 63, 69, 149]. In a media with buffer gas, EIT resonances as narrow as 30-50 Hz have been observed in the lower power regime. The cell is placed inside a 3 layer magnetic shield to screen out the Earth's magnetic field and prevent splitting of Zeeman sublevels.

Significant narrowing of an power broadened EIT resonance has been observed in optically thick media [64, 67, 179]. When the driving field is strong $\Omega_d^2 \gg \gamma\gamma_{bc}$, the width of the EIT resonance in optically thick media is given by

$$\gamma_{EIT} = \frac{\gamma_{bc} + \frac{\Omega_d^2}{\gamma}}{\sqrt{\eta L}} \tag{8.1}$$

where Ω_d is Rabi frequency of the driving field, γ is decay rate of the upper level, L is the cell length, N is density of atoms, and λ is the probe field wavelength. The density of ^{87}Rb at 68^oC is $N = 4.7 \times 10^{11}$ cm^{-3}.

The transmitted laser fields are mixed with another laser field shifted by 60 MHz with respect to the drive field after the cell. This way we are able to distinguish the probe field signal beatnote with the help of a spectrum analyzer.

C. Experimental results

The addition of buffer gas not only leads to narrowing of the EIT resonance, but also to significant change of the EIT resonance shape [180] (see also previous chapter). Namely, for large enough one photon detuning in the vicinity of two-photon resonance, a strong absorption resonance is observed. Such a buffer gas induced absorption

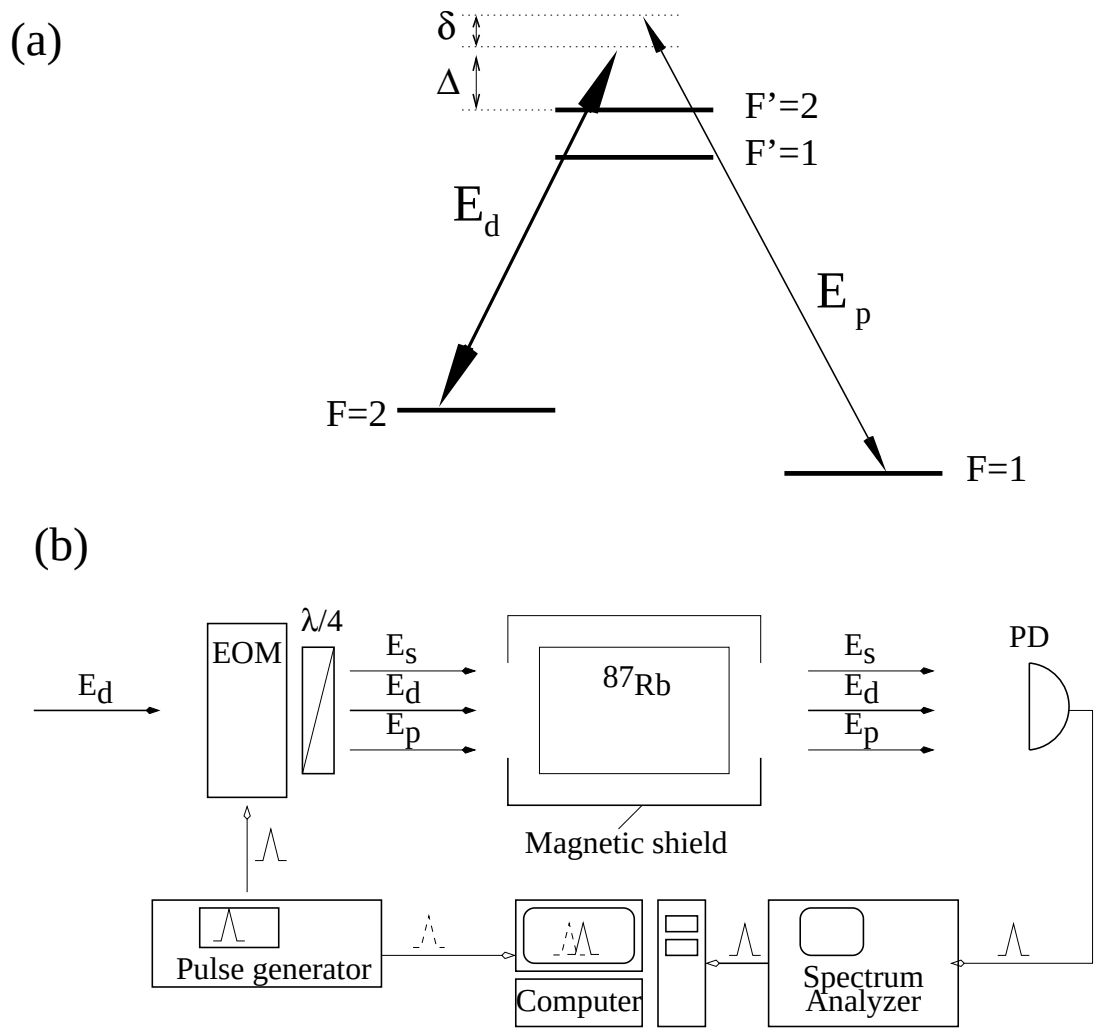

Fig. 58. (a) ^{87}Rb level diagram; (b) simplified setup.

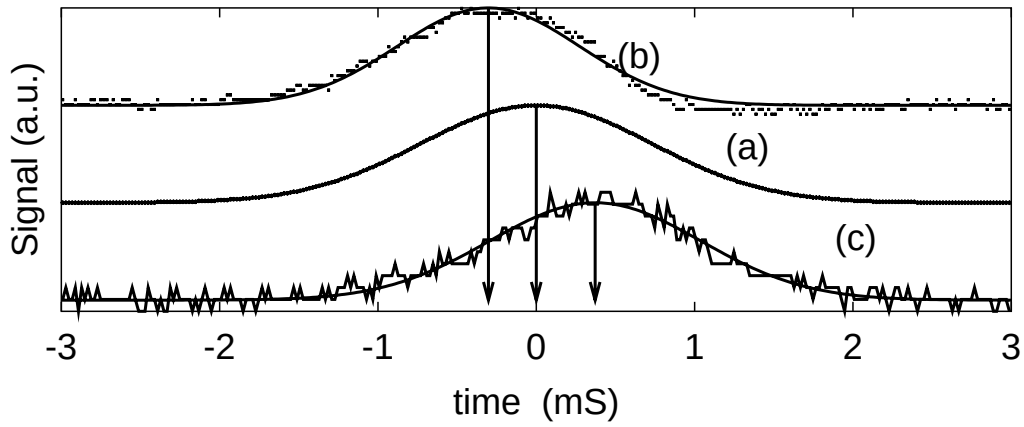

Fig. 59. Examples of pulse delay. (a) is a reference pulse; (b) is taken for one-photon detuning $\Delta = 1.45$ GHz, total laser power 700 μW; (c) is taken for $\Delta = 0$, total laser power 145 μW.

resonance can have higher amplitude and narrower width than the EIT resonance for a properly chosen one-photon detuning. Thus, group velocity is expected to be negative and quite small in magnitude. This was demonstrated experimentally [180].

Examples of pulse delay are shown in Fig. 59. The reader can see that for zero one-photon detuning ($\Delta = 0$), the pulse delay time (τ) is 370 μs, while for $\Delta = 1.45$ GHz, the delay time is -300 μS.

The pulse propagation delay time (τ) is given by

$$\begin{aligned} \tau &= \int_0^L \frac{dx}{v_g(x)} \\ &= \frac{L}{\langle v_g \rangle} = \frac{L}{c} \langle \omega \frac{\partial n}{\partial \omega} \rangle \\ &\approx \frac{L}{c} \frac{A}{\gamma_{EIT}} \end{aligned} \tag{8.2}$$

where L is length of the cell. Above we also utilize Eq. (6.13).

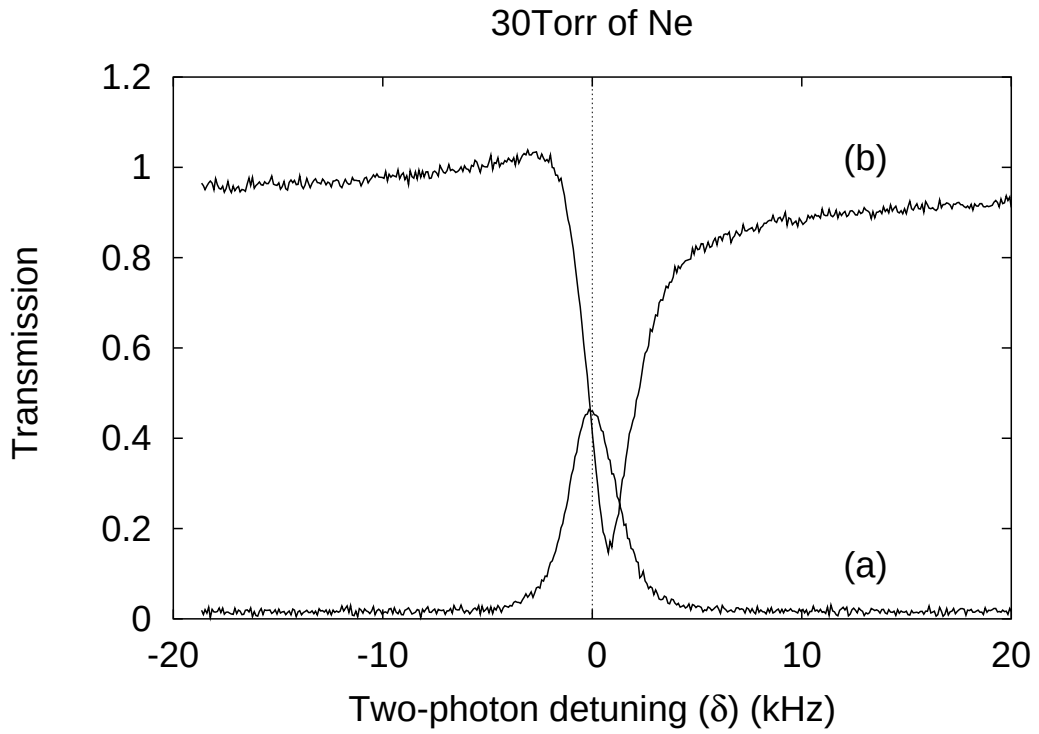

Fig. 60. Examples of resonance shapes for different one-photon detunings (Δ). (a) is taken for $\Delta = 0$ GHz; (b) is taken for $\Delta = 1.45$ GHz. Total power of laser beam is 400 μW, density of atom $N = 4.7 \times 10^{11}$ cm^{-3}.

We vary the one-photon detuning (Δ) of the drive field and then scan the probe field in the vicinity of two-photon resonance and record the transmission signal. Since the one-photon detuning modifies the resonance shape from transparency-like for small detunings (see Fig. 60a) to absorption like for large detunings (see Fig. 60b), we expect modification of the pulse delay from a positive value, or slow group velocity, to a negative delay, or superluminal group velocity. This principally due to the sign of the amplitude A changing from positive to negative, or in other words, the dispersion changes from non-anomalous to anomalous behavior. This dependence of delay time on Δ is shown in Fig. 61.

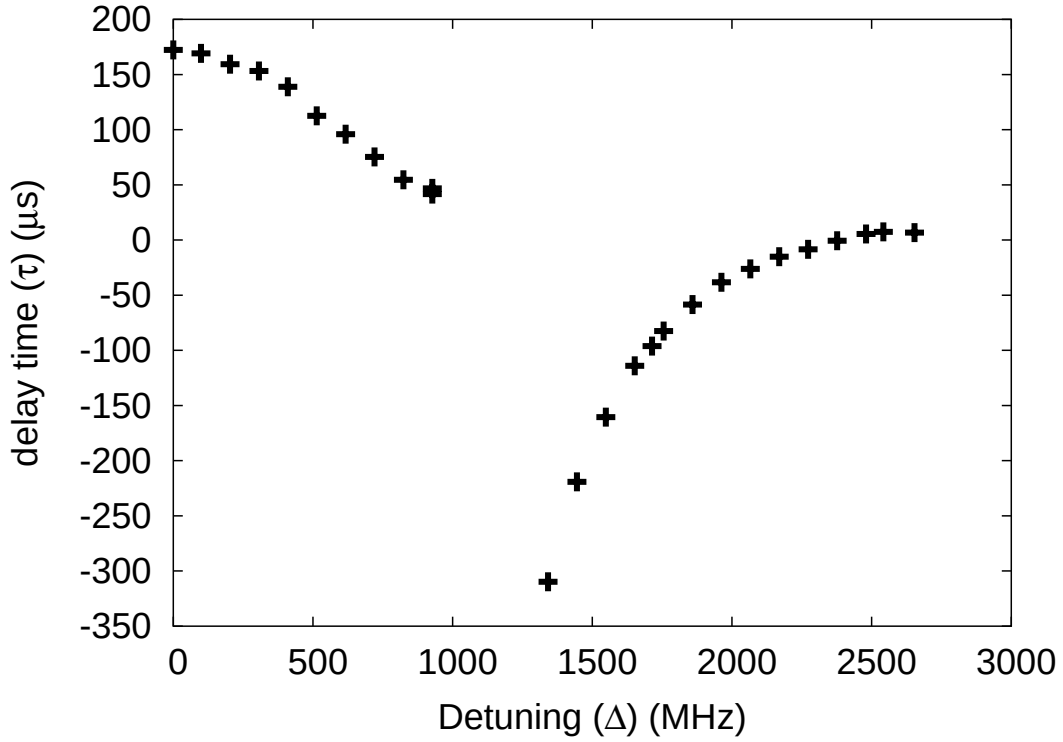

Fig. 61. Positive and negative pulse delay vs one photon detuning. Total power of laser beam is 400 μW, density of atom $N = 4.7 \times 10^{11}$ cm^{-3}.

The dependence is measured in the following way. We start at zero one-photon detuning and then obtain the maximum transmission signal by changing the two-photon detuning. Then we propagate a Gaussian probe field pulse through the medium and measure its delay with respect to the reference pulse. Data are taken in region 0-1 GHz one-photon detuning. The gap in measurements between 1 GHz and 1.4 GHz is associated with experimental difficulties in finding a transparency resonance in this frequency range, because the transmission is too small for meaningful measurements with our apparatus. After this point, we again follow the minimum of transmission by changing two-photon detuning appropriately. An example of two-photon absorption resonance shape is shown in Fig. 60b. The reader can see that at this point the maximum of transparency is barely seen. Decreasing values of τ observed at higher detuning is associated with a decreasing of the resonance strength (A).

We also study the dependence of delay time on the power of the driving laser. First, we measure the delay time for zero one-photon detuning in the EIT regime and second, for 1440 MHz one-photon detuning when the resonance has absorption-like behavior (see Fig. 60). In the first, case according to Eq. (4.15) the width of the resonance is linearly dependent on the driving laser intensity. Thus according to Eq. (8.2), the delay time should be inversely proportional to the drive power for large enough values (so we can neglect change of amplitude A). This observation is similar to [89] where similar behaviour of group delay time on power is demonstrated. However in case of our absorption like resonance, the group delay is negative and increases in magnitude proportionally to the drive power, while the resonance width for large detuning remains close to γ_{bc} level since the correction due to power broadening is of the order of $\Omega_d^2\gamma/\Delta^2$. This means the delay time increases as the power.

We numerically analyze our simple three level model and calculate the delay time

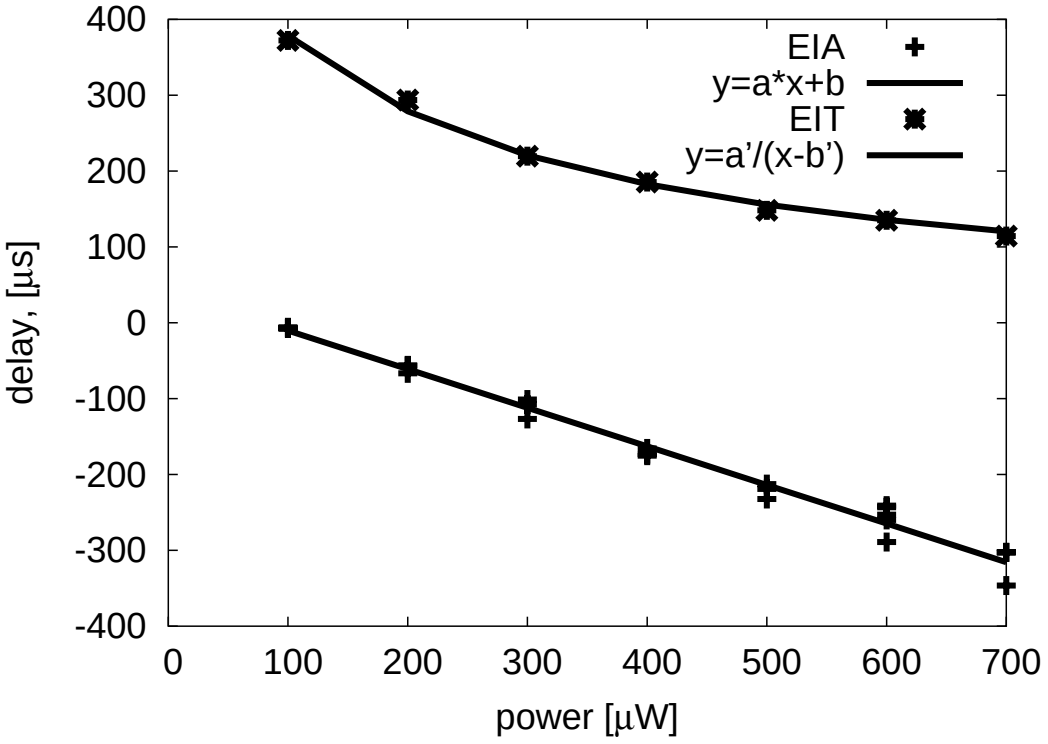

Fig. 62. Positive and negative pulse delay vs power

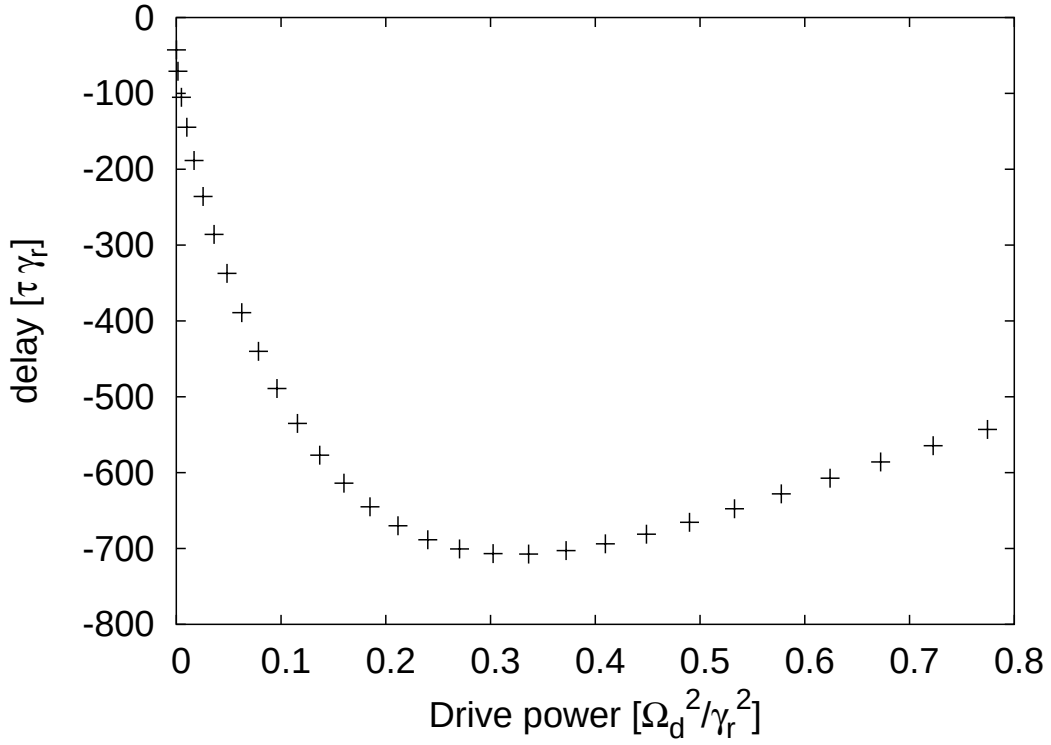

Fig. 63. Numerical calculations of delay time dependence with laser power in the cell with buffer gas. Parameters: $\gamma_{deph} = 10\gamma_r$, $\gamma_{bc} = 5 \times 10^{-4}\gamma_r$, $ku = 50\gamma_r$, $\Omega_d = 0.4\gamma_r$, $\Omega_p = 0.1\gamma_r$.

accordingly to Eq. (8.2). We find that in the region where $\Omega_d^2/\gamma_r^2 \leq 0.18$ the delay time increases proportionally to the laser intensity, and then when power broadening becomes strong enough, the time delay decreases with laser power (see Fig. 9.34) however this region is not covered by our experiment since $\Omega_d \leq .4\gamma_r$.

D. Pulse duration dependences of delay time

It is interesting to compare the dependence of the delay time on pulse duration for the case of EIT and absorption resonance. The Fourier spectrum of the pulse is

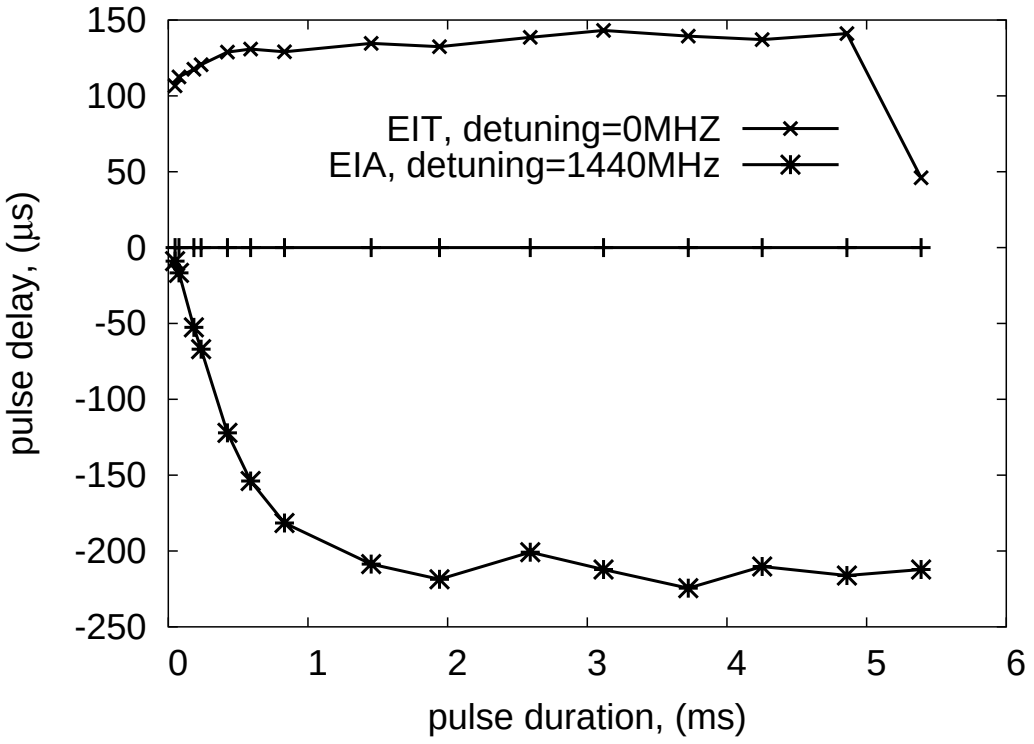

Fig. 64. Delay time with Gaussian pulse duration time.

wider for a shorter pulse. For short enough pulse with spectral width larger then EIT resonance window ($1/t > \gamma_{EIT}$) some Fourier components are outside of the EIT regime and thus have no significant delay. We see in Fig. 64 that for a short pulse, there is a decreasing of delay time due to this process. This is even more pronounced in the case of a absorption resonance when the pulse duration approaches zero, and the delay time also goes to zero (Fig. 64). Similar behavior was observed by Akulshin *et al.* [106] where in the case of a square pulse no delay was observed since such a pulse has all Fourier components.

A similar explanation holds for the dependence of the ratio of outgoing and ingoing Gaussian pulses length vs ingoing pulse duration time. In the case of EIT

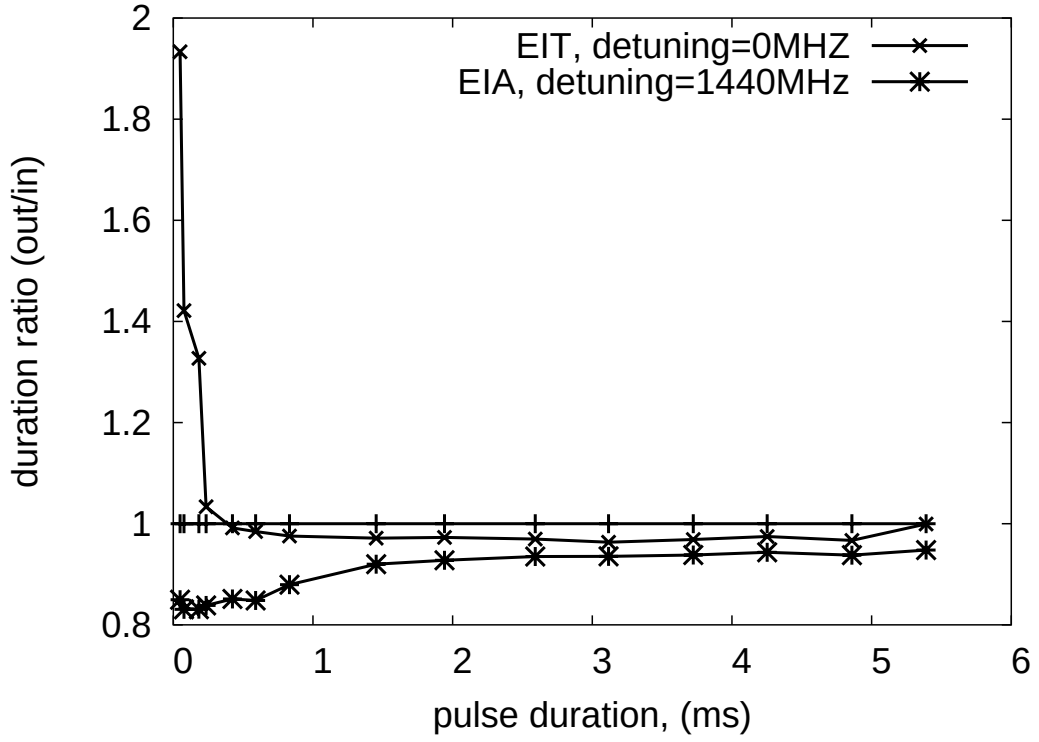

Fig. 65. Ratio of duration times of outgoing and ingoing Gaussian pulses vs ingoing pulse duration time.

narrow EIT resonance cut the larger spectral width of Gaussian pulse and leaves an outgoing duration time in the order of $1/\gamma_{EIT}$ no matter how short was the ingoing pulse (see Fig. 65). In case when the ingoing Gaussian pulse bandwidth $(1/t)$ is smaller then γ_{EIT} no significant change of duration time is observed, and thus the duration ratio stays close to 1. In case of absorption resonance pulse with wider bandwidth, no noticeable reshaping occurs.

E. Discussion

There are many applications for this phase variation $\partial\varphi/\partial\omega$. One example is a magnetometer based on the non-linear Faraday effect. Since the electric field of a plane wave propagating through the medium is given by

$$E(x) = E_0 e^{iknx} = E_0 e^{i\varphi} \tag{8.3}$$

where E is electric field, E_0 is amplitude of this field, and $k = \omega/c$ is wave vector. Then in a thin layer

$$\frac{\partial\varphi}{\partial\omega} = \frac{\omega}{c}\frac{\partial n}{\partial\omega}x + \frac{n}{c}x. \tag{8.4}$$

we neglect second term because of the condition $\omega\partial n/\partial\omega \gg n$ so

$$\frac{\partial\varphi}{\partial\omega} = \frac{\omega}{c}\frac{\partial n}{\partial\omega}x \tag{8.5}$$

Utilizing Eq. 8.2, the phase variation at the end of the cell is

$$\frac{\partial\varphi}{\partial\omega} = \frac{L}{c} < \omega\frac{\partial n}{\partial\omega} >= \tau \tag{8.6}$$

So we see that measurement of delay time τ is a direct tool to find out the phase variation with frequency change. We can estimate the maximal phase difference

$$\Delta\varphi = \frac{\partial\varphi}{\partial\omega}\Delta\omega \approx \frac{\partial\varphi}{\partial\omega}\gamma_{EIT} \approx \tau\gamma_{EIT} \tag{8.7}$$

In our experiment $\tau \approx 3 \cdot 10^{-4}$ S, $\gamma_{EIT} \approx 2\pi \times 2.5 \cdot 10^3$ S^{-1} so $\Delta\varphi \approx 4.7$ rad, this number coincides in order of magnitude with the maximum angle of rotation (10 rad) obtained in [71] for non-linear Faraday rotation in EIT regime on the D_1 line of ^{87}Rb

.

F. Conclusion

We study dependences of the group delay time in ^{87}Rb vapor with buffer gas on power of the laser field and one-photon detuning. We observe linear dependence of negative group delay on power. Variation of one-photon detuning from zero to high values than the homogeneous and inhomogeneous broadening allows us to switch from a regime of positive group delay time to one of negative delay, via modification of the EIT resonance to an absorption-like shape.

As result it is possible to say that the large delay in a coherently prepared medium indicates strong dependence of the refraction index on frequency detuning (sharpness of dispersion). A coherently prepared medium can be used for investigation of different effects which are associated with variation of the refraction index. For instance, proposed to use EIT to measure magnetic fields with extremely high sensitivity [113, 114]. Magnetometer based on EIT was described in [69, 75, 76]. Narrow absorption resonances observed in a coherently prepared medium with buffer gas might help to improve atomic magnetometers. The induced absorption resonance has shown different resonance dependence of the delay (group velocity) on intensity. The delay increases proportionally to the intensity of the laser field for absorption resonance, in the EIT case, it decreases in inversely proportion to the laser power.

CHAPTER IX

COHERENT PROCESS WITH WIDE SPECTRAL BROAD PROBE

A. Introduction

The interaction of an electromagnetic field modulated by phase noise (PN) with media possessing a resonance like absorption or transmission spectrum has been experimentally and theoretically studied. Armstrong [181] pointed out the conversion of PN to amplitude noise in an optical interferometer, then experiments with broad PN radiation from a diode laser passing through an interferometer [182] supported Armstrong's argument, and showed the conversion of intensity fluctuation statistics from Poissonian to Einstein (i.e. exponential intensity distribution). Several experiments were done with PN laser field studying the properties of such field transmitted through a cell with alkali atomic vapor, namely the study of PN conversion to amplitude noise in dense Cs [183] and Rb [184]. There is experimental studies of intensity fluctuations and correlations between drive and probe fields in the EIT regime [185], however we are not aware of any study of the spectral density modification after passing through the medium in the EIT regime.

So far we assumed that the width of the EIT resonance is solely determined by the finite interaction time of atoms with laser fields, and we treated both the probe and drive electro-magnetic fields as monochromatic. In reality, the width of both these fields and their relative frequency fluctuations broaden the EIT resonance. That is why observation of narrow EIT resonance usually requires the use of a phase-lock device which significantly narrows the spectrum of the beat note between the probe and drive fields (in our experiment this beat-note width was less then 100 Hz, which is less then γ_{bc}). Other ways to get coherent probe and drive fields are use of AOM

, EOM or modulation of injection current in the case of diode laser. However these methods have the downside such as additional expenses of buying AOM or EOM , as well as building a phase-lock device. Also in our case the phase-lock device is not very stable, and the EOM produce extra (Stokes) sideband which complicated the analysis of the system.

Experimental observation with non phase-locked lasers leads to a broad EIT resonance width of several MHz, associated with laser linewidth. This effect was theoretically studied by Zubairy *et al.* [81] and experimentally demonstrated by Kim *et al.* [186]. They show that the EIT resonance width is limited by linewidths of the drive and probe fields.

Below we present the way of using incoherent probe or drive fields to observe narrow (less than beat-note spectrum width) EIT resonance.

B. Experiment

The setup for this experiment is described in Chapter III section D. We drive our ^{87}Rb cell with the monochromatic drive field and PN broadened probe field (spectral width $\sim$ 1 MHz). The output of a Standford function generator which produces a white-noise signal with spectral width of 10 MHz is connected to the input of the frequency modulation of a Gigatronics function generator, so the output frequency becomes time dependent

$$f(t) = f_0 + \Delta f(t) \tag{9.1}$$

where f_0 is carrier frequency (6.835 GHz) and $\Delta f(t)$ is noise driven time dependent frequency shift. Since the phase of such oscillation is equal to

$$\varphi(t) = \varphi_0 + f_0 t + \int_{-\infty}^{t} \Delta f(t) dt \tag{9.2}$$

we conclude that we have PN broadened signal. This signal drives an EOM which splits part of the drive field to sidebands corresponding to the probe field, so we obtain the PN broadened probe field instead of a monochromatic probe field which is observed without the PN modulation. The spectral density of the probe signal does not coincide with the distribution of driving frequency because of the limited bandwidth of the EOM response to the modulation frequency.

In canonical EIT resonance observation, the drive field is fixed in frequency and one scans the probe field in the vicinity of the two-photon resonance, looking at the transmission signal with respect to the change of this two-photon detuning.

If one tries to observe the beating frequency of the drive and probe field, she would also measure the beat signal of the drive and second side band which is symmetrically placed with respect to the drive laser frequency. To isolate the probe signal, we introduce an additional field which is shifted by an AOM at 60 MHz with respect to the drive field. This field does not propagate through the ^{87}Rb medium. We observe the beating signal of this additional field and probe field, which occurs at a different frequency from other beat notes. Thus we separate the observation of the probe field from the drive and additional sideband fields. In our PN experiment we record the spectral density of PN broaden transmitted probe field with a spectrum analyzer tuned in the vicinity of the beatnote frequency of the probe and additional fields.

A typical spectral density spectrum is depicted in Fig. 66. Before the cell, the spectral FWHM of the probe field is 980 kHz, and after the cell we see significant narrowing of the spectrum, the FWHM is 4.6 kHz (see also Fig. 67). Also the spectral distribution function is changed, before the cell, we have Gaussian distribution of the spectral density

$$f_{in}(\omega) = e^{-\frac{(\omega-\omega_0)^2}{\omega_w^2}} \tag{9.3}$$

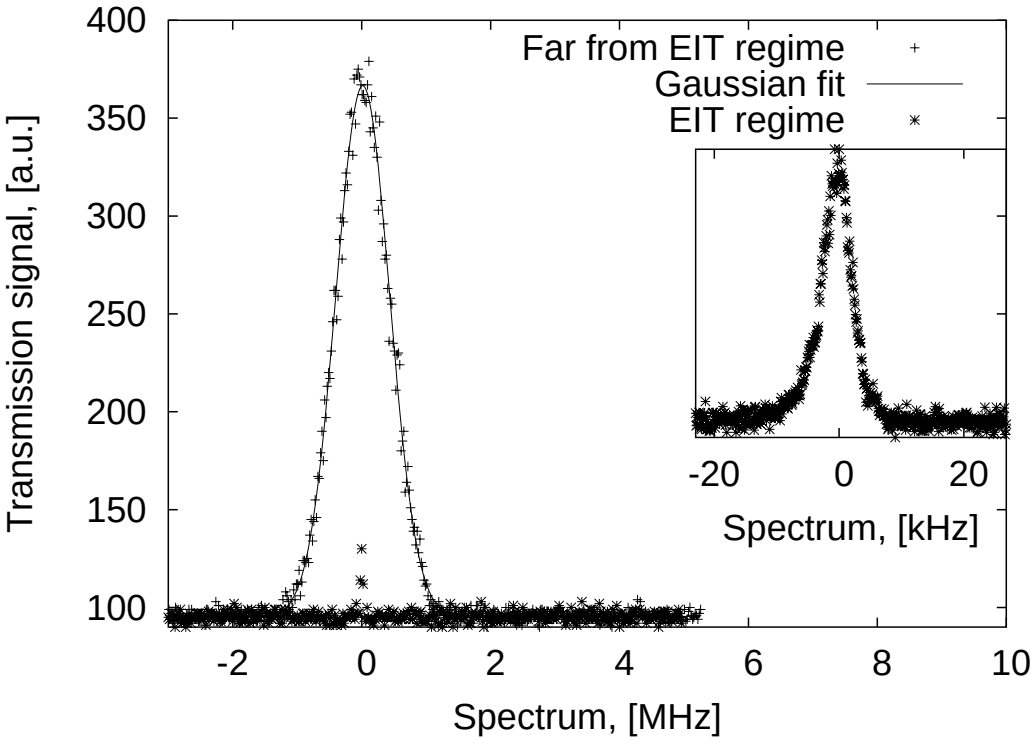

Fig. 66. Spectral density of PN broaden probe field before and after passing the ^{87}Rb cell

where ω_0 is average probe field frequency, ω_w is width of the spectral density spectrum. After the cell the probe field has a Lorentz distribution

$$f_{out} = \frac{\gamma_n^2}{(\omega - \omega_0)^2 + \gamma_n^2} \tag{9.4}$$

where γ_n is width of spectral density spectrum.

In Fig. 67 we compare transmission spectra taken in the similar experimental condition for the cannonical EIT resonance observation (with the coherent drive and probe field) and for the PN broadened probe. Notice that the measured spectra after normalization coincide within our experimental accuracy, which means that $\gamma_n = \gamma_{EIT}$.

C. Discussion

Even though we modulate the phase of our EOM with a source of white noise, due to limited bandwidth of our electronics and the EOM , we did not obtain infinitely broad probe field spectra (which is unphysical anyway). Instead we get a spectral density distribution of the probe electromagnetic field that is limited in width.

1. Very simple model

Transition from phase broadened field to spectral distribution is obtained by the following consideration

$$E_p(t) = E_{p0} e^{-i(\omega_p t + \varphi_p(t))} \tag{9.5}$$

where E_{p0} is the amplitude of the probe field, ω_p is the probe field average frequency, $\varphi_p(t)$ is a random time dependent phase of the electromagnetic field. Taking the Fourier transformation of $E_p(t)$ we obtain the spectral distribution of the probe field

$$E_p(t) = \int E_p(w) e^{-i\omega t} d\omega \tag{9.6}$$

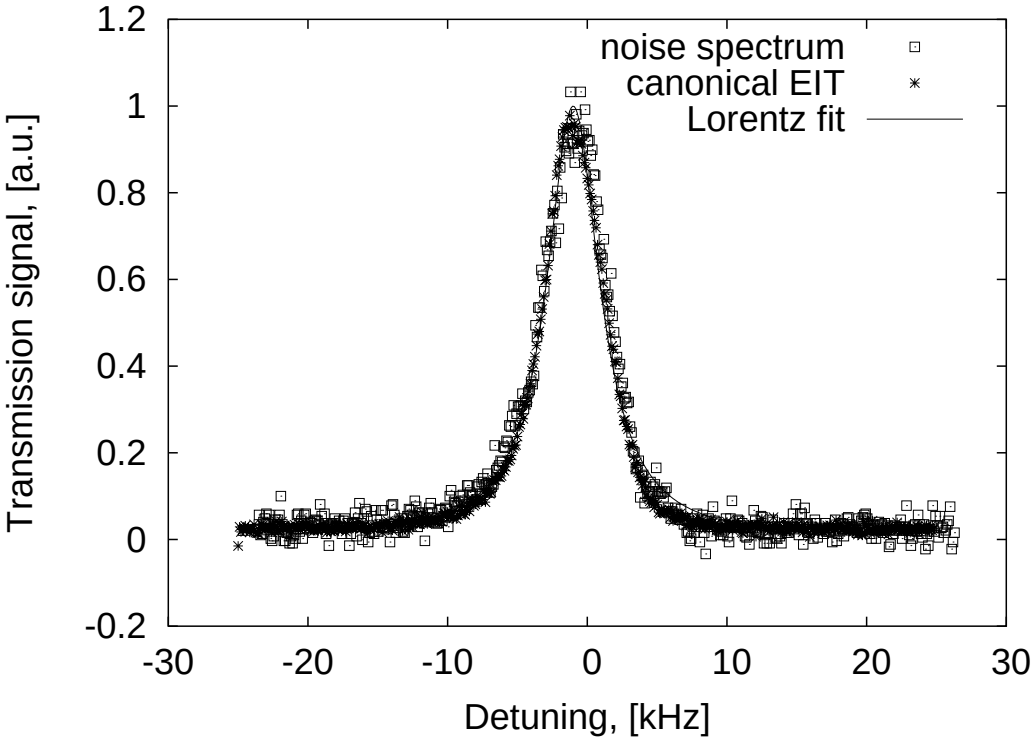

Fig. 67. Comparison of EIT resonance obtained with monochromatic and phase broaden probe field.

where $E_p(\omega)$ is the intensity of the spectral component of the probe field with frequency ω.

Now we assume that the drive field is monochromatic. We assume that we can apply all previously derived equations for density matrix Eqs. (2.61-9.14) and susceptibility Eq. (4.14) for each Fourier component independently from other components. Since the susceptibility does not depend on the power of the probe beam for weak probe power, we conclude that the spectral density signal of light transmitted through an optically thin cell is given by following expression

$$f_{out}(\omega) = E_p(w)\chi'(\omega, \omega_d, \Omega_d) \tag{9.7}$$

where $\chi'(\omega, \omega_d, \Omega_d)$ is given by Eq. (4.14).

In the case when the input probe field spectra is much broader than the EIT resonance, we can neglect dependence of $E_p(\omega)$ on ω and just take $E_p(\omega) = E_p(\omega_p) = E_p$. This explains the coincidence of spectra in Fig. 67.

2. More general approach

Let us write the phase-noise broadened probe and drive field as

$$E_p(t) = E_{p0}e^{-i(\omega_p t+\varphi_p(t))}, E_d(t) = E_{d0}e^{-i(\omega_d t+\varphi_d(t))} \tag{9.8}$$

Then

$$\dot{\rho}_{ab} = -(\Gamma_{ab} + \dot{\varphi}_p)\rho_{ab} + i\Omega_p(\rho_{bb} - \rho_{aa}) + i\Omega_d\rho_{cb} \tag{9.9}$$

$$\dot{\rho}_{ca} = -(\Gamma_{ca} - \dot{\varphi}_d)\rho_{ca} + i\Omega_d^*(\rho_{aa} - \rho_{cc}) - i\Omega_p^*\rho_{cb} \tag{9.10}$$

$$\dot{\rho}_{cb} = -(\Gamma_{cb} + \dot{\varphi}_p - \dot{\varphi}_d)\rho_{cb} - i\Omega_p\rho_{ca} + i\Omega_d^*\rho_{ab} \tag{9.11}$$

In the case when the probe and drive field are phase correlated ($\dot{\varphi}_d = \dot{\varphi}_p$) then ρ_{cb} term remains the same as in the case of monochromatic probe and drive fields (this is the essence of phase-lock technique).

It can be shown that if the phase fluctuation are Brownian such that $\langle\varphi_d\rangle = 0$, $\langle\varphi_p\rangle = 0$, and $\langle\dot{\varphi}_d(t)\dot{\varphi}_d(t')\rangle = 2D_d\delta(t'-t)$, $\langle\dot{\varphi}_p(t)\dot{\varphi}_p(t')\rangle = 2D_p\delta(t'-t)$ then [81, 186]

$$\dot{\rho}_{ab} = -(\Gamma_{ab} + D_p)\rho_{ab} + i\Omega_p(\rho_{bb} - \rho_{aa}) + i\Omega_d\rho_{cb} \tag{9.12}$$

$$\dot{\rho}_{ca} = -(\Gamma_{ca} + D_d)\rho_{ca} + i\Omega_d^*(\rho_{aa} - \rho_{cc}) - i\Omega_p^*\rho_{cb} \tag{9.13}$$

$$\dot{\rho}_{cb} = -(\Gamma_{cb} + D_p + D_d)\rho_{cb} - i\Omega_p\rho_{ca} + i\Omega_d^*\rho_{ab} \tag{9.14}$$

so we see that the solution remains the same with proper modification of Γ_{ab}, Γ_{ca}, and Γ_{cb}. But the main modification is that the EIT resonance is now broadened by the $D_p + D_d$ term.

But let us have a look at propagation of the following signal

$$S(t) = \Omega_p(t)\Omega_d^*(t). \tag{9.15}$$

where signal (S) corresponds to the amplitude of the measured beatnote signal.

$$\frac{\partial S}{\partial z} = -i\eta\rho_{ab}\Omega_d^* + i\eta\rho_{ca}\Omega_p \tag{9.16}$$

We substitute ρ_{ab} and ρ_{ca} as solutions of the Eqs. (2.45–2.46) where we assume that $\dot{\rho}_{ab} = \dot{\rho}_{ca} = 0$ (adiabatic approximation). We do this because bandwidth of the PN is less then γ. However we have to keep term corresponding to $\dot{\rho}_{cb}$ since Γ_{cb} is smaller then bandwidth of PN . Then

$$\frac{\partial S}{\partial z} = \eta\left(\frac{n_{ab}}{\Gamma_{ab}} - \frac{n_{ca}}{\Gamma_{ca}}\right)S - \eta\left(\frac{|\Omega_d|^2}{\Gamma_{ab}} + \frac{|\Omega_p|^2}{\Gamma_{ca}}\right)\rho_{cb} \tag{9.17}$$

$$\dot{\rho}_{cb} = -\left(\Gamma_{cb} + \frac{|\Omega_d|^2}{\Gamma_{ab}} + \frac{|\Omega_p|^2}{\Gamma_{ca}}\right)\rho_{cb} + \left(\frac{n_{ab}}{\Gamma_{ab}} - \frac{n_{ca}}{\Gamma_{ca}}\right)S \tag{9.18}$$

At the next step let us see how the correlation signal ($R(\tau) = \langle SS_\tau \rangle$) propagates

$$\frac{\partial}{\partial z}\langle SS_\tau\rangle = 2\eta\left(\frac{n_{ab}}{\Gamma_{ab}} - \frac{n_{ca}}{\Gamma_{ca}}\right)\langle SS_\tau\rangle - 2\eta\left(\frac{|\Omega_d|^2}{\Gamma_{ab}} + \frac{|\Omega_p|^2}{\Gamma_{ca}}\right)\langle S\rho_{cb}(\tau)\rangle \tag{9.19}$$

$$\frac{\partial}{\partial \tau}\langle S\rho_{cb}(\tau)\rangle = -\left(\Gamma_{cb} + \frac{|\Omega_d|^2}{\Gamma_{ab}} + \frac{|\Omega_p|^2}{\Gamma_{ca}}\right)\langle S\rho_{cb}(\tau)\rangle + \left(\frac{n_{ab}}{\Gamma_{ab}} - \frac{n_{ca}}{\Gamma_{ca}}\right)\langle SS_\tau\rangle \tag{9.20}$$

Now let us present spectral density of the correlation function of the signal (I_ω)

$$\langle S(t,z)S(t+\tau,z)\rangle = \int I_\omega e^{-i\omega\tau}d\omega \tag{9.21}$$

and assuming that the signal and coherence correlation expressed as following

$$\langle S(t,z)\rho_{cb}(t+\tau,z)\rangle = \int \rho_\omega e^{-i\omega\tau}d\omega \tag{9.22}$$

we obtain

$$\rho_\omega = \frac{\left(\frac{n_{ab}}{\Gamma_{ab}} - \frac{n_{ca}}{\Gamma_{ca}}\right)I_\omega}{\Gamma_{cb} + \frac{|\Omega_d|^2}{\Gamma_{ab}} + \frac{|\Omega_p|^2}{\Gamma_{ca}} - i\omega} \tag{9.23}$$

$$\frac{\partial}{\partial z}I_\omega = 2\eta\frac{(\Gamma_{cb} - i\omega)\left(\frac{n_{ab}}{\Gamma_{ab}} - \frac{n_{ca}}{\Gamma_{ca}}\right)}{\Gamma_{cb} + \frac{|\Omega_d|^2}{\Gamma_{ab}} + \frac{|\Omega_p|^2}{\Gamma_{ca}} - i\omega}I_\omega \tag{9.24}$$

Assuming that $\Omega_p \ll \Omega_d$ all population is at state $|b\rangle$

$$\frac{\partial}{\partial z}I_\omega = 2\eta\frac{(\Gamma_{cb} - i\omega)}{\Gamma_{cb} + \frac{|\Omega_d|^2}{\Gamma_{ab}} + \frac{|\Omega_p|^2}{\Gamma_{ca}} - i\omega}\frac{1}{\Gamma_{ab}}I_\omega \tag{9.25}$$

The term in the front of I_ω in left hand side of above equation coincides with the expression for susceptibility in Eq. 4.9 and thus all formalism derived above for the probe field propagation is applied for the spectral density of the beatnote signal correlation function propagation. For example, the expression for the width of the EIT signal is identical to the expression for the width of the spectral density of the correlation function.

D. Applications

As we have just shown, all formal apparatus developed for calculation of EIT properties is valid for the spectral density of the beatnote signal of the incoherent probe as well. Thus we can apply our general knowledge about EIT properties for the case of the incoherent probe and see what possible application are.

1. Modification of correlation function

Let us say that our spectral broadened probe field has following spectral distribution $S_p(\omega)$ then

$$< |S|^2 >= I_p = \int |S(w)|^2 d\omega = \int I_\omega d\omega \tag{9.26}$$

where $E_p(\omega)$ and I_ω are spectral distribution of the electromagnetic field and its intensity.

Then the correlation function $R(\tau)$ defined as

$$R(\tau) =< S(t)S(t+\tau) > \tag{9.27}$$

can be expressed through the spectral density of intensity as [187]

$$R(\tau) = \int I_\omega e^{-i\omega\tau} d\omega \tag{9.28}$$

and on the other hand

$$I_\omega = \frac{1}{2\pi} \int R(\tau) e^{i\omega\tau} d\tau \tag{9.29}$$

Using Eqs. 9.3 and 9.4 we obtain

$$R_{in}(\tau) = \frac{1}{2\pi} \int e^{-\frac{(\omega-\omega_p)^2}{\omega_w^2}} e^{-i\omega\tau} d\omega = \frac{\omega_w}{2\sqrt{\pi}} e^{-\frac{\omega_w^2\tau^2}{4} - i\omega_p\tau} \tag{9.30}$$

$$R_{out}(\tau) = \frac{1}{2\pi} \int \frac{\gamma_n^2}{(\omega-\omega_0)^2 + \gamma_n^2} e^{-i\omega\tau} d\omega = \frac{\gamma_n}{\pi} e^{-\gamma_n|\tau| - i\omega_0\tau} \tag{9.31}$$

From Eq. 9.28 we see that by changing the spectral density we change the correlation function I_ω as well. As we can see in Fig. 66 we modify input spectrum from broad Gaussian to narrow Lorentz at the output of the cell. Thus we significantly increase the correlation time of the output probe field τ_{out} with respect to the correlation time of the ingoing probe field τ_{in}. Characteristic coherence time $\tau_{in} = 2/\omega_w$ for the input probe field is much smaller then the characteristic coherence time of the output radiation $\tau_{out} = 2/\gamma_n = 2/\gamma_{EIT}$, since width $\omega_w \gg \gamma_{EIT}$.

If one is required to obtain a source with long coherence time source of radiation with low coherence, use of coherent media under condition of EIT resonance would be a good tool for that.

Let us note that the narrow EIT resonance behaves as narrow signal spectral filter, we supply wide spectrally broadened probe field and obtain in the output of the cell a filtered signal with the width of the spectrum of the order of several kHz (see for example Fig. 66. Also this filter has variable spectral width, we can change the spectral width of the filter by varying several experimental parameters such as a density of ^{87}Rb atoms and applied power of the probe or drive field. We know that the width of the EIT changes with the density of atoms

$$\gamma_{EIT} = \frac{\gamma_{bc} + \frac{\Omega^2}{\gamma}}{\sqrt{\eta L}} \tag{9.32}$$

where γ_{bc} is decay rate of the ground levels coherence, Ω is Rabi frequency of the driving field, γ is decay rate of upper level, L is cell length, N is density of atoms, λ is the probe field wave length.

So the higher the density the narrow is the EIT resonance. Since the density of ^{87}Rb atoms can be easily changed by changing the temperature of the cell it gives us nice control over the width of EIT. This can also be achieved if we change the power of the drive or probe laser which can be done very quickly by changing current of the

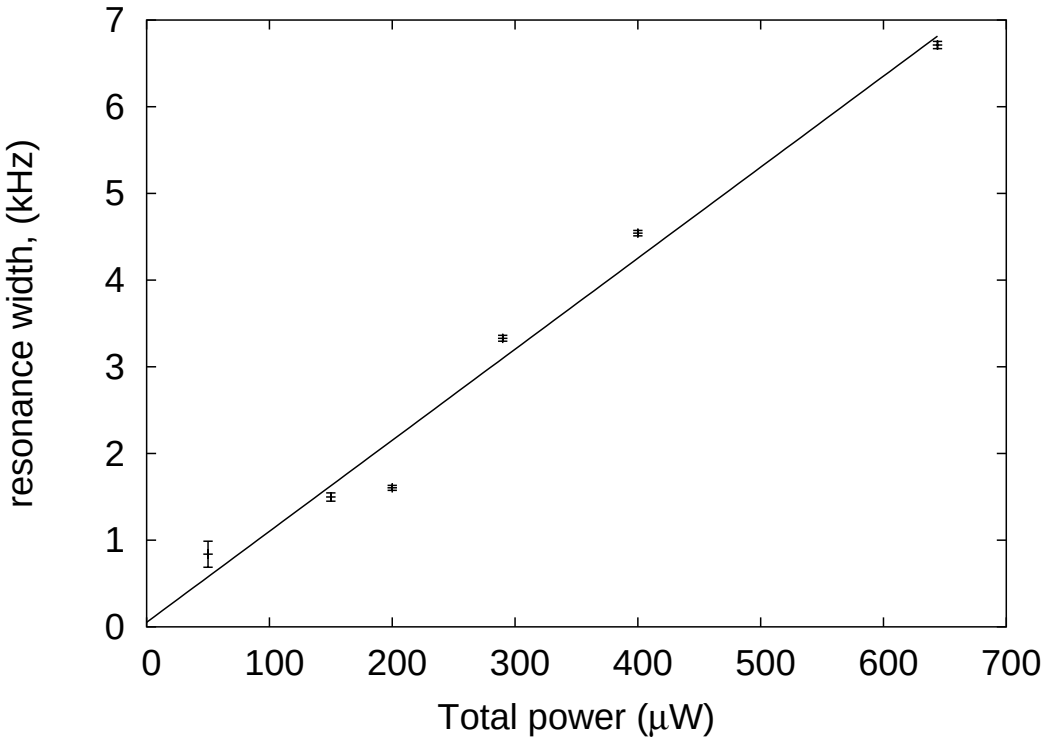

Fig. 68. Dependence of spectral width of transmitted trough the cell probe field vs total power under condition of EIT resonance.

lasers or applying neutral density filter to the laser field, or by several others way. We will be able to change power broadening of the EIT resonance width and thus spectral filter bandwidth. This point is illustrated in Fig. 68, where we measure dependence of transmitted spectral width of the signal on the power of the drive and probe lasers (power of both laser is changed with the same constant proportionality by varying the angle between two crossed polarizers). All of the above is applied to the correlation function modification. So we can modify correlation time in a controllable fashion.

Also we can tune the position of the EIT resonance, and thus change the central frequency of our spectral signal filter. This may be done, for example, by applying a

magnetic field and splitting the EIT resonance to several parts, where the position of the EIT resonance depends on the magnetic field (see Fig. 69). Other mechanism can be used for this as well, for example, the Stark shift of the EIT resonance depends on laser power. Or as we show in previous section, the position of the two photon resonance is tied to the ground level splitting and only slightly changes with one-photon detuning, we can see that changing the drive one-photon detuning we will change the frequency of transmitted field or central frequency of the filter according to the two-photon resonance condition

$$\omega_p = \omega_d + \omega_{gs} \tag{9.33}$$

where ω_{gs} is ground level splitting frequency (≈ 6.835 GHz for ^{87}Rb).

2. Magnetometer

A simple magnetometer (similar to that suggested by Wynands *et al.* [69]) is also possible with this technique. Since the position of different magnetic sublevels is dependent on magnetic field (Zeeman splitting) it means that in nonzero magnetic field we will observe several EIT resonances corresponding to the transitions between different magnetic sublevels.

The difference in the position of these levels, and hence difference in frequency of the EIT two photon resonance position, is well known and given by following expression ([188] page 37)

$$\Delta\omega_{eit}^{\pm}(m, m' = m - 1) = 2\pi(\Gamma^{\pm}B \mp (2m - 1)GB^2) \tag{9.34}$$

where B is magnetic field, m and m' are the quantum number of different Zeeman sublevels, $\Gamma^{\pm}$ and G are constants that are different for different atoms. Sign "+" corresponds to magnetic sublevels with quantum number $F = I + 1/2$ and sign "-

" corresponds to $F = I - 1/2$, where I is nuclear spin of the atom. For ^{87}Rb , $\Gamma^{+} = 699605$ Hz/G, $\Gamma^{-} = 702399$ Hz/G and $G = 71.8$ Hz/G^2.

If we use a probe field with spectral width larger then $\omega_{EIT}(m, m')$, we will get after the cell the filtered probe field with frequencies corresponding to two photon resonances for different Zeeman sublevels. This can be detected on a spectrum analyzer (see Figs. 69). Similar results based on buffer gas induced absorption (BGIA) resonance discussed in Chapter VII are shown in Fig. 70. Also we can detect the beat note frequency corresponding to the frequency equal to $\Delta\omega_{EIT}(m, m')$ on a frequency counter. From the measurement of this frequency we can easily calculate the magnetic field B since the other parameters are known.

3. Modification of the spectral density distribution and spectral hole burning

Recalling the properties of the BGIA resonances described in the Chapter VII, we can not only narrow the transmitted spectrum, but also burn a hole in such spectral density distribution, or at least significantly suppress the amplitude of the spectral harmonics corresponding to the two-photon resonance. An example of this is shown in Fig. 71. One photon-detuning increases from zero from bottom curve up to 1.3 GHz on the top curve.

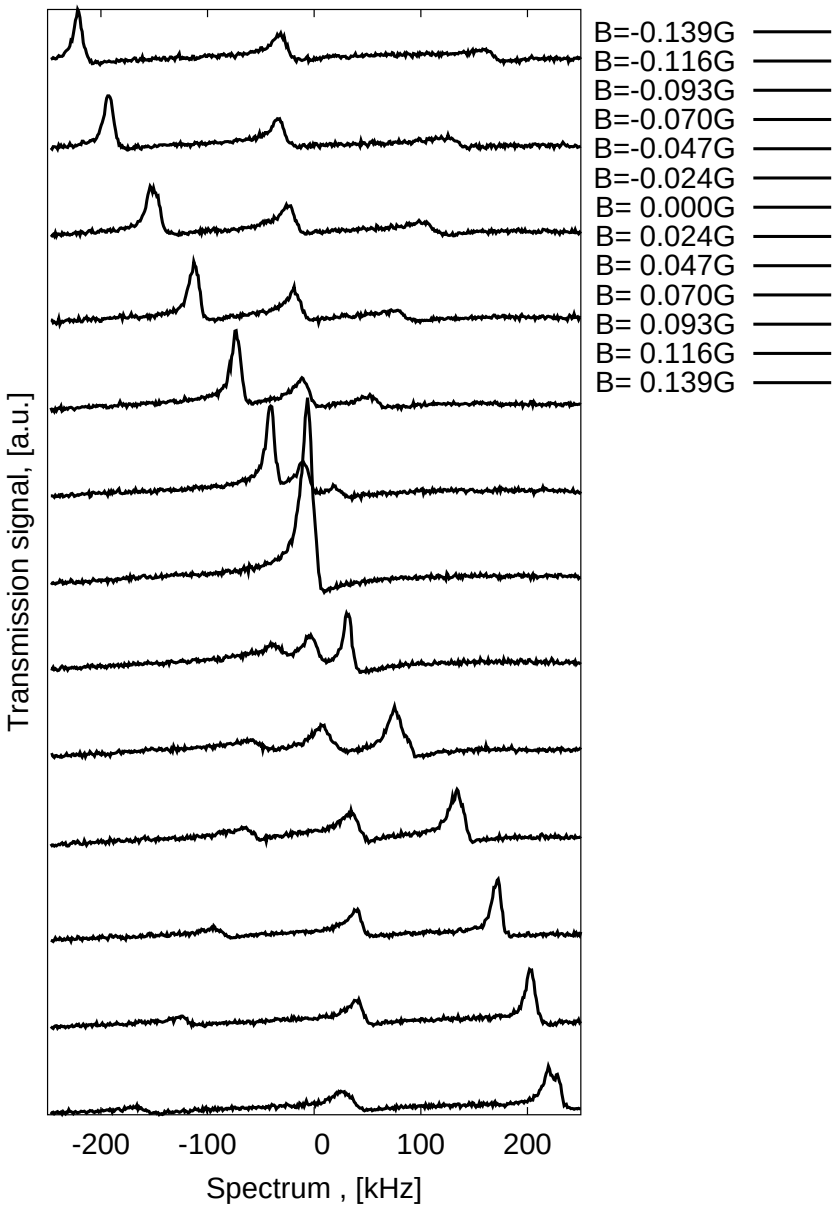

Fig. 69. Transmission spectra of noise broaden probe field for different magnetic field (voltages applied to internal solenoid) taken in EIT regime.

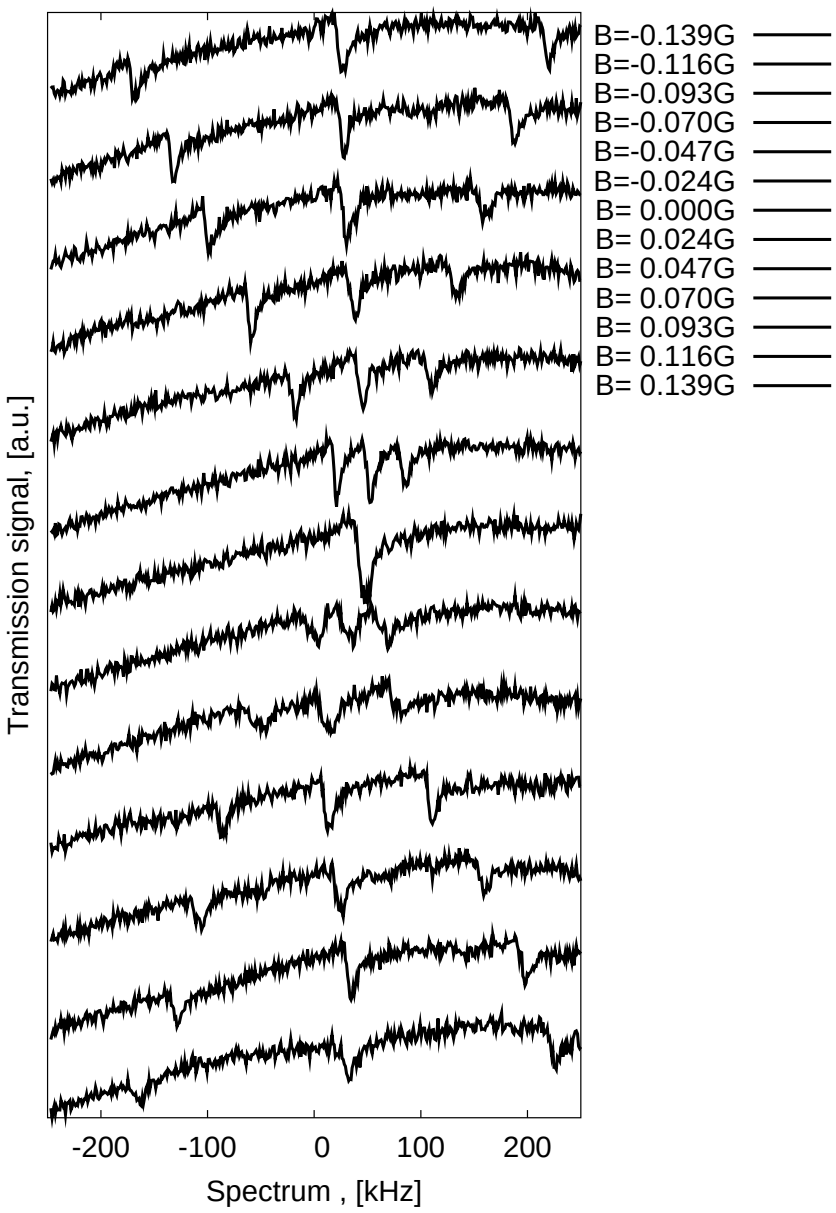

Fig. 70. Transmission spectra of noise broaden probe field for different magnetic field (voltages applied to internal solenoid) taken in BGIA regime.

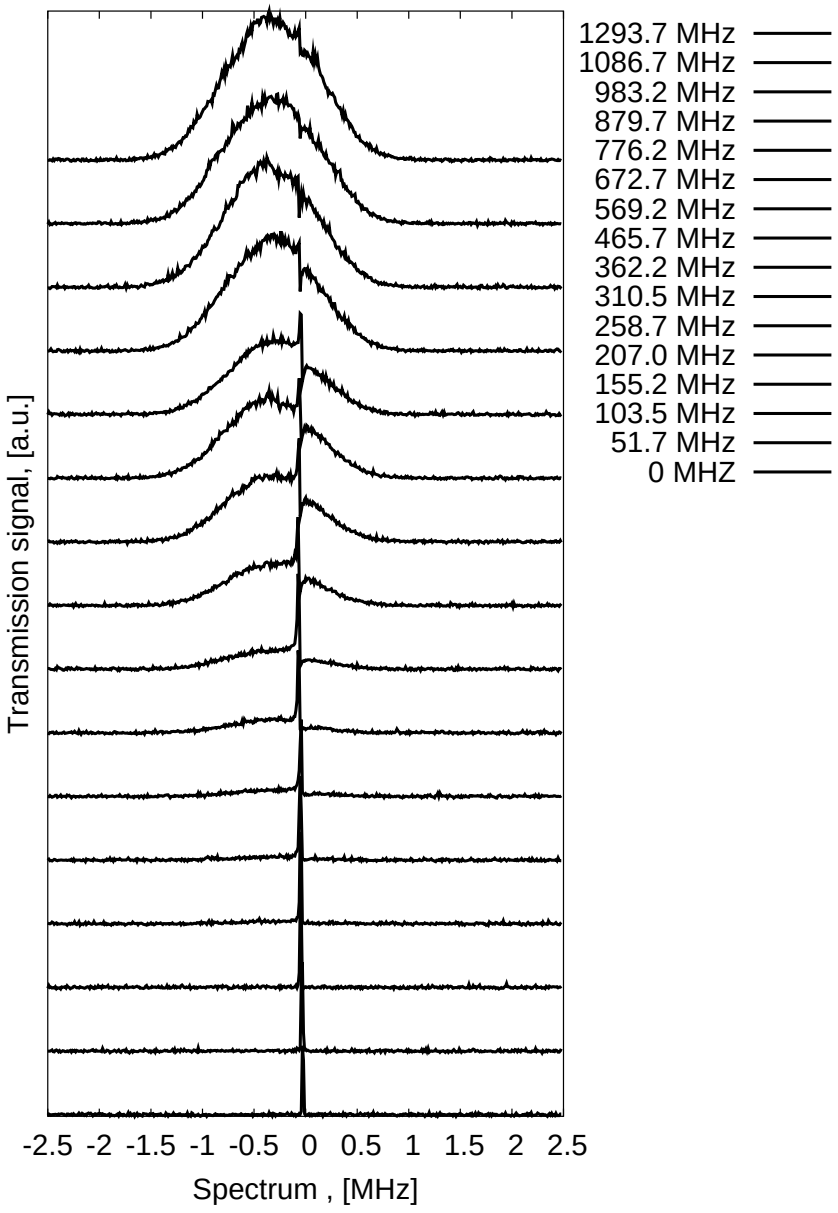

Fig. 71. Various transmission spectral density distribution for noise broaden probe signal with different one-photon detuning of drive field. Detuning grows from zero for bottom curve up to 1.3 GHz for the top curve.

CHAPTER X

CONCLUSION

In this work we have studied properties of coherent media. We have studied the drive and probe power dependences on width of the EIT resonance. We show the connection between the width of the resonance and the group velocity of probe light pulse propagation in the media under conditions of EIT . We show that the addition of buffer gas to the ^{87}Rb cell dramatically changes the properties of the EIT regime. It changes not only the width of the resonance, but also the shape of the EIT resonances and leads to observation of an absorption-like resonance for large one-photon drive detunings. Also it changes the dispersive properties of the media. We show that group velocity of probe field is smaller for the blue one-photon detuning of the drive field in a buffered cell.

Under the conditions leading to a new absorption resonance regime, we find large negative pulse delay which corresponds to a "fast" light regime where the speed of light is negative (less then 100 m/S).

Furthermore, we demonstrate that even in the case of phase noise broadened probe field, we can observe a narrow beatnote signal with spectral width coinciding with that of the EIT resonance. Several applications of this technique for magnetometry, spectral holeburning, correlation time modification are outlined.

REFERENCES

[1] W. Hanle, Z. Phys. **30**, 93 (1924).

[2] G. Moruzzi and F. Strumia, *The Hanle Effect and Level-Crossing Spectroscopy* (Plenum Press; New York and London, 1991).

[3] M. O. Scully and M. S. Zubairy, *Quantum Optics* (Cambridge University Press, Cambridge, UK, 1997).

[4] E. Alexandrov, M. Chaika, and G. Khvostenko, *Interference of Atomic States* (Springer-Verlag; Berlin, 1993).

[5] G. Alzetta, A. Gozzini, L. Moi, and G. Orriols, Nouvo Cimento Soc. Ital. Fis. B-Gen. Phys. Relativ. Astron. Math. Phys. Methods **36**, 5 (1976).

[6] E. Arimondo and G. Orriols, Nuovo Cimento Lett. **17**, 333 (1976).

[7] K. Zaheer and M. S. Zubairy, Phys. Rev. A **39**, 2000 (1989).

[8] G. S. Agarwal and N. Nayak, J. Phys. B-At. Mol. Opt. Phys. **19**, 3385 (1986).

[9] P. M. Radmore and P. L. Knight, J. Phys. B-At. Mol. Opt. Phys. **15**, 561 (1982).

[10] P. M. Radmore and P. L. Knight, Phys. Lett. A **102**, 180 (1984).

[11] B. J. Dalton and P. L. Knight, Opt. Commun. **42**, 411 (1982).

[12] G. Alzetta, L. Moi, and G. Orriols, Nouvo Cimento Soc. Ital. Fis. B-Gen. Phys. Relativ. Astron. Math. Phys. Methods **52**, 209 (1979).

[13] J. D. Stettler, C. M. Bowden, N. M. Witriol, and J. H. Eberly, Phys. Lett. A **73**, 171 (1979).

[14] H. R. Gray, R. M. Whitley, and C. R. Stroud, Opt. Lett. **3**, 218 (1978).

[15] R. M. Whitley and C. R. Stroud, Phys. Rev. A **14**, 1498 (1976).

[16] B. D. Agapyev, M. B. Gornyi, B. G. Matisov, and Y. V.Rozhdestvenskii, Usp. Fiz. Nauk **163**, 1 (1993).

[17] E. Arimondo, Progress in Optics **XXXV**, 259 (1996).

[18] S. E. Harris, J. E. Field, and A. Imamoglu, Phys. Rev. Lett. **64**, 1107 (1990).

[19] J. E. Field, K. H. Hahn, and S. E. Harris, Phys. Rev. Lett. **67**, 3062 (1991).

[20] K. J. Boller, A. Imamoglu, and S. E. Harris, Phys. Rev. Lett. **66**, 2593 (1991).

[21] K. H. Hahn, D. A. King, and S. E. Harris, Phys. Rev. Lett. **65**, 2777 (1990).

[22] J. P. Marangos, J. Mod. Opt. **45**, 471 (1998).

[23] S. E. Harris, Phys. Today **50**, 36 (1997).

[24] M. O. Scully, S. Y. Zhu, and A. Gavrielides, Phys. Rev. Lett. **62**, 2813 (1989).

[25] M. O. Scully, Phys. Rev. Lett. **67**, 1855 (1991).

[26] K. Hakuta, L. Marmet, and B. P. Stoicheff, Phys. Rev. Lett. **66**, 596 (1991).

[27] O. Kocharovskaya, Phys. Rep.-Rev. Sec. Phys. Lett. **219**, 175 (1992).

[28] O. A. Kocharovskaya and Y. I. Khanin, Jetp Lett. **48**, 630 (1988).

[29] M. O. Scully and M. Fleischhauer, Phys. Rev. Lett. **69**, 1360 (1992).

[30] D. J. Fulton, S. Shepherd, R. R. Moseley, B. D. Sinclair, and M. H. Dunn, Phys. Rev. A **52**, 2302 (1995).

[31] Y. Q. Li and M. Xiao, Opt. Lett. **21**, 1064 (1996).

[32] J. M. Zhao, L. R. Wang, L. T. Xiao, Y. T. Zhao, W. B. Yin, and S. T. Jia, Opt. Commun. **206**, 341 (2002).

[33] K. Yamamoto, K. Ichimura, and N. Gemma, Phys. Rev. A **58**, 2460 (1998).

[34] H. Lee and M. O. Scully, Found. Phys. **28**, 585 (1998).

[35] J. A. Vaccaro, A. V. Durrant, D. Richards, S. A. Hopkins, H. X. Chen, and K. E. Hill, J. Mod. Opt. **45**, 315 (1998).

[36] C. Fort, F. S. Cataliotti, T. W. Hansch, M. Inguscio, and M. Prevedelli, Opt. Commun. **139**, 31 (1997).

[37] S. A. Hopkins, E. Usadi, H. X. Chen, and A. V. Durrant, Opt. Commun. **138**, 185 (1997).

[38] S. D. Badger, I. G. Hughes, and C. S. Adams, J. Phys. B-At. Mol. Opt. Phys. **34**, L749 (2001).

[39] J. J. Clarke, W. A. van Wijngaarden, and H. X. Chen, Phys. Rev. A **6402**, 023818 (2001).

[40] D. McGloin, D. J. Fulton, and M. H. Dunn, Opt. Commun. **190**, 221 (2001).

[41] J. R. Boon, E. Zekou, D. McGloin, and M. H. Dunn, Phys. Rev. A **59**, 4675 (1999).

[42] S. Shepherd, D. J. Fulton, and M. H. Dunn, Phys. Rev. A **54**, 5394 (1996).

[43] R. R. Moseley, S. Shepherd, D. J. Fulton, B. D. Sinclair, and M. H. Dunn, Opt. Commun. **119**, 61 (1995).

[44] G. G. Padmabandu, G. R. Welch, I. N. Shubin, E. S. Fry, D. E. Nikonov, M. D. Lukin, and M. O. Scully, Phys. Rev. Lett. **76**, 2053 (1996).

[45] A. S. Zibrov, M. D. Lukin, D. E. Nikonov, L. W. Hollberg, M. O. Scully, and V. L. Velichansky, Laser Phys. **5**, 553 (1995).

[46] E. S. Fry, X. F. Li, D. Nikonov, G. G. Padmabandu, M. O. Scully, A. V. Smith, F. K. Tittel, C. Wang, S. R. Wilkinson, and S. Y. Zhu, Phys. Rev. Lett. **70**, 3235 (1993).

[47] A. Nottelmann, C. Peters, and W. Lange, Phys. Rev. Lett. **70**, 1783 (1993).

[48] Y. F. Li and J. F. Sun, Acta Phys. Sin. **52**, 547 (2003).

[49] P. S. Bhatia, G. R. Welch, and M. O. Scully, J. Opt. Soc. Am. B-Opt. Phys. **18**, 1587 (2001).

[50] D. A. Cardimona and D. H. Huang, Phys. Rev. A **65**, 033828 (2002).

[51] M. Fleischhauer, C. H. Keitel, L. M. Narducci, M. O. Scully, S. Y. Zhu, and M. S. Zubairy, Opt. Commun. **94**, 599 (1992).

[52] A. Imamoglu and S. E. Harris, Opt. Lett. **14**, 1344 (1989).

[53] A. Imamoglu, J. E. Field, and S. E. Harris, Phys. Rev. Lett. **66**, 1154 (1991).

[54] A. Lyras, X. Tang, P. Lambropoulos, and J. Zhang, Phys. Rev. A **40**, 4131 (1989).

[55] S. E. Harris and J. J. MacKlin, Phys. Rev. A **40**, 4135 (1989).

[56] A. Imamoglu, Phys. Rev. A **40**, 2835 (1989).

[57] S. E. Harris, Phys. Rev. Lett. **62**, 1033 (1989).

[58] P. P. Sorokin and J. H. Glownia, Astron. Astrophys. **384**, 350 (2002).

[59] A. S. Zibrov, M. D. Lukin, D. E. Nikonov, L. Hollberg, M. O. Scully, and V. L. Velichansky, Laser Physics **5**, 563 (1995).

[60] A. S. Zibrov, M. D. Lukin, D. E. Nikonov, L. Hollberg, M. O. Scully, V. L. Velichansky, and H. G. Robinson, Phys. Rev. Lett **75**, 1499 (1995).

[61] S. Brandt, A. Nagel, R. Wynands, and D. Meschede, Phys. Rev. A **56**, R1063 (1997).

[62] J. Vanier, A. Godone, and F. Levi, Phys. Rev. A **58**, 2345 (1998).

[63] M. Erhard and H. Helm, Phys. Rev. A **63**, 043813 (2001).

[64] M. D. Lukin, M. Fleischhauer, A. S. Zibrov, H. G. Robinson, V. L. Velichansky, L. Hollberg, and M. O. Scully, Phys. Rev. Lett. **79**, 2959 (1997).

[65] A. M. Akulshin, A. A. Celikov, and V. L. Velichansky, Opt. Commun. **84**, 139 (1991).

[66] A. M. Akulshin, S. Barreiro, and A. Lezama, Phys. Rev. A **57**, 2996 (1998).

[67] A. Javan, O. Kocharovskaya, H. Lee, and M. O. Scully, Phys. Rev. A **66**, 013805 (2002).

[68] A. V. Taichenachev, A. M. Tumaikin, and V. I. Yudin, Jetp Lett. **72**, 119 (2000).

[69] R. Wynands and A. Nagel, Appl. Phys. B **68**, 1 (1998).

[70] D. Budker, V. Yashchuk, and M. Zolotorev, Phys. Rev. Lett. **81**, 5788 (1998).

[71] I. Novikova, A. B. Matsko, and G. R. Welch, Opt. Lett. **26**, 1016 (2001).

[72] V. A. Sautenkov, M. D. Lukin, C. J. Bednar, I. Novikova, E. Mikhailov, M. Fleischhauer, V. I. Velichansky, G. R. Welch, and M. O. Scully, Phys. Rev. A **62**, 023810 (2000).

[73] I. Novikova, A. B. Matsko, and G. R. Welch, J. Mod. Opt. **49**, 2565 (2002).

[74] I. Novikova and G. R. Welch, J. Mod. Opt. **49**, 349 (2002).

[75] M. Stahler, S. Knappe, C. Affolderbach, W. Kemp, and R. Wynands, Europhysics Lett. **54**, 323 (2001).

[76] A. Nagel, L. Graf, A. Naumov, E. Mariotti, V. B. D. Meschede, and R. W. and, Europhysics Lett. **44**, 31 (1998).

[77] S. Knappe, R. Wynands, J. Kitching, H. G. Robinson, and L. Hollberg, J. Opt. Soc. Am. B-Opt. Phys. **18**, 1545 (2001).

[78] S. E. Harris, J. E. Field, and A. Kasapi, Phys. Rev. A **46**, R29 (1992).

[79] O. Schmidt, R. Wynands, Z. Hussein, and D. Meschede, Phys. Rev. A **53**, R27 (1996).

[80] F. Renzoni and E. Arimondo, Opt. Commun. **178**, 345 (2000).

[81] S. Sultana and M.S.Zubairy, Phys. Rev. A **49**, 438 (1994).

[82] O. Kocharovskaya, P. Mandel, and M. O. Scully, Phys. Rev. Lett. **74**, 2451 (1995).

[83] U. Rathe, M. Fleischhauer, S. Y. Zhu, T. W. Hansch, and M. O. Scully, Phys. Rev. A **47**, 4994 (1993).

[84] M. Fleischhauer, C. H. Keitel, M. O. Scully, C. Su, B. T. Ulrich, and S. Y. Zhu, Phys. Rev. A **46**, 1468 (1992).

[85] M. Fleischhauer, C. H. Keitel, M. O. Scully, and C. Su, Opt. Commun. **87**, 109 (1992).

[86] M. O. Scully and S. Y. Zhu, Opt. Commun. **87**, 134 (1992).

[87] A. S. Zibrov, M. D. Lukin, L. Hollberg, D. E. Nikonov, M. O. Scully, H. G. Robinson, and V. L. Velichansky, Phys. Rev. Lett **76**, 3935 (1996).

[88] L. V. Hau, S. E. Harris, Z. Dutton, and C. H. Behroozi, Nature **397**, 594 (1999).

[89] M. M. Kash, V. A. Sautenkov, A. S. Zibrov, L. Hollberg, G. R. Welch, M. D. Lukin, Y. Rostovtsev, E. S. Fry, and M. O. Scully, Phys. Rev. Lett. **82**, 5229 (1999).

[90] D. Budker, D. F. Kimball, S. M. Rochester, and V. V. Yashchuk, Phys. Rev. Lett. **83**, 1767 (1999).

[91] A. Godone, F. Levi, and S. Micalizio, Phys. Rev. A **66**, 043804 (2002).

[92] D. F. Phillips, A. Fleischhauer, A. Mair, R. L. Walsworth, and M. D. Lukin, Phys. Rev. Lett. **86**, 783 (2001).

[93] C. Liu, Z. Dutton, C. H. Behroozi, and L. V. Hau, Nature **409**, 490 (2001).

[94] A. S. Zibrov, A. B. Matsko, O. Kocharovskaya, Y. V. Rostovtsev, G. R. Welch, and M. O. Scully, Phys. Rev. Lett. **88**, 103601 (2002).

[95] C. Liu, Z. Dutton, C. H. Behroozi, and L. V. Hau, Nature **409**, 490 (2001).

[96] J. T. Manassah and I. Gladkova, Laser Phys. **11**, 801 (2001).

[97] A. B. Matsko, Y. V. Rostovtsev, O. Kocharovskaya, A. S. Zibrov, and M. O. Scully, Phys. Rev. A **6404**, 043809 (2001).

[98] A. S. Zibrov, A. B. Matsko, O. Kocharovskaya, Y. V. Rostovtsev, G. R. Welch, and M. O. Scully, Phys. Rev. Lett. **88**, 103601 (2002).

[99] A. Mair, J. Hager, D. F. Phillips, R. L. Walsworth, and M. D. Lukin, Phys. Rev. A **65**, 031802 (2002).

[100] M. Kozuma, D. Akamatsu, L. Deng, E. W. Hagley, and M. G. Payne, Phys. Rev. A **66**, 031801 (2002).

[101] G. Juzeliunas, M. Masalas, and M. Fleischhauer, Phys. Rev. A **67**, 023809 (2003).

[102] T. N. Dey and G. S. Agarwal, Phys. Rev. A **67**, 033813 (2003).

[103] A. B. Matsko, Y. V. Rostovtsev, M. Fleischhauer, and M. O. Scully, Phys. Rev. Lett. **86**, 2006 (2001).

[104] A. B. Matsko, Y. V. Rostovtsev, H. Z. Cummins, and M. O. Scully, Phys. Rev. Lett. **84**, 5752 (2000).

[105] L. J. Wang, A. Kuzmich, and A. Dogariu, Nature **406**, 277 (2000).

[106] A. M. Akulshin, A. Cimmino, A. I. Sidorov, P. Hannaford, and G. I. Opat, Phys. Rev. A **67**, 011801(R) (2003).

[107] A. V. Taichenachev, A. M. Tumaikin, and V. I. Yudin, Phys. Rev. A **61**, 011802 (2000).

[108] C. Y. Ye, Y. V. Rostovtsev, A. S. Zibrov, and Y. M. Golubev, Opt. Comm. **207**, 227 (2002).

[109] P. R. Hemmer, D. P. Katz, J. Donoghue, M. Croningolomb, M. S. Shahriar, and P. Kumar, Opt. Lett. **20**, 982 (1995).

[110] M. Jain, H. Xia, G. Y. Yin, A. J. Merriam, and S. E. Harris, Phys. Rev. Lett. **77**, 4326 (1996).

[111] A. S. Zibrov, M. D. Lukin, and M. O. Scully, Phys. Rev. Lett. **83**, 4049 (1999).

[112] M. O. Scully, Physics Reports **219**, 191 (1992).

[113] M. O. Scully and M. Fleischhauer, Phys. Rev. Lett. **69**, 1360 (1992).

[114] M. Fleischhauer and M. O. Scully, Phys. Rev. A **49**, 1973 (1994).

[115] M. T. Johnsson and M. Fleischhauer, Phys. Rev. A **66**, 043808 (2002).

[116] Y. L. Zhang, L. Jiang, Z. R. Sun, L. E. Ding, and Z. G. Wang, Chin. Phys. **12**, 174 (2003).

[117] Y. Wu, J. Saldana, and Y. F. Zhu, Phys. Rev. A **67**, 013811 (2003).

[118] M. T. Johnsson and M. Fleischhauer, Phys. Rev. A **66**, 043808 (2002).

[119] Y. F. Li, Y. P. Niu, and J. F. Sun, Phys. Lett. A **301**, 195 (2002).

[120] G. Juzeliunas and H. J. Carmichael, Phys. Rev. A **65**, 021601 (2002).

[121] B. S. Ham, P. R. Hemmer, M. K. Kim, and S. M. Shahriar, Laser Phys. **9**, 788 (1999).

[122] C. Dorman and J. P. Marangos, Phys. Rev. A **58**, 4121 (1998).

[123] C. Dorman, J. P. Marangos, and J. C. Petch, J. Mod. Opt. **45**, 1123 (1998).

[124] C. Dorman, I. Kucukkara, and J. P. Marangos, Opt. Commun. **180**, 263 (2000).

[125] S. E. Harris and A. V. Sokolov, Phys. Rev. Lett. **81**, 2894 (1998).

[126] R. S. Bennink, R. W. Boyd, C. R. Stroud, and V. Wong, Phys. Rev. A **6303**, 033804 (2001).

[127] M. Fleischhauer, U. Rathe, and M. O. Scully, Phys. Rev. A **46**, 5856 (1992).

[128] U. Rathe, M. Fleischhauer, and M. O. Scully, Phys. Rev. A **54**, 3961 (1996).

[129] A. B. Matsko, I. Novikova, G. R. Welch, D. Budker, D. F. Kimball, and S. M. Rochester, Phys. Rev. A **66**, 043815 (2002).

[130] D. Budker, W. Gawlik, D. Kimball, S. Rochester, V. Yashchuk, and A. Weis, Rev. Mod. Phys. **74**, 1153 (2002).

[131] V. Chickarmane and S. V. Dhurandhar, Phys. Rev. A **54**, 786 (1996).

[132] E. Arimondo, Phys. Rev. A **54**, 2216 (1996).

[133] M. Graf, E. Arimondo, E. S. Fry, D. E. Nikonov, G. G. Padmabandu, M. O. Scully, and S. Zhu, Phys. Rev. A **51**, 4030 (1995).

[134] A. V. Taichenachev, V. I. Yudin, R. Wynands, M. Stähler, J. Kitching, and L. Hollberg, Phys. Rev. A **67**, 033810 (2003).

[135] S. Knappe, M. Stahler, C. Affolderbach, A. Taichenachev, V. Yudin, and R. Wynands, Appl. Phys. B **76**, 57 (2003).

[136] J. D. Jackson, *Classical Electrodynamics* (Wiley, New York, 1975).

[137] L. D. Landau and E. M. Lifshitz, *The Classical Theory of Fields*, Vol. 2 (Pergamon Press, Oxford, 1975).

[138] S. Mukamel, *Principles of Nonlinear Optical Spectroscopy* (Oxford University Press, 1995).

[139] M. Lukin, Ph.D. dissertation, Texas A&M University, College Station (1998).

[140] C.Y.Ye and A.S.Zibrov, Phys. Rev. A **65**, 023806 (2002).

[141] C. Ottinger, R. Scheps, G. W. York, and A. Gallagher, Phys. Rev. A **11**, 1815 (1975).

[142] J. Vanier and C. Audoin, *The Quantum Phisics of Atomic Frequency Standards*, Vol. 1 (Adam Hilger; Philadelphia, 1989).

[143] S. H. Autler and C. H. Townes, Phys. Rev. **100**, 703 (1955).

[144] Y. Rostovtsev, I. Protsenko, H. Lee, and A. Javan, Journal of Modern Optics **49**, 2501 (2002).

[145] H.Lee, Y. Rostovtsev, C.J.Bednar, and A. Javan, Appl. Phys. B **76**, 33 (2003).

[146] V. A. Sautenkov, M. M. Kash, V. L. Velichansky, and G. R. Welch, Laser Phys. **9**, 889 (1999).

[147] O. Kocharovskaya, Y. Rostovtsev, and M. O. Scully, Phys. Rev. Lett. **86**, 628 (2001), URL http://link.aps.org/doi/10.1103/PhysRevLett.86.628.

[148] Y. V. Rostovtsev, O. Kocharovskaya, and M. O. Scully, Journal of Modern Optics **49**, 2637 (2002).

[149] M. Erhard, S. Nußmann, and H. Helm, Phys. Rev. A **62**, 061802(R) (2000).

[150] S. I. Kanorsky, A. Weis, and J. Skalla, Appl. Phys. B **60**, S165 (1995).

[151] D. Budker, D. J. Orlando, and V. Yashchuk, Am. J. Phys. **67**, 584 (1999).

[152] H. G. Robinson, E. S. Ensberg, and H. G. Dehmelt, Bull. Am. Phys. Soc. **3**, 9 (1958).

[153] M. A. Bouchiat and J. Brossel, Phys. Rev. **147**, 41 (1966).

[154] E. B. Alexandrov, M. V. Balabas, D. Budker, D. S. English, D. F. Kimball, C. H. Li, and V. Yashchuk, Phys. Rev. Lett **66**, 042903 (2002).

[155] A. Lipsich, S. Barreiru, P. Valente, and A. Lezama, Opt. Commun. **190**, 185 (2001).

[156] H. X. Chen, A. V. Durrant, J. P. Marangos, and J. A. Vaccaro, Phys. Rev. A **58**, 1545 (1998).

[157] E. E. Mikhailov, Y. Rostovtsev, and G. R. Welch, Journal of Modern Optics **49**, 2535 (2002).

[158] C. Affolderbach, A. Nagel, S. Knappe, S. Jung, D. Wiedenmann, and R. Wynands, Applied Physics B **70**, 407 (1999).

[159] R. Bernheim, *Optical Pumping* (W. A. Benjamin, Inc., New York, 1965).

[160] W. Happer, Rev. Mod. Phys. **44**, 169 (1972).

[161] C. Affolderbach, S. Knappe, R. Wynands, A. V. Taichenachev, and V. I. Yudin, Phys. Rev. A **65**, 043810 (2002).

[162] A. Lazema, S. Barreiro, and A. M. Akulshin, Phys. Rev. A **59**, 4732 (1999).

[163] A. Lipsich, S. Barreiro, A. M. Akulshin, and A. Lazema, Phys. Rev. A **61**, 053803 (2000).

[164] A. V. Taichenachev, A. M. Tumaikin, and V. I. Yudin, JETP Lett. **69**, 819 (1999).

[165] M. Kwon, K. Kim, H. S. Moon, H. D. Park, and J. B. Kim, J. Phys. B **34**, 2951 (2001).

[166] Y. Dancheva, G. Alzetta, S. Cartaleva, M. Taslakov, and C. Andreeva, Opt. Comm. **178**, 103 (2000).

[167] G. Alzetta, S. Cartaleva, Y. Dancheva, C. Andreeva, S. Gozzini, L. Botti, and A. Rossi, J. of Opt. B **3**, 181 (2001).

[168] F. Renzoni, C. Zimmermann, P. Verkerk, and E. Arimondo, J. Opt. B **3**, S7 (2001).

[169] F. Renzoni, S. Cartaleva, G. Alzetta, and E. Arimondo, Phys. Rev. A **63**, 065401 (2001).

[170] C. Andreeva, S. Cartaleva, Y. Dancheva, V. Biancalana, A. Burchianti, C. Marinelli, E. Mariotti, L. Moi, and K. Nasyrov, Phys. Rev. A **66**, 012502 (2002).

[171] H. Failache, P. Valente, G. Ban, V. Lorent, and A. Lezama, LANL e-Print archive (2002), URL http://arxiv.org/abs/quant-ph/0211065.

[172] H. Lee, Y. Rostovtsev, C. J. Bednar, and A. Javan, Appl. Phys. B **76**, 33 (2003).

[173] M. D. Lukin, M. Fleischhauer, A. S. Zibrov, H. G. Robinson, V. L. Velichansky, L. Hollberg, and M. O. Scully, Phys. Rev. Lett. **79**, 2959 (1997).

[174] S. E. Harris and L. V. Hau, Phys. Rev. Lett. **82**, 4611 (1999).

[175] C. Affolderbach, M. Stahler, S. Knappe, and R. Wynands, Appl. Phys. B **75**, 605 (2002).

[176] D. Budker, D. F. Kimball, S. M. Rochester, V. V. Yashchuk, and M. Zolotorev, Phys. Rev. A **62**, 043403 (2000).

[177] J. Kitching, S. Knappe, and L. Hollberg, Appl. Phys. Lett. **81**, 553 (2002).

[178] M. Merimaa, T. Lindvall, I. Tittonen, and E. Ikonen, J. Opt. Soc. Am. B **20**, 273 (2003).

[179] V. Sautenkov, M. Kash, V. Velichansky, and G. Welch, Laser Physics **9**, 889 (1999).

[180] E. Mikhailov, V. Sautenkov, Y. Rostovtsev, and G. Welch, submitted to JOSA B (2003).

[181] J. A. Armstrong, J. Opt. Soc. Am. **56**, 1024 (1966).

[182] R. C. Neelen, D. M. Boersma, G. N. M. P. van Exter, and J. P. Woerdman, Phys. Rev. Lett. **69**, 593 (1992).

[183] M. Bahoura and A. Clairon, Opt. Lett. **26**, 926 (2001).

[184] H. Robinson, V. Vasiliev, V. Velichanskiy, L. Hollberg, and A. Zibrov, *Diode Laser Noise Conversion and Reduction in Rubidium*, Vol. 1A-7 (14th International Conference on Atomic Physics, 1994).

[185] C. G. Alzar, L. Cruz, J. A. Gomez, M. F. Santos, and P. Nussenzveig, Europhysics. Lett. **61**, 485 (2003).

[186] H. Kim, K. Kwon, and J.B.Kim, Journal of the Korean Physical Society **30**, 407 (1997).

[187] S.A.Ahmanov, Y.E.Dyakov, and A.S.Chirkin, *Vvedenie v Statisticheskuyu Radiofiziku i Optiku* (Nauka, Moscow, 1981).

[188] N. M. Pomerantsev, V. Rizhkov, and G. V. Skrotskiy, *Fizicheskie Osnovi Kvantovoy Optiki* (Nauka, Moscow, 1972).

VITA

Name:	Eugeniy E. Mikhailov
Date and Place of birth:	November 5, 1975, Mitishi, USSR
Citizenship:	Russian
Address:	Department of Physics, Texas A&M University,
	College Station, TX 77843-4242, USA
E-mails:	evmik@leona.physics.tamu.edu; evmik@tamu.edu

Education

1998 - present	Graduate student at Texas A&M University, GPR 3.7.
	Ph.D. in Physics (August, 2003)
February, 1998	Diploma (BS)
	in Engineering Physics/Solid State Physics,
	Moscow State Engineering Physics Institute
1992 - 1998	Student at Moscow State Engineering Physics Institute

Experience

1998-present	Physics Department, Texas A&M University
	Teaching assistant (undergraduate and graduate courses)
	Research assistant (Experimental Quantum Optics)
1997-1998	Frequency Standard Laboratory, Lebedev Physics Institute, Moscow
	Research assistant (Quantum Electronics)

The typist for this dissertation was Eugeniy E. Mikhailov.